

<http://researchcommons.waikato.ac.nz/>

## Research Commons at the University of Waikato

### Copyright Statement:

The digital copy of this thesis is protected by the Copyright Act 1994 (New Zealand).

The thesis may be consulted by you, provided you comply with the provisions of the Act and the following conditions of use:

- Any use you make of these documents or images must be for research or private study purposes only, and you may not make them available to any other person.
- Authors control the copyright of their thesis. You will recognise the author's right to be identified as the author of the thesis, and due acknowledgement will be made to the author where appropriate.
- You will obtain the author's permission before publishing any material from the thesis.

# LANTHANIDE LUMINESCENCE AND ITS APPLICATIONS IN FORENSIC SCIENCE



THE UNIVERSITY OF  
**WAIKATO**  
*Te Whare Wānanga o Waikato*

A thesis  
submitted in partial fulfilment  
of the requirements for the degree  
of

**Master of Science in Chemistry**

at

**The University of Waikato**

by

**ANTONY J. PARNELL**

---

**The University of Waikato**

**2011**

## Abstract

Lanthanide compounds, specifically those containing europium and terbium can exhibit luminescent properties when combined with ligands that promote this characteristic. Lanthanide luminescence has proven to have an array of useful applications, one of which is the formation of luminescent powders for exposure of latent fingerprints. The aim of this study was to synthesise a novel ligand to support luminescent character in europium and terbium compounds, and then dope these compounds in to talcum powder. This resulting powder would ideally give exposure of latent fingerprints that can then be enhanced, through excitation of the luminescent compounds dispersed in the powder.

A novel  $(\text{Me})_3\text{CN}(\text{CH}_2\text{P}(\text{O})\text{Ph}_2)_2$  ligand ( $\text{p}=\text{o}$ ) was synthesised, and in turn was used to synthesis a range of  $\text{Ln}(\beta\text{-diketonate})_3(\text{p}=\text{o})$  compounds. These compounds were assessed for potential luminescent activity, and doped into talcum powder. These powders were then appraised for their prospective use as latent fingerprint exposing agents.

Through modification of a published procedure, the  $(\text{Me})_3\text{CN}(\text{CH}_2\text{P}(\text{O})\text{Ph}_2)_2$  ligand was synthesised, and characterised by Electrospray Ionisation (ESI) Mass spectrometry, Nuclear Magnetic Resonance (NMR) spectroscopy, Infra-red (IR) spectroscopy, melting point analysis and elemental analysis. With  $\beta$ -diketonate ligands acetylacetone (acac) and thenoyltrifluoroacetone (tta), lanthanide metals lanthanum, europium and terbium and the ( $\text{p}=\text{o}$ ) ligands a series of novel compounds were synthesised ( $\text{Ln}(\beta\text{-diketonate})_3(\text{p}=\text{o})$ ). These compounds were characterised by the methods listed above.

Using the neutral ligands 1,10-phenanthroline (phen) and 2,2-bipyridine (bipy), a series of  $\text{Eu/Tb}(\text{acac/tta})_3(\text{phen/bipy})$  compounds were

synthesised and doped into talcum powder, to investigate the effects on particle and structure character of the doped talcum powders. Talcum powder was also sonicated to investigate the effect of this on particle size, along with effect on use as a fingerprinting agent. Laser diffraction and Scanning Electron Microscopy studies informed of a notable decrease in particle size with sonication, and an increase in specific surface area. However the effect of this process on increasing exposure of latent fingerprints was deemed too insignificant to justify the procedure.

The compounds  $\text{Eu/Tb}(\text{acac}/\text{tta})_3(\text{phen}/\text{bipy})$ ,  $(\text{Eu/Tb}(\beta\text{-diketonate})_3(\text{p}=\text{o}))$  and  $[\text{H}_2\text{NMe}_2]_3[\text{Eu/Tb}(2,6\text{-dpa})_3]\cdot 2\text{H}_2\text{O}$  were investigated for luminescent activity. Fluorescence spectroscopy determined the dominant emission wavelengths from 254 nm and 312 nm excitation were at 510 nm and 625 nm respectively. The talcum powders, doped with the luminescent compounds were analysed for luminescent activity. Direct screening with an ultra-violet (UV) lamp with emission wavelengths of 254 nm and 312 nm informed of the powders with the most intensely observed luminescent emissions. From these results,  $\text{Eu}(\text{tta})_3(\text{p}=\text{o})$ ,  $\text{H}_2\text{NMe}_2]_3[\text{Eu}(2,6\text{-dpa})_3]\cdot 2\text{H}_2\text{O}$ ,  $\text{Tb}(\text{acac})_3(\text{p}=\text{o})$  and  $\text{H}_2\text{NMe}_2]_3[\text{Tb}(2,6\text{-dpa})_3]\cdot 2\text{H}_2\text{O}$  were chosen as the most promising candidates for more in-depth investigation of latent fingerprint exposure potential. Furthermore, it was determined that the novel  $(\text{Me})_3\text{CN}(\text{CH}_2\text{P}(\text{O})\text{Ph}_2)_2$  ligand was successful as a neutral ligand for supporting luminescence.

The powders were trialled by several variables, including surface, powder quantity, age of latent print, temperature, and the brush used to determine their effectiveness. Powders were compared to commercial Greenwop and Redwop fingerprint powders, as these were the most similar industrial samples in terms of use. Through trials in the laboratory and the police fingerprinting laboratory, it was determined that the doped talcum



powders were inferior to the commercial “wop” samples in terms of latent print definition under UV conditions. However, the talcum powders had several useful applications, specifically the dual effect of exposing prints clearly under UV and non-UV conditions. It was concluded the best application for the fingerprint powders was on smooth surfaces such as glass, with a gradual application of powder. Small amounts of powder gave more clarity under non-UV print exposure, but higher quantities of powder were required to get ample luminescent intensity under UV conditions.

## Acknowledgements

First and foremost, I must express my gratitude to my supervisor, Bill Henderson. His willingness to lend his vast knowledge was invaluable for this thesis, and I thank him for his support.

Thank you to all the lab techs throughout the department, specifically Pat, Wendy and Annie. Pat and Wendy were always on hand to help me get whatever various compounds I needed while making sure I wasn't letting my safety requirements lapse, so I thank them for that. Annie was a great help during my battles with the fluorescence spectrometer, her assistance in that task was highly appreciated.

I am very grateful to Godfrey Shouler and the other members of the Hamilton City police fingerprinting department. The resources they provided me along with their input were an important part of this thesis, and I thank them for it.

To all my friends who have provided humour and insight along the way, whether related to the task or not, thank you. In particular Jacob Jaine, who has always been willing to discuss ideas and lend his abilities, this helped immensely.

My family, specifically my parents and brother, have always given me nothing but unwavering support and I can't thank them enough for this. Their encouragement and interest throughout this work has meant a lot to me.

And to my partner Parva, who has always lovingly been there to help me throughout my academia. Having such an intelligent and caring person to keep me motivated has made this a less daunting task, and I express my utmost gratitude to her for this.

# Table of Contents

<b>Abstract .....</b>	<b>ii</b>
<b>Acknowledgements .....</b>	<b>v</b>
<b>Table of Contents .....</b>	<b>vi</b>
<b>List of Figures .....</b>	<b>xi</b>
<b>List of Tables.....</b>	<b>xiv</b>
<b>List of Abbreviations.....</b>	<b>xvi</b>
<b>1 Introduction .....</b>	<b>1</b>
1.1 History .....	1
1.2 Types and compositions of fingerprints .....	2
1.3 Typical methods for exposure of fingerprints.....	4
1.4 Development of new methods of latent print exposure .....	8
1.5 Aim of this research .....	8
<b>2 Synthesis of a novel aminomethylbis(phosphine oxide) ligand, and subsequent use to synthesise a novel series of lanthanide <math>\beta</math>-diketonate compounds.....</b>	<b>10</b>
2.1 Introduction.....	10
2.1.1 $\beta$ -Diketonate and Neutral Ligands.....	10
2.1.2 Aminomethylphosphines .....	11
2.1.3 Applications of lanthanide coordination compounds.....	13
2.1.4 Scope of this chapter .....	15
2.2 Method .....	16
2.2.1 Materials and instrumentation.....	16
2.2.2 Synthesis of $(\text{Me})_3\text{CN}(\text{CH}_2\text{P}(\text{O})\text{Ph}_2)_2$ .....	18

2.2.3	Synthesis of lanthanide compounds .....	19
2.3	Results .....	20
2.3.1	(Me) <sub>3</sub> CN(CH <sub>2</sub> P(O)Ph <sub>2</sub> ) <sub>2</sub> ligand.....	20
2.3.2	Lanthanide compounds .....	24
2.4	Discussion.....	28
2.4.1	Analysis of data for (Me) <sub>3</sub> CN(CH <sub>2</sub> P(O)Ph <sub>2</sub> ) <sub>2</sub> .....	28
2.4.2	Analysis of data for lanthanide compounds.....	29
2.5	Chapter summary.....	31
<b>3</b>	<b>Structure and particle character of talcum and fingerprinting powders.....</b>	<b>32</b>
3.1	Introduction.....	32
3.1.1	Structure and composition of talc.....	32
3.1.2	Physical makeup of fingerprinting powders .....	33
3.1.3	Use of laser diffraction and SEM for analysis of particle size and morphology .....	33
3.2	Methods .....	35
3.2.1	Materials and instrumentation.....	35
3.2.2	Manufacture of powders.....	36
3.2.3	Processing of powders.....	37
3.2.4	Evaluation of the adhesion of powders to latent prints .....	38
3.3	Results .....	38
3.3.1	Mastersizer analysis.....	38
3.3.2	SEM analysis .....	42
3.3.3	Powder adhesion analysis .....	48

3.4	Discussion.....	49
3.4.1	Particle size and morphology of talcum powder and doped talcum powders.....	49
3.4.2	Particle size and morphology of commercial fingerprinting powders .....	50
3.4.3	Effect of particle size on effectiveness of talcum powder print exposure .....	52
3.5	Chapter Summary .....	52
<b>4</b>	<b>Lanthanide Luminescence.....</b>	<b>54</b>
4.1	Introduction.....	54
4.1.1	Factors influencing luminescent intensity .....	55
4.1.2	Applications of lanthanide luminescence .....	58
4.1.3	Analysis of luminescent compounds .....	59
4.2	Methods .....	62
4.2.1	Chemicals and instrumentation.....	62
4.2.2	Synthesis of lanthanide compounds .....	62
4.2.3	Analysis of luminescent character .....	63
4.3	Results .....	64
4.3.1	Excitation and emission spectra of $\text{Ln}(\beta\text{-diketonate})_3(\text{phen/bipy})$ .....	64
4.3.2	Excitation and emission spectra of $\text{Ln}(\beta\text{-diketonate})_3(\text{p=O})...$	68
4.3.3	Excitation and emission spectra of Greenwop and Redwop.	70
4.3.4	Excitation and emission spectra of $[\text{H}_2\text{NMe}_2]_3[\text{Eu}(2,6\text{-dpa})_3].2\text{H}_2\text{O}$ and $[\text{H}_2\text{NMe}_2]_3[\text{Tb}(2,6\text{-dpa})_3].2\text{H}_2\text{O}$ .....	71
4.3.5	Observed luminescent intensity of fingerprint powders .....	71

4.4	Discussion.....	75
4.4.1	Analysis of excitation and emission spectra of lanthanide complexes.....	75
4.4.2	Analysis of doped talcum powders under UV excitation.....	76
4.4.3	Effectiveness of the $(\text{Me})_3\text{CN}(\text{CH}_2\text{P}(\text{O})\text{Ph}_2)_2$ ligand compared to 1,10-phenanthroline and 2,2-bipyridine.....	77
4.5	Chapter Summary .....	77
<b>5</b>	<b>Evaluation of doped talcum powders for detection of latent fingerprints.....</b>	<b>79</b>
5.1	Introduction.....	79
5.1.1	Methods for print comparison .....	79
5.1.2	Powder methods for exposing latent fingerprints .....	80
5.1.3	Applications for this research .....	81
5.2	Methods .....	82
5.2.1	Materials and instrumentation.....	82
5.2.2	Fingerprint trials .....	82
5.2.3	Imaging of exposed fingerprints.....	84
5.2.4	Police fingerprinting laboratory.....	85
5.3	Results .....	85
5.3.1	Surface trials.....	85
5.3.2	Powder quantity trials.....	92
5.3.3	Feather brush trials .....	95
5.3.4	Print age trials.....	97
5.3.5	Temperature trials.....	100

5.3.6	Police laboratory results.....	101
5.4	Discussion.....	104
5.4.1	Quality of doped talcum powders compared to commercial Greenwop/Redwop samples .....	104
5.4.2	Factors influencing best use of the doped talcum powders for latent print exposure.....	105
5.4.3	Assessment of powders by police fingerprinting officers....	106
5.5	Chapter summary.....	107
<b>6</b>	<b>Conclusions and recommendations .....</b>	<b>109</b>
6.1	Conclusions .....	109
6.1.1	Synthesis of $(\text{Me})_3\text{CN}(\text{CH}_2\text{P}(\text{O})\text{Ph}_2)_2$ ligand and $\text{Ln}(\beta\text{-diketonate})_3(\text{p}=\text{o})$ compounds .....	109
6.1.2	Analysis of particle character of doped talcum powders ....	109
6.1.3	Analysis of luminescent character of lanthanide complexes .....	110
6.1.4	Evaluation of doped talcum powders for their performance in exposing latent fingerprints.....	111
6.2	Future recommendations .....	111
<b>7</b>	<b>References.....</b>	<b>113</b>

## List of Figures

Figure 1.1: Graph of search hits for “development of latent fingerprints” from 1940 - 2010 on Google Scholar. ....	2
Figure 1.2: Structure of methyl cyanoacrylate. ....	6
Figure 1.3: Reaction of Ninhydrin with amino acid.....	6
Figure 1.4: Structure of DFO.....	7
Figure 2.1: Acetylacetonate, a $\beta$ -diketonate ligand. ....	11
Figure 2.2: 1,10- phenanthroline, a bulky neutral ligand. ....	11
Figure 2.3: Structure of a diphenyl substituted aminomethylphosphine, where R= any hydrocarbon group.....	12
Figure 2.4: General synthetic route to phosphine oxide from phosphonium salt precursor. ....	12
Figure 2.5: Structure of Eu(fod) <sub>3</sub> .....	13
Figure 2.6: Structure of (Me) <sub>3</sub> CN(CH <sub>2</sub> P(O)Ph <sub>2</sub> ) <sub>2</sub> . ....	16
Figure 2.7: Diagram of vapour diffusion set up. ....	18
Figure 2.8: Structure of MeN(CH <sub>2</sub> P(O)Ph <sub>2</sub> ) <sub>2</sub> .....	20
Figure 2.9: <sup>31</sup> P NMR spectrum of the (Me) <sub>3</sub> CN(CH <sub>2</sub> P(O)Ph <sub>2</sub> ) <sub>2</sub> ligand with a singlet at 27.83 ppm. ....	21
Figure 2.10: <sup>1</sup> H NMR spectrum of the (Me) <sub>3</sub> CN(CH <sub>2</sub> P(O)Ph <sub>2</sub> ) <sub>2</sub> ligand.....	21
Figure 2.11: ESI-MS spectrum of the (Me) <sub>3</sub> CN(CH <sub>2</sub> P(O)Ph <sub>2</sub> ) <sub>2</sub> ligand, followed by isotope pattern of the [M+Na] <sup>+</sup> peak observed. ....	22
Figure 2.12: Calculated isotope pattern of the (Me) <sub>3</sub> CN(CH <sub>2</sub> P(O)Ph <sub>2</sub> ) <sub>2</sub> ligand, with a complexed Na <sup>+</sup> ion.....	23
Figure 2.13: ESI mass spectrum of Eu(acac) <sub>3</sub> (p=o), with isotope pattern of [Eu(acac) <sub>2</sub> (p=o)] <sup>+</sup> ion.....	25
Figure 2.14: Simulated isotope pattern of [Eu(acac) <sub>2</sub> (p=o)] <sup>+</sup> ion.....	26
Figure 3.1: Particle size distribution of talcum powder. ....	39



Figure 3.2: Particle size comparison of talcum powder to sonicated talcum powders.....	40
Figure 3.3: Particle size comparison of EU3 talcum powder and 4 hour sonicated EU3 talcum powder. ....	41
Figure 3.4: Particle size comparison of TB3 talcum powder and 8 hour sonicated TB3 talcum powder.....	41
Figure 3.5: Particle size distribution of Greenwop powder.....	42
Figure 3.6: SEM image of talcum powder. ....	43
Figure 3.7: SEM image of talcum powder doped with $\text{Eu}(\text{tta})_3(\text{phen})$ .....	44
Figure 3.8: SEM image of talcum powder sonicated for 8 hours. ....	45
Figure 3.9: SEM image of talcum powder doped with $\text{Eu}(\text{tta})_3(\text{phen})$ , sonicated for 4 hours. ....	45
Figure 3.10: SEM image of Greenwop at 350x magnification.....	46
Figure 3.11: SEM image of a Greenwop particle at 2000x magnification...	46
Figure 3.12: SEM image of Redwop at 350x magnification.....	47
Figure 3.13: SEM image of Redwop at 3000x magnification.....	47
Figure 3.14: Fingerprints exposed by talcum and “wop” powders. From left to right, top to bottom: A) unmodified talcum powder B) 2 hour sonicated, C) 4 hour sonicated D) 6 hour sonicated E) 8 hour sonicated F) Greenwop G) Redwop.....	48
Figure 4.1: Jablonski diagram showing energy transfers and electronic states of a molecule <sup>[59]</sup> . ....	54
Figure 4.2: Main luminescent levels (red) and fundamental levels of lanthanide(III) ions <sup>[60]</sup> .....	55
Figure 4.3: Modified Jablonski diagram displaying luminescence sensitisation through ligand interaction <sup>[63]</sup> . 1S* or S = singlet state, 3T* or T = triplet state, A = absorption, F = fluorescence, P = phosphorescence, k = rate constant, r = radiative, nr = non-radiative, nr = non-radiative, IC = internal conversion, ISC = intersystem crossing, ILCT (indices IL) =	

intraligand charge transfer, LMCT (indices LM) = ligand-to-metal charge transfer.....	57
Figure 4.4: Reproduced diagram of a fluorescence spectrometer.....	60
Figure 4.5: Structure of 2,6-dipicolinic acid.....	63
Figure 4.6: Emission spectrum of $\text{Eu}(\text{tta})_3(\text{phen})$ , excited at 254 nm. ....	65
Figure 4.7: Emission spectrum of $\text{Tb}(\text{acac})_3(\text{phen})$ at 312 nm excitation....	66
Figure 4.8: Excitation spectrum of $\text{Eu}(\text{tta})_3(\text{phen})$ at 625 nm emission. ....	67
Figure 4.9: Excitation spectra of $\text{Tb}(\text{acac})_3(\text{bipy})$ at 510 nm emission.....	68
Figure 4.10: Emission spectrum of $\text{Eu}(\text{tta})_3(\text{p}=\text{o})$ at 254 nm excitation.....	69
Figure 4.11: Excitation spectrum of $\text{Tb}(\text{tta})_3(\text{p}=\text{o})$ at 625 nm emission. ....	70
Figure 4.12: Emission spectrum of $[\text{H}_2\text{NMe}_2]_3[\text{Eu}(\text{2,6-dpa})_3] \cdot 2\text{H}_2\text{O}$ at 254 nm excitation.....	71
Figure 5.1: Latent print exposed with $\text{Tb}(\text{acac})_3(\text{p}=\text{o})$ print under frigid conditions.....	100
Figure 5.2: Images of talcum powder exposed prints on glass with no UV. A) $\text{Eu}(\text{tta})_3(\text{p}=\text{o})$ B) $[\text{H}_2\text{NMe}_2]_3[\text{Eu}(\text{2,6-dpa})_3] \cdot 2\text{H}_2\text{O}$ C) $\text{Tb}(\text{acac})_3(\text{p}=\text{o})$ D) $[\text{H}_2\text{NMe}_2]_3[\text{Tb}(\text{2,6-dpa})_3] \cdot 2\text{H}_2\text{O}$ .....	101
Figure 5.3: Images of prints exposed with $\text{Eu}(\text{tta})_3(\text{p}=\text{o})$ powder. A) no UV B) 350 nm excitation.....	102
Figure 5.4: Fingerprint on glass exposed with $\text{Eu}(\text{tta})_3(\text{p}=\text{o})$ powder, exposed with 350 nm light.....	103
Figure 5.5: Fingerprint on plastic exposed with $\text{Eu}(\text{tta})_3(\text{p}=\text{o})$ powder, exposed with 350 nm light.....	103
Figure 5.6: Fingerprints on aluminium exposed with $\text{Eu}(\text{tta})_3(\text{p}=\text{o})$ powder, exposed with 350 nm light.....	103

## List of Tables

Table 1.1: Organic and inorganic constituents of eccrine secretions <sup>[5]</sup> . ....	3
Table 1.2: Composition of sebum <sup>[6]</sup> . ....	4
Table 2.1: Lanthanum, europium and terbium complexes synthesised in this study. ....	15
Table 2.2: Theoretical and experimental elemental compositions of phosphine oxide ligand. ....	24
Table 2.3: Melting points of Ln(tta) <sub>3</sub> (p=O) compounds. ....	27
Table 2.4: Table of elemental compositions of synthesised Ln( $\beta$ -diketonate) <sub>3</sub> (p=O) compounds, with experimental values in brackets to the right of the theoretical values. ....	28
Table 3.1: Compounds doped in to talcum powder for particle character analysis. ....	36
Table 3.2: Powders and time sonicated. ....	37
Table 3.3: Particle sizes of talcum powders. ....	39
Table 3.4: Particle sizes of sonicated talcum powders. ....	40
Table 4.1: Compounds that were analysed by fluorescence spectroscopy. ....	61
Table 4.2: Summary of powders exhibiting red luminescence. ....	73
Table 4.3: Summary of powders exhibiting green luminescence. ....	74
Table 4.4: Alternate emission wavelengths for lanthanide compounds. ....	75
Table 5.1: Surface trials for fingerprint powders. ....	83
Table 5.2: Red luminescent powders on glass, displayed with and without UV excitation. ....	86
Table 5.3: Green luminescent powders on glass, displayed with and without UV excitation. ....	87
Table 5.4: Red luminescent powders on aluminium, displayed with and without UV excitation. ....	88

Table 5.5: Green luminescent powders on aluminium, displayed with and without UV excitation. ....	89
Table 5.6: Red luminescent powders on a plastic bank note, displayed with UV excitation. ....	90
Table 5.7: Green luminescent powders on a plastic bank note, displayed with UV excitation. ....	91
Table 5.8: A comparison of red luminescent powders, applied in quantities of 0.005 g, 0.01 g and 0.02 g. ....	93
Table 5.9: A comparison of green luminescent powders, applied in quantities of 0.005 g, 0.01 g and 0.02 g. ....	94
Table 5.10: Comparison of doped talcum powders when applied with a feather or badger hair brush. ....	97
Table 5.11: A comparison of red luminescent powders, applied to prints immediately, after 6 hours, after 24 hours and after 72 hours. ....	98
Table 5.12: A comparison of green luminescent powders, applied to prints immediately, after 6 hours, after 24 hours and after 72 hours. ....	100

## List of Abbreviations

2,6-dpa	2,6-dipicolinic acid
acac	acetylacetonate
bipy	2,2-bipyridine
cm <sup>-1</sup>	Wavenumbers
DFO	1,8-diazafluoren-9-one
DMF	N,N-dimethylformamide
ESI-MS	Electrospray Mass Spectrometry
fod	tris(6,6,7,7,8,8,8-heptafluoro-2,2-dimethyl-3,5-octanedionato)
FT-IR	Fourier Transform Infra-Red
IUPAC	International Union of Pure and Applied Chemistry
<i>m/z</i>	Mass to Charge Ratio
Me	Methyl Group
Nd-YAG	Neodymium-Yttrium Aluminum Garnet
nm	Nanometres
NMR	Nuclear Magnetic Resonance
p=O	(Me) <sub>3</sub> CN(CH <sub>2</sub> P(O)Ph <sub>2</sub> ) <sub>2</sub>
Ph	Phenyl

phen	1,10-phenanthroline
ppm	Parts Per Million
SEM	Scanning Electron Microscopy
tta	thenoyltrifluoroacetate
UV	Ultra-violet
μm	Micrometres
XRD	X-ray Diffraction

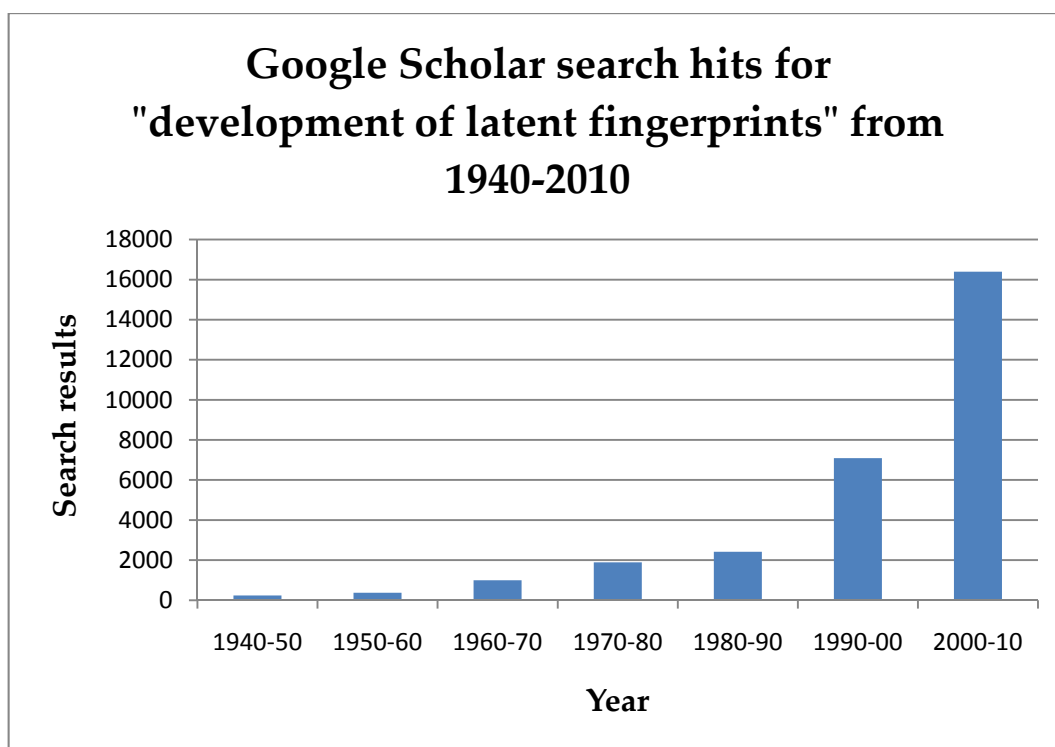
# 1 Introduction

## 1.1 History

The use of fingerprints for identification dates back as far as 1885 B.C. In ancient Babylonian times, fingerprints were pressed into clay tablets to authenticate written contracts. By 246 B.C., Chinese officials sealed documents with fingerprints, also with clay tablets. The Japanese were observed to be sealing contracts with fingerprints by 702 A.D. The first significant discovery in the modern era was by Nehemiah Grew, who published the first paper on the ridges of skin on the fingers and palms<sup>[1]</sup>. In 1788, Johan Mayer wrote the first paper recognising the uniqueness of fingerprints to the individual, and in 1892 Sir Francis Galton published the book *Finger Prints* which included a detailed model for fingerprint analysis and identification, and encouraged their use in forensic science<sup>[2]</sup>. With further expansion through the next decade, the practice of fingerprinting criminals was introduced into the United States by Deputy Commissioner Joseph A. Faurot of the New York City police department.

The basic process of using a fingerprint as evidence involves taking a clear image of a print at the scene of a crime, and matching that to one taken of the person in question. This is usually taken through application of a thin layer of printing ink to their finger, which is pressed onto a contrasting surface<sup>[3]</sup>. Fingerprints are highly important pieces of evidence for several reasons. Fingerprints are unique to individuals (even identical twins), with an estimated chance of 1 in 64 billion of two individuals sharing a finger print<sup>[3]</sup>. This level of certainty makes the discovery of a person's prints at a crime scene a powerful piece of evidence in placing them there. Furthermore the use of fingerprints is well established, with a robust history of research into their development for use as evidence. Figure 1.1

shows a graph of search results on Google Scholar for the term “development of latent fingerprints”, from 1940 to 2010.



*Figure 1.1: Graph of search hits for “development of latent fingerprints” from 1940 - 2010 on Google Scholar.*

The graph shows a relatively long history of research into the topic, and a surge in publications in the last 30 years as new methods have been developed. A search of New Zealand law database Lexis gave 633 cases where the term “fingerprint” was a key term.

## 1.2 Types and compositions of fingerprints

Imaging of fingerprints is an extremely varied process that is constantly being refined and improved. The main components of fingerprints targeted by imaging agents are eccrine sweat (water soluble) and sebum (water insoluble). These components are secreted by the eccrine glands and sebaceous glands, respectively. Other components of a print include apocrine secretions, epidermic substances and environmental contaminants. All components were found to differ in levels depending on



the age of the person from which the print was taken<sup>[4]</sup>. Fingerprints can be distinguished into three categories: plastic, visible and latent. Plastic prints occur when the ridges on the finger leave a negative image in a soft surface, such as paint or oil. Visible prints are a positive image left by a coating of a substance on the ridges of the fingerprint, pressed against a surface. Latent prints occur through a coating of sweat and oils on the ridges of the print leaving a positive image on a surface. Latent prints very commonly require chemical exposure.

Different methods for exposing latent fingerprints must be chosen depending on the surface and conditions under which prints were left. Factors such as the porosity and moisture on a surface determine which component of eccrine or sebaceous secretions should be targeted by the imaging agent. Table 1.1 shows the composition of eccrine secretions, while Table 1.2 shows the composition of sebum.

<u>Organic</u>	<u>Inorganic</u>
Amino acids	Water
Urea	Chlorides
Uric acid	Metal ions
Lactic acid	Sulfates
Monosaccharides and disaccharides	Phosphates
Creatinine	Ammonia
Choline	

*Table 1.1: Organic and inorganic constituents of eccrine secretions<sup>[5]</sup>.*

<u>Components</u>	<u>Composition</u>
Wax monoesters	25%
Triglycerides	41%
Free fatty acids	16%
Squalene	12%
Sterols and other hydrocarbons	6%

*Table 1.2: Composition of sebum<sup>[6]</sup>.*

A typical print will consist of over 98% water, with other constituents in trace amounts. These trace components can be exposed through various chemical reactions, leading to a range of imaging methods that can be used depending on the circumstances.

### **1.3 Typical methods for exposure of fingerprints**

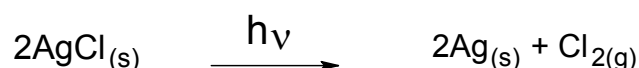
Powder methods are one of the simplest and broadest methods for exposing prints. By distributing a powder over an area, initial latent prints can be detected on site for more precise exposure in a laboratory scenario later. Still, these methods require skill and care. Fine brushes must be used as not to damage the structure of the latent print. Powders often consist of two parts, an adhesive and a colorant. The adhesive absorbs onto the sweat residue, and the colorant absorbs onto the adhesive. A typical adhesive may be starch or silica gel, with inorganic salts or organic dyes used as the colorant<sup>[7]</sup>. Metal powders (such as oxides of iron, manganese and titanium) have proven useful, as they can be milled to extremely fine

powders which provide good print clarity. Powder methods are further elaborated upon in chapter 5.

Classic chemical tests for exposing latent prints involve silver nitrate or iodine. The silver nitrate method works through reaction with chloride ions in a latent print. A solution of 3%  $\text{AgNO}_3$  is applied to a surface being examined, and subsequently reacts with any chloride ions:



On exposure to light, the silver chloride undergoes photochemical decomposition, exposing the prints with silver metal:



Iodine fuming is another classic technique for print exposure. Through sublimation of iodine, the non-polar  $\text{I}_2$  molecule adsorbs onto lipid materials in the print. The latent print then takes on the brown colour of the iodine. The colour fades from the print after a short time, leading to methods for fixing the iodine in the print. The use of 7,8-benzoflavone has proven useful for this, fixing the print as a deep blue colour<sup>[5]</sup>.

The “Super Glue” method of developing prints is another which uses fuming of latent prints. The active ingredient in the Super Glue is a cyanoacrylate ester, which through a polymerisation reaction with components of the latent prints gives a white polymer on the print. The structure of this ester is given in Figure 1.2. While many components of a print can cause this polymerisation reaction (water,  $\text{OH}^-$ ) it is unsure as to what exactly in the print causes the polymerisation to happen so precisely to the latent print<sup>[9]</sup>. The white polymer can be further enhanced by a range of methods. The polymer can be coloured for contrasting purposes,

through sublimation of organic dyes 1-amino-2-phenoxy-4-hydroxy-anthraquinone and 1,4-bis(ethylamino)anthraquinone giving red and blue colours respectively<sup>[10]</sup>.

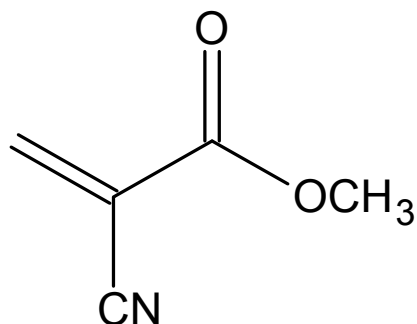


Figure 1.2: Structure of methyl cyanoacrylate.

Ninhydrin (2,2-Dihydroxyindane-1,3-dione) is a compound that reacts with free amines to give Ruhemann's purple. Ninhydrin reacts with the amino acids present in the eccrine sweat in latent prints, visualising the prints in Ruhemann's purple. The following diagram (Figure 1.3) shows the reaction of ninhydrin with an amino acid to give Ruhemann's purple.

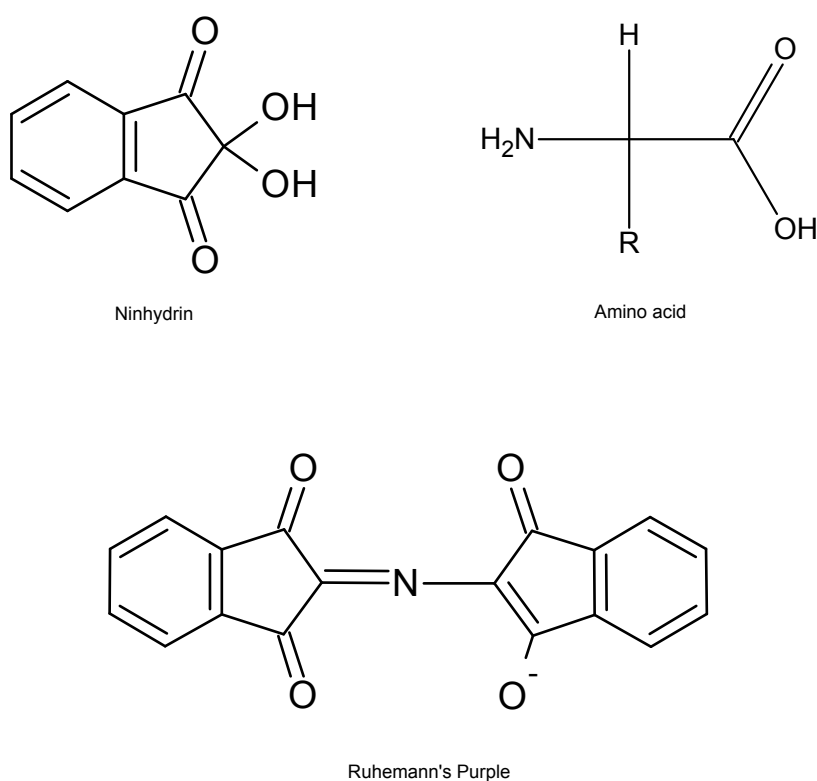
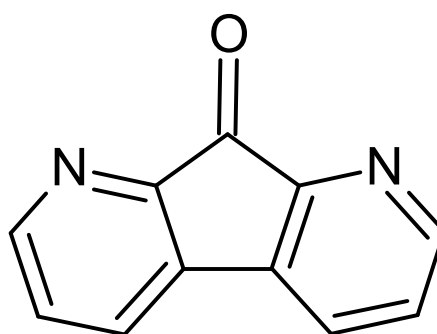


Figure 1.3: Reaction of Ninhydrin with amino acid.

The Ruhemann's purple structure is highly conjugated, however it is twisted which lowers conjugation. By making the structure co-planar the rigidity of the system increases, thus increasing the fluorescent intensity of the compound. This can be achieved through treatment with zinc chloride. Reaction with zinc chloride forms a complex which pulls the Ninhydrin rings into coplanar alignment. The increased conjugation results in fluorescence at ~560 nm, from illumination at ~488 nm. DFO or 1,8-diazafluoren-9-one is another compound used for luminescent exposure of latent prints. It operates in the same way as Ninhydrin (reaction with amino acids) but does not require treatment with zinc chloride to exhibit fluorescence. Excitation at ~470 nm results in fluorescence at ~570 nm<sup>[11]</sup>. The structure of DFO is given in Figure 1.4.



*Figure 1.4: Structure of DFO.*

Due to the characteristic luminescence exhibited by europium and terbium, there are numerous publications in the literature regarding their applications to fingerprinting. Research has been undertaken to form Ruhemann's purple-type complexes with europium and terbium from various Ninhydrin analogues, increasing luminescent intensities of the  $\text{Eu}^{3+}$  and  $\text{Tb}^{3+}$  ions<sup>[12]</sup>. More details on the use of lanthanide luminescence in forensic science are given in chapter 4.

## **1.4 Development of new methods of latent print exposure**

While fingerprinting has long been established as an important tool for use in forensics, there remain problems with the technique. While the theory behind the uniqueness of prints to the individual is sound, in practice there is a level of subjective interpretation when comparing one fingerprint to another. Furthermore, there is question over the standard number of matching minutiae that are required to confirm a match between prints, and also whether there should be a standard at all<sup>[13]</sup>. While there are various ways in which these issues can be addressed (such as improved automation systems), increasing resolution and accuracy of latent print exposure is central to achieving a positive identification between two prints. Therefore it is important that fingerprinting techniques are constantly refined to achieve the utmost accuracy, so permissibility as evidence in court is not brought into question.

Through discussion with a member of the fingerprinting unit of the Hamilton Central police department, several factors regarding the nature of print exposing powders were identified. The officer in question explained that “clogging” was a problem sometimes experienced in powder applications. This was described as the powder clumping together when applied to a surface, obscuring print detail. Furthermore the officer described that some powders disperse in air, potentially aggravating breathing which is undesirable.

## **1.5 Aim of this research**

The aim of this research is to synthesise a series of novel lanthanide compounds that exhibit luminescence, and dope these compounds into

talcum powder ideally giving a product that can expose latent fingerprints. Lanthanide compounds will be designed using a novel ligand along with a series of  $\beta$ -diketonates, which have well established support for luminescent activity in lanthanide compounds. These compounds will be analysed for their luminescent properties to determine which would have the best potential as fingerprinting powders. The lanthanide doped powders will be assessed for their particle character, specifically particle size and surface area to gain insight into the particle characteristics that support activity as a latent fingerprint powder. Finally the powders will be trialled in a range of conditions to evaluate their effectiveness in exposing latent fingerprints. Ultimately this should yield a novel print exposing powder, with information on the circumstances under which it can best perform.

## 2 Synthesis of a novel aminomethylbis(phosphine oxide) ligand, and subsequent use to synthesise a novel series of lanthanide $\beta$ -diketonate compounds

### 2.1 Introduction

The coordination chemistry of the lanthanide elements is dominated by the trivalent ions that all lanthanides form. Lanthanide complexes typically have coordination numbers of 7 - 12<sup>[14]</sup>, and have a rapid rate of ligand exchange in solution. Due to the lanthanide contraction, coordination number tends to decrease across the series, as the coordination of lanthanides is mainly controlled by steric factors<sup>[15]</sup>. Spectroscopic data show early lanthanides (La - Eu) coordinate 9 water molecules while the later (Dy - Lu) coordinate 8. The trivalent lanthanide ions are hard acceptors, making them ideal for forming complexes with ligands containing oxygen donors. Furthermore, with the strong affinity of lanthanides for water, chelating polydentate ligands are preferred to monodentate ligands as it is difficult for them to displace water molecules from the inner coordination sphere. Thus common complexes of lanthanide ions often contain  $\beta$ -diketonates or other polydentate oxygen donor ligands.

#### 2.1.1 $\beta$ -Diketonate and Neutral Ligands

$\beta$ -diketonate complexes of lanthanides have the general formula  $\text{Ln}(\text{R}^1\text{CO.CH.CO.R}^2)_3$ . The acetylacetonate complexes are made through a simple one pot synthesis combining a lanthanide salt and acetylacetone, with addition of NaOH as a base<sup>[15]</sup>. These complexes crystallise as hydrates; however inclusion of a bulky neutral ligand (such as phenanthroline) can block coordination of water molecules. Fluorinated diketones such as thenoyltrifluoroacetone have also been shown to form



useful complexes when synthesised with a neutral ligand, and have applications in solvent extraction of lanthanides<sup>[16]</sup>.  $\beta$ -Diketonate complexes with blocked off inner coordination spheres have found useful application as luminescent materials. These ligands behave as antennae chromophores, moieties which absorb photons and transfer energy to the metal ion, and are a simple strategy for increasing luminescent efficiency in a molecule<sup>[17]</sup>. Figures 2.1 and 2.2 show examples of a  $\beta$ -diketonate ligand and a neutral ligand.

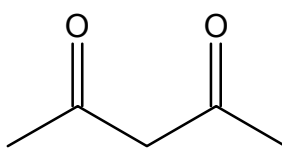


Figure 2.1: Acetylacetonate, a  $\beta$ -diketonate ligand.

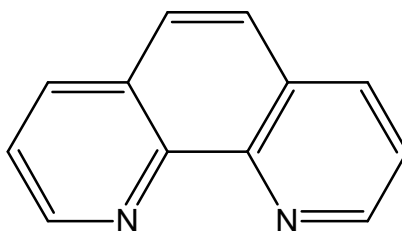


Figure 2.2: 1,10-phenanthroline, a bulky neutral ligand.

### 2.1.2 Aminomethylphosphines

Aminomethylphosphines were first discovered by Coates and Hoyer in 1962, through a reaction of a hydroxymethylphosphine with an excess of primary and secondary amine<sup>[18]</sup>. While there are a variety of aminomethylphosphines that have been prepared, the dominant chemistry has primarily been using phenyl and diphenyl substituted phosphines<sup>[19]</sup>. Aminomethylphosphines have proven to have application in flame retardation<sup>[20]</sup> and catalysis, where they are useful water soluble

ligands for complexation with transition metals<sup>[21]</sup>. Figure 2.3 shows the structure of a diphenyl substituted aminomethylphosphine.

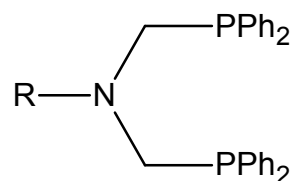


Figure 2.3: Structure of a diphenyl substituted aminomethylphosphine, where R= any hydrocarbon group.

Bidentate bis(diphenylphosphinomethyl)amino ligands have been shown to be extremely useful in a wide range of complexes, due to their influence on the stability of complexes<sup>[22]</sup>, their ease of synthesis and relatively cheap starting materials<sup>[23]</sup>. Due to their easy synthetic routes these compounds can be extremely versatile, with their donor atoms and positions easily modified. These ligands can be reacted to give oxides, which donate electron density through hard oxygen donors more preferentially to lanthanide ions. The phenyl ring substituents on the phosphorus atoms give conjugation which may increase energy transfer in luminescent metal complexes, which makes them ideal for this research. A simplified diagram of the route to the synthesis of an aminobis(methylphosphine oxide) is demonstrated in Figure 2.4.

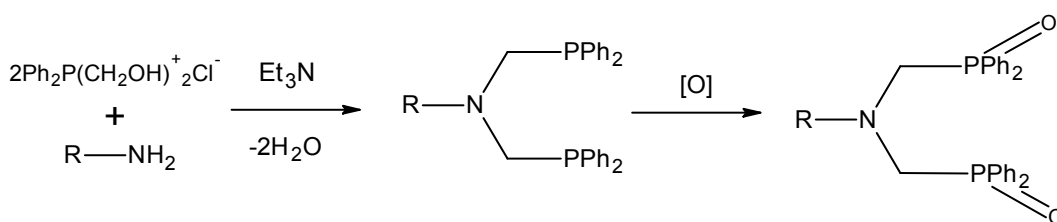


Figure 2.4: General synthetic route to phosphine oxide from phosphonium salt precursor.

The phosphonium salt  $\text{Ph}_2\text{P}(\text{CH}_2\text{OH})_2^+\text{Cl}^-$  is an ideal starting material as it is easily synthesised from inexpensive triphenylphosphine, and is reactive

towards amines. This allows for a range of aminomethylphosphines to be synthesised from the starting material. Manipulation of the R group on the phosphine is useful for modifying the properties of a compound.

### 2.1.3 Applications of lanthanide coordination compounds

One of the earliest applications for coordination compounds of lanthanides was that of lanthanide shift reagents. *Tris*(6,6,7,7,8,8,8-heptafluoro-2,2-dimethyl-3,5-octanedionato)europium (more commonly known as  $\text{Eu}(\text{fod})_3$ ) was found to give substantial peak shift in NMR spectra, without significant broadening of the spectrum<sup>[24]</sup>. This allowed for resolution of closely spaced signals when analysing compounds. Due to advances in NMR spectrometers, the use of shift reagents has become largely redundant. However  $\text{Eu}(\text{fod})_3$  has found use as a Lewis acid catalyst in organic synthesis<sup>[25]</sup>, and as a reagent for the luminescent visualisation of latent fingerprints<sup>[26]</sup>. The compound consists of three bidentate fod ligands, coordinated through oxygen donors to the  $\text{Eu}(\text{III})$  centre, Figure 2.5.

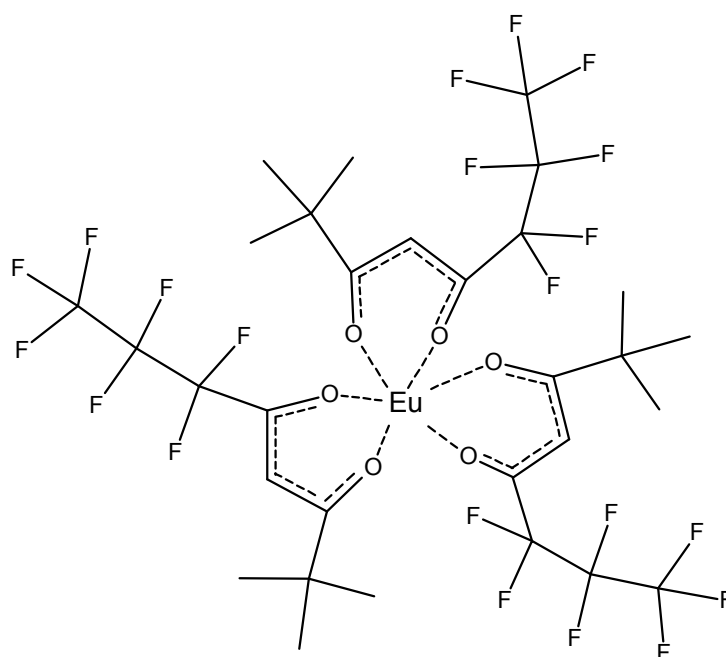


Figure 2.5: Structure of  $\text{Eu}(\text{fod})_3$ .

The use of phosphine oxide and related phosphorylic ligands to form lanthanide complexes is a topic which has been covered widely in the literature. In the recovery of products from spent nuclear fuel, phosphine oxide compounds are often used to extract lanthanide cations<sup>[27]</sup>. Extraction of lanthanides from ore and solutions, and separation of lanthanides from actinide elements is a common application for the coordination chemistry of lanthanides. The use of chelating phosphine oxide ligands is common place for such extractions. Early research by Siddall for DuPont shows a series of bidentate phosphine oxide ligands which are useful for the extraction of cerium, promethium and americium from nitric acid<sup>[28]</sup>.

These techniques have been expanded, and have proven useful in the reprocessing of highly active wastes. Various phosphonate ligands have been trialled to optimise separation of actinides and lanthanides from highly active nuclear wastes<sup>[29]</sup>. The literature shows a large body of work undertaken on complexation of lanthanides by phosphine oxide ligands. Phosphonopyridyl N,P oxides have been shown to chelate lanthanide ions while displacing water from the inner coordination sphere<sup>[30]</sup>, and research on the use of methylphosphonic acid ligands has shown the ability to complex neodymium under hydrothermal conditions<sup>[31]</sup>. There is also a body of work detailing the complexes formed by aminobis(methylphosphine oxide) ligands. Complexes of copper<sup>[32]</sup>, palladium and platinum<sup>[33]</sup> have been published, with the ligands donating through oxygen and nitrogen atoms. The aminobis(methylphosphine oxide) ligand has also been used to give hydrophilicity to complexes of platinum and palladium for anti-cancer applications<sup>[33]</sup>. Phosphine oxides have been proven to act as useful

antenna chromophore ligands for the sensitisation of lanthanide luminescence<sup>[34]</sup>.

### 2.1.4 Scope of this chapter

The complexes in this research were based on complexes synthesised by Melby<sup>[35]</sup>, using acetylacetone (acac) and thenoyltrifluoroacetone (tta) as bidentate oxygen donor anionic ligands, and phenanthroline (phen) and bipyridine (bipy) were used as bidentate nitrogen donor neutral ligands. The phosphine oxide ligand (p=O) was substituted in place of the neutral ligand in the synthesis. The lanthanide metals used were lanthanum, europium and terbium. At the time of writing, the price of one gram of lanthanum nitrate hexahydrate was \$1.57 whereas europium nitrate pentahydrate and terbium nitrate hexahydrate were \$84.63 and \$53.45 respectively. Therefore it was economically responsible to use lanthanum to test the methods first, as it has almost identical reactivity as europium and terbium. Europium and terbium both have extensively proven use in luminescence, as further detailed in chapter 4. Table 2.1 shows the range of complexes that were synthesised.

	<b><u>Phen</u></b>	<b><u>bipy</u></b>	<b><u>p=O</u></b>
La(acac) <sub>3</sub>	La(acac) <sub>3</sub> (phen)	La(acac) <sub>3</sub> (bipy)	La(acac) <sub>3</sub> (p=O)
La(tta) <sub>3</sub>	La(tta) <sub>3</sub> (phen)	La(tta) <sub>3</sub> (bipy)	La(tta) <sub>3</sub> (p=O)
Eu(acac) <sub>3</sub>	Eu(acac) <sub>3</sub> (phen)	Eu(acac) <sub>3</sub> (bipy)	Eu(acac) <sub>3</sub> (p=O)
Eu(tta) <sub>3</sub>	Eu(tta) <sub>3</sub> (phen)	Eu(tta) <sub>3</sub> (bipy)	Eu(tta) <sub>3</sub> (p=O)
Tb(acac) <sub>3</sub>	Tb(acac) <sub>3</sub> (phen)	Tb(acac) <sub>3</sub> (bipy)	Tb(acac) <sub>3</sub> (p=O)
Tb(tta) <sub>3</sub>	Tb(tta) <sub>3</sub> (phen)	Tb(tta) <sub>3</sub> (bipy)	Tb(tta) <sub>3</sub> (p=O)

Table 2.1: Lanthanum, europium and terbium complexes synthesised in this study.

The aminobis(methylphosphine oxide) ligand synthesised for this research was a novel compound, and thus it was necessary to undertake rigorous characterisation of the ligand and the metal complexes it formed. Several techniques were used, including melting point studies, multinuclear nuclear magnetic resonance spectroscopy, electrospray ionisation mass spectroscopy, infra-red spectroscopy, elemental analysis and x-ray diffraction spectroscopy. Figure 2.6 gives the structure of the aminobis(methylphosphine oxide) that was attempted.

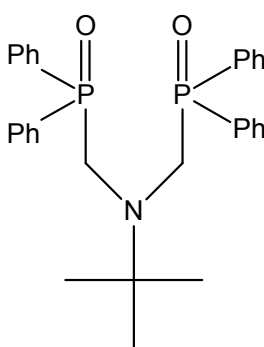


Figure 2.6: Structure of  $(Me)_3CN(CH_2P(O)Ph_2)_2$ .

## 2.2 Method

### 2.2.1 Materials and instrumentation

The phosphine oxide ligand was synthesised from the phosphonium salt  $Ph_2P(CH_2OH)_2^+Cl^-$  starting material, which was sourced from the laboratory and synthesised by published methods<sup>[19]</sup> when more was required. *Tert*-butylamine was sourced from J.T Baker Chemical Company, while triethylamine and  $Na_2SO_4$  was sourced from Sigma-Aldrich. Drum grade dichloromethane was also used.

For the synthesis of the lanthanide complexes, lanthanum nitrate hexahydrate, europium nitrate hexahydrate, terbium nitrate hexahydrate, acetylacetone (acac) and thenoyltrifluoroacetone (tta) were purchased from Sigma-Aldrich. Synthesis grade 1,10-phenanthroline was obtained

from May and Baker LTD, and 2,2-bipyridine from BDH Laboratory supplies was used. Drum grade 95% ethanol solvent was also used for synthesis. The following instruments were used for all characterisation in this research:

- Bruker AC300 NMR spectrometer fitted with a multi-nuclear probe for  $^1\text{H}$ ,  $^{13}\text{C}$  and  $^{31}\text{P}$  NMR
- Bruker MicrOTOF<sup>TM</sup> electrospray ionisation mass spectrometer for ion mass and isotope pattern analysis, run in positive ion mode
- Perkin Elmer spectrum 100 FT-IR for Infra-red spectroscopy
- Buchi melting point Mm-560 for melting point data

Elemental analysis was also undertaken to assist with characterisation. A sample of the compound was sent away for analysis to the University of Otago. The samples were desiccated overnight to remove any solvent or water impurities. The samples were analysed for composition of carbon, hydrogen and nitrogen.

XRD spectroscopy requires a single unit cell crystal of the compound being analysed to obtain suitable data. Crystal growth was attempted using vapour diffusion, where a low polarity solvent is diffused into a high polarity solvent, ideally giving gradual growth of a unit cell crystal. A vial containing the dissolved compound is placed into a larger vial containing the alternate polarity solvent. Figure 2.7 demonstrates the vapour diffusion procedure.

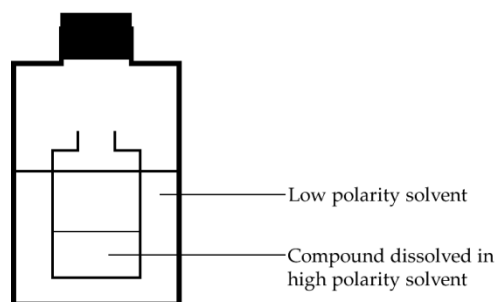


Figure 2.7: Diagram of vapour diffusion set up.

A series of different diffusions were set up, using chloroform and diethyl ether and dichloromethane and diethyl ether. A series were run at room temperature, and another refrigerated. The vials were left for several days, and monitored for crystal growth. Ultimately no suitable crystals were achieved from these methods.

### 2.2.2 Synthesis of $(\text{Me})_3\text{CN}(\text{CH}_2\text{P}(\text{O})\text{Ph}_2)_2$

The  $(\text{Me})_3\text{CN}(\text{CH}_2\text{P}(\text{O})\text{Ph}_2)_2$  ligand was synthesised through a modification of the literature method<sup>[23]</sup> for the synthesis of  $(\text{Me})_3\text{CN}(\text{CH}_2\text{P}(\text{O})\text{Ph}_2)_2$ , and is detailed as follows.

For synthesis of the the phosphine oxide ligand, 0.92 mmol of the phosphonium salt was dissolved in 15 mL of a 2:1 mixture of  $\text{H}_2\text{O}:\text{EtOH}$ . While stirring, 2.65 mmol of triethylamine was added, followed by 0.46 mmol of *tert*-butylamine. The mixture was then refluxed for one hour, and on completion was extracted with dichloromethane. After drying with  $\text{Na}_2\text{SO}_4$  the solvent was removed by rotary evaporation, yielding a brown oil. The oil was then dissolved in methanol, with addition of dichloromethane to obtain complete dissolution. An excess (3 mL) of  $\text{H}_2\text{O}_2$  was added dropwise while stirring the mixture. The dichloromethane was then removed using a rotary evaporator. Water was then added dropwise



to precipitate out the product,  $(\text{Me})_3\text{CN}(\text{CH}_2\text{P}(\text{O})\text{Ph}_2)_2$ . The product was then filtered and dried under vacuum.

### 2.2.3 Synthesis of lanthanide compounds

The lanthanide complexes were synthesised through published methods<sup>[35]</sup>, suitably scaled down. The lanthanide metals were interchanged in the synthesis for each respective complex.

Lanthanide complexes with acac ligands were synthesised as follows. In a 50 mL round bottom flask 1.5 mmol of acac, 1.5 mL of 1M NaOH and 0.5 mmol of the neutral ligand were added to 5 mL of hot 95% ethanol. While stirring, 0.5 mmol of the lanthanide nitrate hexahydrate was added drop wise after being dissolved in 5 mL of distilled water. A precipitate formed immediately. After stirring for an hour the precipitate was filtered, and washed with 5 mL of distilled water and 5 mL of ethanol. The precipitate was then dried under vacuum.

A different method<sup>[36]</sup> was utilised for the synthesis of complexes with the tta ligands. In a 50 mL round bottom flask, to a hot mixture of 12.5 mL 95% ethanol and 1.25 mL water 0.5 mmol of lanthanide nitrate hexahydrate and 1.5 mmol of tta was added. While the solution was stirring, 0.75 mL of 2M NaOH was added. NaCl precipitated instantly, and was filtered out immediately. After filtration, 0.5 mmol of the neutral ligand was added drop wise after having been dissolved in 2.5 mL of ethanol. A precipitate appeared almost instantly. After stirring for an hour, the precipitate was filtered, washed with 5 mL of distilled water and 5 mL of ethanol and dried under vacuum.

## 2.3 Results

### 2.3.1 (Me)<sub>3</sub>CN(CH<sub>2</sub>P(O)Ph<sub>2</sub>)<sub>2</sub> ligand

To determine successful synthesis of the (Me)<sub>3</sub>CN(CH<sub>2</sub>P(O)Ph<sub>2</sub>)<sub>2</sub> ligand, the NMR shifts were compared with shifts from an aminobis(methylphosphine oxide) of similar structure in the literature. Figure 2.8 shows the structure of MeN(CH<sub>2</sub>P(O)Ph<sub>2</sub>)<sub>2</sub>, which differs from the synthesised compound only in the methyl group on the nitrogen. This compound was used to compare NMR and IR data for characterisation of the synthesised (Me)<sub>3</sub>CN(CH<sub>2</sub>P(O)Ph<sub>2</sub>)<sub>2</sub>. The literature indicates a singlet at 29.8 ppm was present in the <sup>31</sup>P NMR spectrum of MeN(CH<sub>2</sub>P(O)Ph<sub>2</sub>)<sub>2</sub><sup>[37]</sup>. Figure 2.9 displays a <sup>31</sup>P NMR spectrum and Figure 2.10 displays a <sup>1</sup>H NMR spectrum taken of the synthesised (Me)<sub>3</sub>CN(CH<sub>2</sub>P(O)Ph<sub>2</sub>)<sub>2</sub>. The <sup>31</sup>P NMR spectrum showed a singlet peak at 27.83 ppm. The <sup>1</sup>H NMR spectrum showed a doublet of multiplets from 7.3 - 7.7 ppm, and singlets at 3.96 and 0.99 ppm.

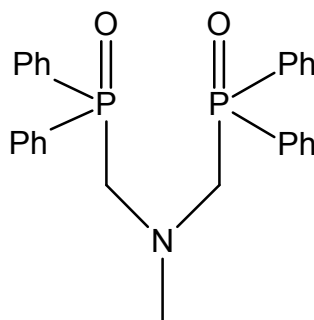


Figure 2.8: Structure of MeN(CH<sub>2</sub>P(O)Ph<sub>2</sub>)<sub>2</sub>.

Results from ESI-MS further supported the NMR evidence. A sample was analysed with NaCl added to the solution to promote ionisation of the [M+Na]<sup>+</sup> species. An abundant peak at *m/z* 524 indicated presence of the (Me)<sub>3</sub>CN(CH<sub>2</sub>P(O)Ph<sub>2</sub>)<sub>2</sub> ligand complexed with Na<sup>+</sup>. Figure 2.11 displays an ESI-MS spectrum taken of the phosphine oxide and NaCl in methanol, and the isotope pattern observed on the spectrum. Comparison of the

isotope pattern of the  $m/z$  524 peak shows correlation with simulated isotope pattern of the ligand with a  $\text{Na}^+$  ion, which is shown in Figure 2.12.

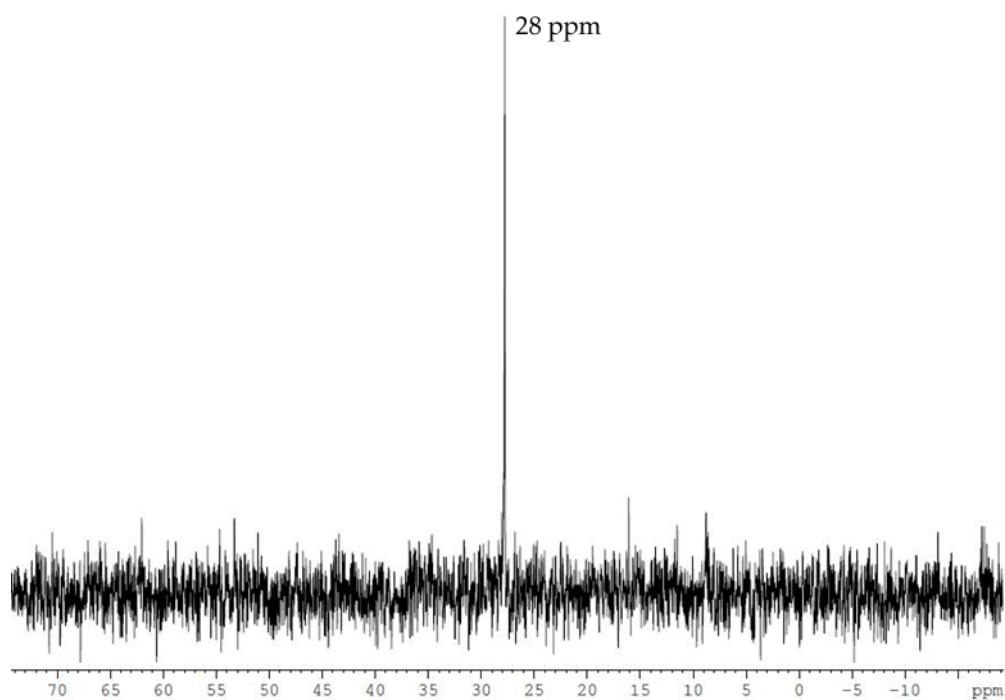


Figure 2.9:  $^{31}\text{P}$  NMR spectrum of the  $(\text{Me})_3\text{CN}(\text{CH}_2\text{P}(\text{O})\text{Ph}_2)_2$  ligand with a singlet at 27.83 ppm.

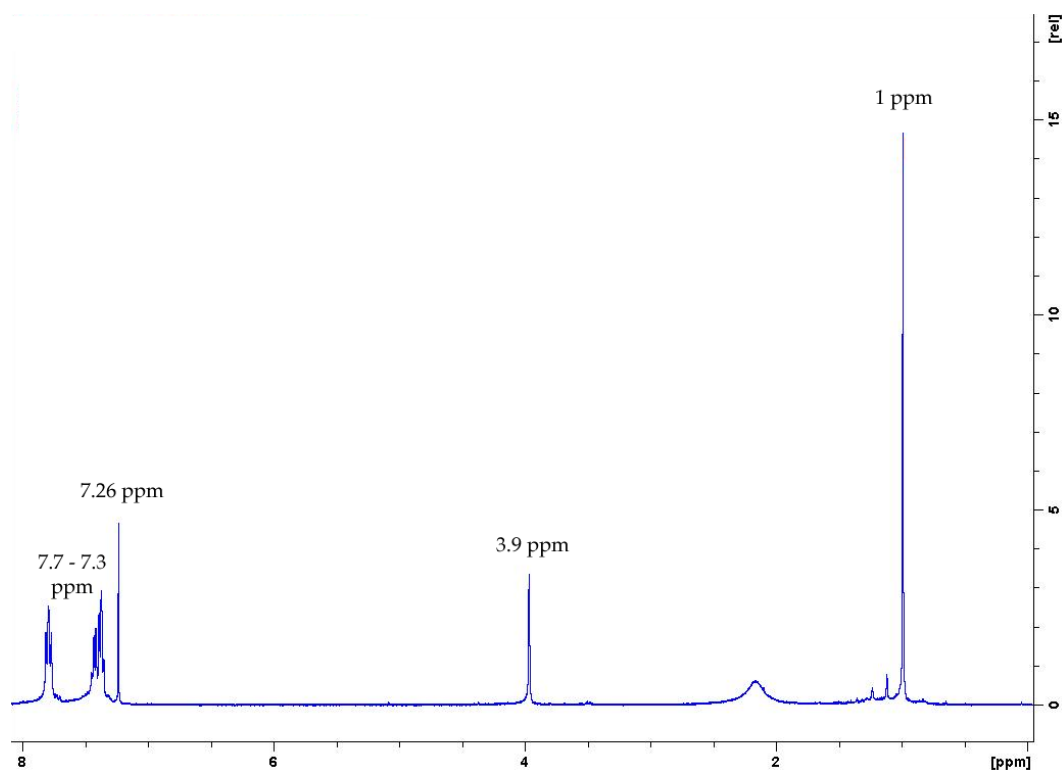


Figure 2.10:  $^1\text{H}$  NMR spectrum of the  $(\text{Me})_3\text{CN}(\text{CH}_2\text{P}(\text{O})\text{Ph}_2)_2$  ligand.

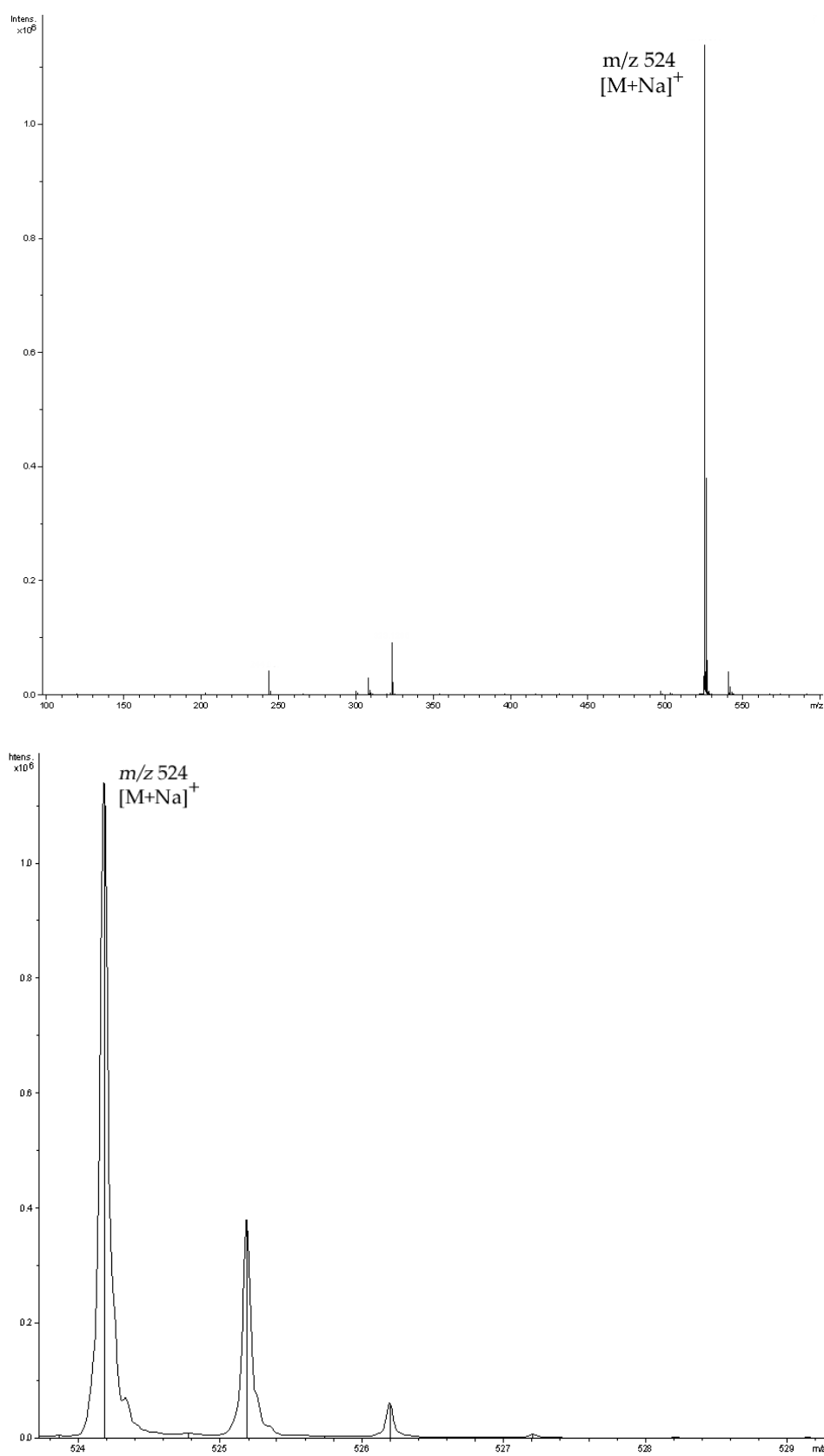


Figure 2.11: ESI-MS spectrum of the  $(\text{Me})_3\text{CN}(\text{CH}_2\text{P}(\text{O})\text{Ph}_2)_2$  ligand, followed by isotope pattern of the  $[\text{M}+\text{Na}]^+$  peak observed.

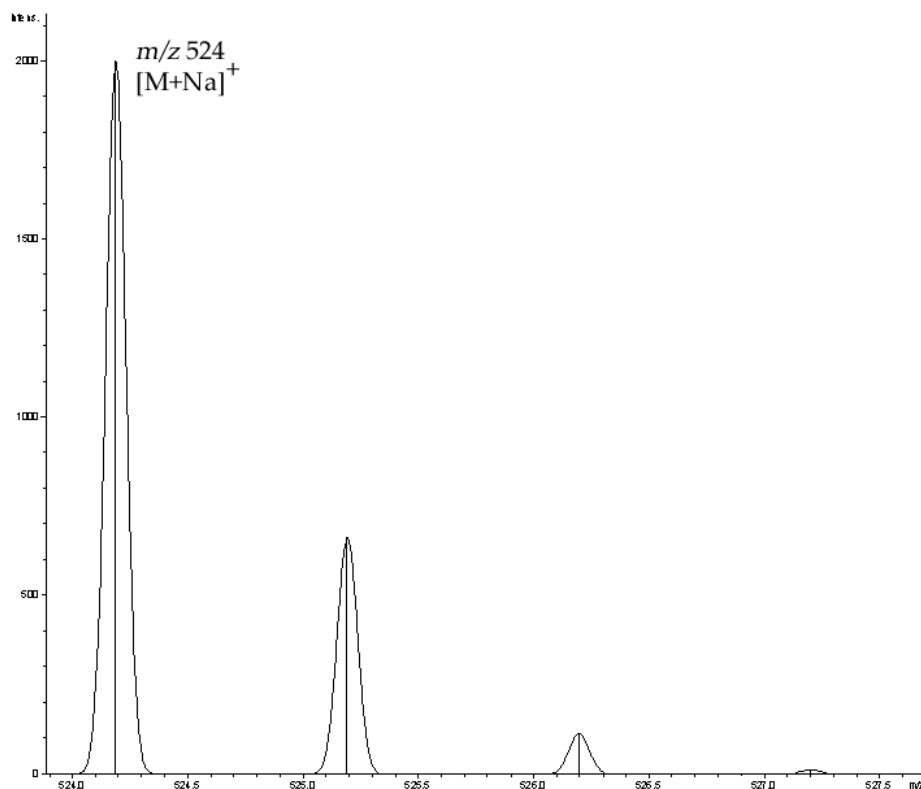


Figure 2.12: Calculated isotope pattern of the  $(Me)_3CN(CH_2P(O)Ph_2)_2$  ligand, with a complexed  $Na^+$  ion.

Infrared spectroscopy was used to analyse for the presence of the phosphorus oxygen double bond, which literature studies stated at around  $1189\text{ cm}^{-1}$  on the comparative  $MeN(CH_2P(O)Ph_2)_2$  compound<sup>[37]</sup>. The IR spectrum of  $(Me)_3CN(CH_2P(O)Ph_2)_2$  displayed a P=O stretch at  $1196\text{ cm}^{-1}$ . Melting point analysis gave a melting point of  $113.5\text{ }^\circ\text{C} - 115.1\text{ }^\circ\text{C}$ .

Elemental analysis of the  $(Me)_3CN(CH_2P(O)Ph_2)_2$  ligand was used. Table 2.2 gives the theoretical and experimental elemental compositions of the ligand.

	<u>Carbon</u>	<u>Hydrogen</u>	<u>Nitrogen</u>
Theoretical	71.83%	6.64%	2.79%
Experimental	68.14%	6.70%	2.73%

Table 2.2: Theoretical and experimental elemental compositions of phosphine oxide ligand.

Once the phosphine oxide ligand was successfully characterised, it was used in the synthesis of the lanthanide complexes. These complexes were then characterised through NMR, ESI-MS and Infrared spectroscopy, using the same instruments stated earlier.

### 2.3.2 Lanthanide compounds

The lanthanide complexes were synthesised using the methods stated earlier, with the  $(\text{Me})_3\text{CN}(\text{CH}_2\text{P}(\text{O})\text{Ph}_2)_2$  used as the neutral ligand in the reaction.  $\text{Eu}(\text{acac})_3(\text{p}=\text{o})$ ,  $\text{Tb}(\text{acac})_3(\text{p}=\text{o})$ ,  $\text{La}(\text{acac})_3(\text{p}=\text{o})$  and  $\text{La}(\text{tta})_3(\text{p}=\text{o})$  were all collected as white solids, where as  $\text{Eu}(\text{tta})_3(\text{p}=\text{o})$  and  $\text{Tb}(\text{tta})_3(\text{p}=\text{o})$  were collected as yellow solids.

#### 2.3.2.1 ESI Mass spectrometry

The ESI mass spectra of the compounds was dominated mainly by peaks of  $[\text{Ln}(\beta\text{-diketonate})_2(\text{p}=\text{o})]^+$  and  $[\text{Ln}(\beta\text{-diketonate})_2(\text{p}=\text{o})_2]^+$ . These ions correlate with the loss of a  $\beta$ -diketonate ligand in the electrospray process, a fragmentation process which is supported by the literature<sup>[38]</sup>. Calculated isotope patterns of these ions also matched with the patterns observed on the spectra. Another common peak observed correlated to an ion of  $[(\text{p}=\text{o})\text{Na}]^+$ . This suggested a free ligand complexing with a  $\text{Na}^+$  ion. Calculated isotope patterns further backed up this hypothesis, as they matched that observed in the spectra. Figure 2.13 shows the ESI MS of  $\text{Eu}(\text{acac})_3(\text{p}=\text{o})$ , which displays ions of  $[(\text{p}=\text{o})\text{Na}]^+$ ,  $[(\text{p}=\text{o})_2\text{Na}]^+$ ,  $[\text{Eu}(\text{acac})_2(\text{p}=\text{o})]^+$  and  $[\text{Eu}(\text{acac})_2(\text{p}=\text{o})_2]^+$ . The isotope pattern of the most dominant lanthanide fragmentation ion of  $[\text{Eu}(\text{acac})_2(\text{p}=\text{o})]^+$  is also shown,

and correlates with the simulated pattern of  $[\text{Eu}(\text{acac})_2(\text{p}=\text{o})]^+$  in Figure 2.14.

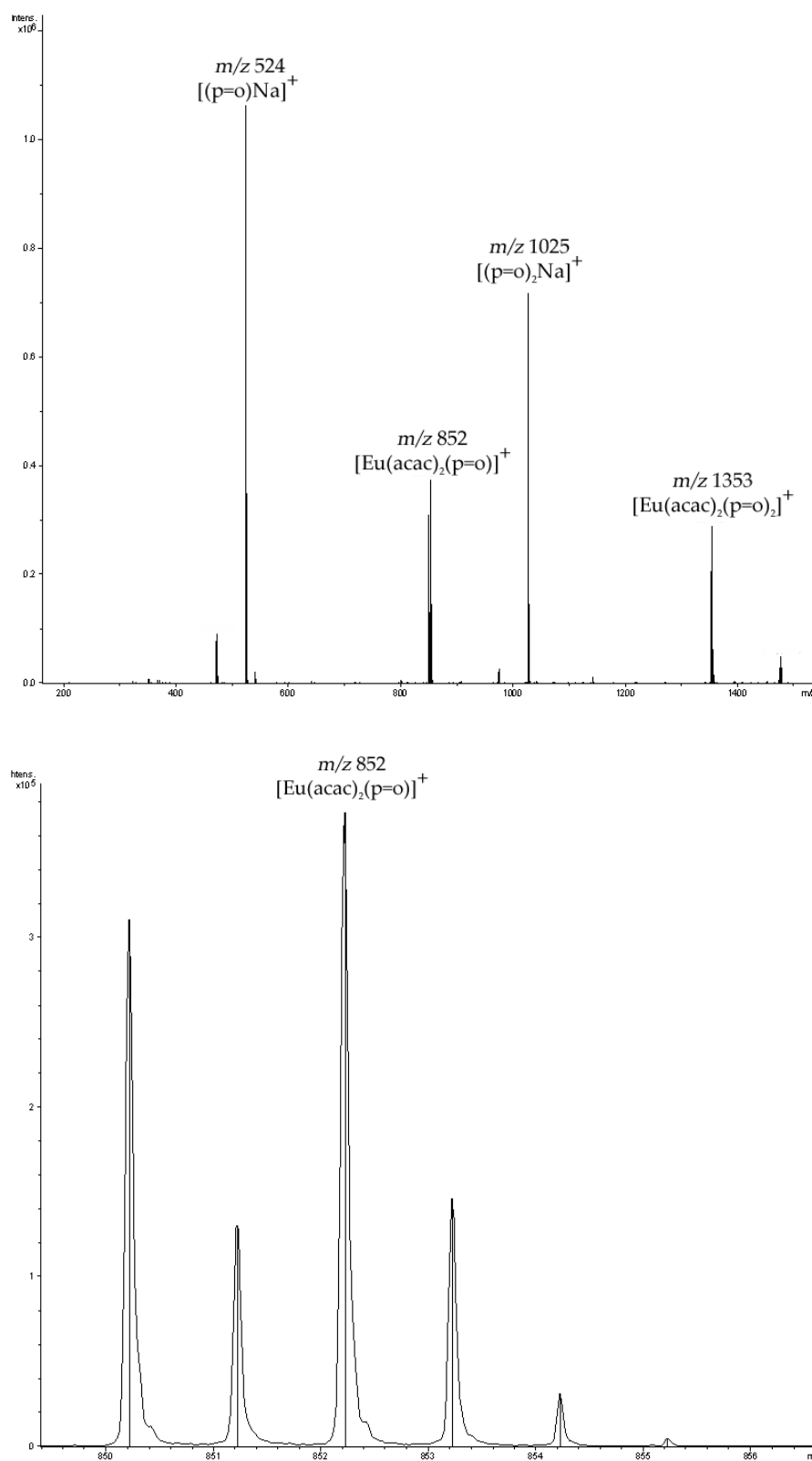


Figure 2.13: ESI mass spectrum of  $\text{Eu}(\text{acac})_3(\text{p}=\text{o})$ , with isotope pattern of  $[\text{Eu}(\text{acac})_2(\text{p}=\text{o})]^+$  ion.

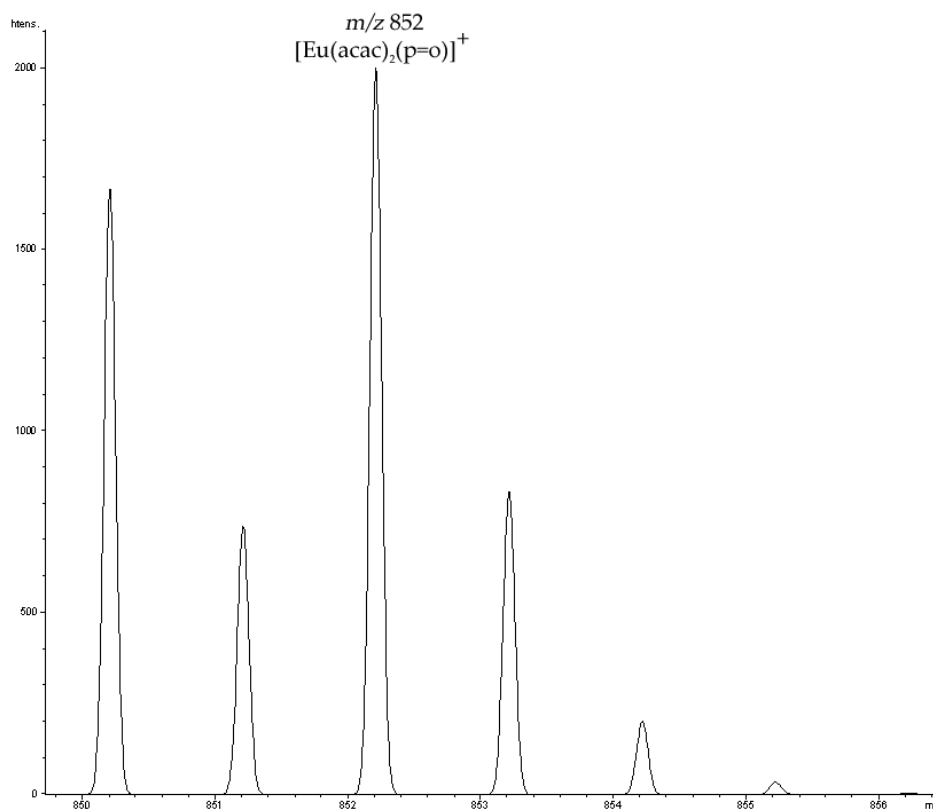


Figure 2.14: Simulated isotope pattern of  $[Eu(acac)_2(p=O)]^+$  ion.

### 2.3.2.2 Nuclear magnetic resonance spectroscopy

$^1H$  and  $^{31}P$  NMR were used for characterisation of the lanthanide compounds. Due to the nature of the lanthanide compounds used in this research, NMR data was at times of low quality, with non uniform results. This is discussed further in the discussion section. The  $^1H$  NMR spectra was similar for most of the compounds, with the main differences arising from the difference between the acac and tta ligands. The  $^{31}P$  NMR was mostly consistent, with a singlet located at *ca.* 27 ppm for the majority of the compounds.

### 2.3.2.3 Infrared spectroscopy

The main purpose of IR spectroscopy was to determine the existence of a P=O stretch on the complexes, which would indicate the presence of the  $(Me)_3CN(CH_2P(O)Ph_2)_2$  ligand on the complexes. A suspected P=O peak at around  $1189\text{ cm}^{-1}$  was present on all complexes.



#### 2.3.2.4 Melting point analysis

The melting point studies were vastly different between compounds containing acac and tta ligands. For all compounds containing acac ligands, a melting point could not be obtained as the compounds turned black and decomposed at certain heats. However, melting points for tta compounds were obtained successfully, and are detailed in Table 2.3.

<u>Compound</u>	<u>Melting point (°C)</u>
La(tta) <sub>3</sub> (p=O)	128.1 - 135.3
Eu(tta) <sub>3</sub> (p=O)	166.8 - 170.9
Tb(tta) <sub>3</sub> (p=O)	155.1 - 159.3

*Table 2.3: Melting points of Ln(tta)<sub>3</sub>(p=O) compounds.*

#### 2.3.2.5 Elemental analysis

Samples of each compound were also submitted to the University of Otago for elemental analysis. Theoretical calculations of elemental compositions are shown in Table 2.4, with the experimental elemental compositions in brackets next to theoretical values.

	<u>Carbon</u>	<u>Hydrogen</u>	<u>Nitrogen</u>
La(acac) <sub>3</sub> (p=O)	57.62% (54.10%)	5.81% (6.06%)	1.49% (1.49%)
Eu(acac) <sub>3</sub> (p=O)	56.82% (52.50%)	5.73% (5.53%)	1.47% (1.48%)
Tb(acac) <sub>3</sub> (p=O)	56.41% (46.33%)	5.69% (5.53%)	1.46% (0.64%)
La(tta) <sub>3</sub> (p=O)	49.73% (50.81%)	3.48% (3.83%)	1.07% (1.78%)
Eu(tta) <sub>3</sub> (p=O)	49.24% (49.31%)	3.45% (3.51%)	1.06% (1.11%)
Tb(tta) <sub>3</sub> (p=O)	48.98% (48.87%)	3.43% (3.45%)	1.06% (1.10%)

Table 2.4: Table of elemental compositions of synthesised Ln( $\beta$ -diketonate)<sub>3</sub>(p=O) compounds, with experimental values in brackets to the right of the theoretical values.

## 2.4 Discussion

### 2.4.1 Analysis of data for (Me)<sub>3</sub>CN(CH<sub>2</sub>P(O)Ph<sub>2</sub>)<sub>2</sub>

Synthesis of an aminobis(methylphosphine oxide) ligand, followed by a series of lanthanide complexes were attempted through use of literature methods. The (Me)<sub>3</sub>CN(CH<sub>2</sub>P(O)Ph<sub>2</sub>)<sub>2</sub> ligand was characterised through comparing experimental IR, NMR and melting point data with literature data of the compound MeN(CH<sub>2</sub>P(O)Ph<sub>2</sub>)<sub>2</sub>. With the structure differing only in that the R group on the nitrogen is a methyl group instead of a *tert*-butyl group, it provided a suitable comparison. ESI mass spectrometry and elemental analysis were also used for characterisation.

The mass spectrum data provided good evidence to suggest the compound had been successfully synthesised. The peak at *m/z* 524 was in high abundance, and indicated the presence of the ligand having formed a complex with a Na<sup>+</sup> ion. This was further supported by the matching theoretical and experimental isotope patterns.

When comparing with the compound  $\text{MeN}(\text{CH}_2\text{P}(\text{O})\text{Ph}_2)_2$ , the  $^{31}\text{P}$  NMR and IR data were also positive. Experimental  $^{31}\text{P}$  NMR data gave a singlet peak at 27.8 ppm, while the comparison compound had a singlet at 29.8 ppm. Experimental IR data gave a notable  $\text{P}=\text{O}$  stretch at  $1196\text{ cm}^{-1}$  which was similar to the comparison data of  $1189\text{ cm}^{-1}$ .  $^1\text{H}$  NMR data appeared to also agree with literature data. The literature data details a singlet at 2.62 ppm resulting from the methyl group on the nitrogen, however due to the *tert*-butyl group on the synthesised phosphine a peak at 0.99 ppm was observed instead. The peak was further upfield as there was less electron deshielding from the nitrogen. Furthermore two small peaks were observed slightly down field of the 0.99 ppm peak, due to long range coupling effects. The other peaks observed coincided with the literature data, a peak at 3.9 ppm from the  $\text{CH}_2$  groups, and a multiplet of peaks from 7.3 - 7.7 ppm from the phenyl rings on the phosphorus. A solvent peak for  $\text{CDCl}_3$  was also observed at 7.26 ppm. There was sufficient agreement between experimental and comparison data from elemental analysis, along with promising ESI-MS data to conclude that the synthesis had been successful, and enough evidence to progress with synthesis of the lanthanide complexes utilising the newly synthesised ligand.

#### 2.4.2 Analysis of data for lanthanide compounds

While ESI-MS, IR and elemental analysis provide robust methods for determining structural information, due to the nature of these complexes NMR data can be unreliable. Similar to the compound  $\text{Eu}(\text{fod})_3$ , the europium and terbium complexes in this research have NMR shift reagent properties, which gives alters the expected chemical shift in the NMR spectra. Furthermore, their quick relaxation times give a small FID pulse

which negatively impacts the signal to noise ratio of the signal. Because of these effects, quality spectra for  $\text{Tb}(\text{acac})_3(\text{p}=\text{o})$  and  $\text{Tb}(\text{tta})_3(\text{p}=\text{o})$  were unobtainable, and peaks in the  $\text{Eu}(\text{acac})_3(\text{p}=\text{o})$  and  $\text{Eu}(\text{tta})_3(\text{p}=\text{o})$  were not properly resolved.

The ESI-MS provided supporting evidence that all compounds had been successfully synthesised. Several ions were common on all spectra, notably  $[\text{Ln}(\beta\text{-diketonate})_2(\text{p}=\text{o})]^+$  and  $[\text{Ln}(\beta\text{-diketonate})_2(\text{p}=\text{o})_2]^+$  ions. As the spectra were taken under positive ion mode, the dissociation of a negatively charged  $\beta$ -diketonate was a dominant mechanism in the electrospray process. In all cases the experimental isotope pattern matched that of the theoretical one, giving good evidence in favour of successful synthesis.

The  $^1\text{H}$  NMR spectrum of  $\text{Eu}(\text{acac})_3(\text{p}=\text{o})$  shows several singlet peaks between 1 and 2 ppm, one of which is a broad peak. These peaks result from the methyl groups on  $(\text{Me})_3\text{CN}(\text{CH}_2\text{P}(\text{O})\text{Ph}_2)_2$  and acac ligands. The broad peak is likely unresolved due to the poor FID pulse obtained when running scans. The singlet at 4 ppm is due to the  $\text{CH}_2$  groups from the phosphine oxide ligand, and has been shifted downfield due to deshielding from the electronegative nitrogen atom. The two broad peaks around 7.4 - 7.8 ppm are likely unresolved multiplets from the phenyl groups on the phosphine oxide ligand.

$^{31}\text{P}$  NMR of all complexes gave a shift similar to that of the free phosphine oxide ligand, around 28 ppm. Literature shows that phosphine oxide complexes of lanthanides and actinides results in a  $^{31}\text{P}$  NMR shift similar to that of the free ligand, which was a positive indication for successful compound synthesis. The exception to this was the  $^{31}\text{P}$  NMR shift of

$\text{Eu}(\text{tta})_3(\text{p}=\text{o})$ , which after repeated experiments was observed around -70 ppm. This was a significant anomaly, and can be attributed to the unpredictable behaviour of the compound under NMR conditions.

IR spectra of the compounds were all relatively consistent, with a peak around  $1189\text{ cm}^{-1}$  in all spectra, arising from the  $\text{P}=\text{O}$  stretch in the aminobis(methylphosphine oxide) ligand. Peaks were also present around  $1600\text{ cm}^{-1}$ , due to the  $\text{C}=\text{O}$  stretch from the  $\beta$ -diketonate ligands on the complexes. While theoretical and experimental data was in good consensus for the  $\text{Ln}(\text{tta})_3(\text{p}=\text{o})$  compounds, agreement was notably poorer for the  $\text{Ln}(\text{acac})_3(\text{p}=\text{o})$  compounds.

## 2.5 Chapter summary

A novel ligand,  $(\text{Me})_3\text{CN}(\text{CH}_2\text{P}(\text{O})\text{Ph}_2)_2$  was synthesised and then characterised by a range of techniques. Once sufficient evidence was gained that the synthesis was successful, the ligand was used to synthesise a range of novel lanthanide  $\beta$ -diketonate complexes, consisting of acetylacetone (acac) and thenoyltrifluoroacetone (tta)  $\beta$ -diketonate ligands. These compounds were also characterised by a range of methods. Through investigation and assessment of data obtained from the characterisation process, it was determined that the compounds were successfully synthesised.

### **3 Structure and particle character of talcum and fingerprinting powders**

#### **3.1 Introduction**

##### **3.1.1 Structure and composition of talc**

Many of the earliest methods of print exposure involve use of fine powders, with the exposure occurring through adhesion of the fine particulates to the lipid component of the print. Simple household talcum powder has proven to give reasonable print definition through a simple soft brushing application, and is contained in some fingerprint powder formulations<sup>[39]</sup>. Due to the different locations and processes of mining, not all talc minerals are identical, however many generalisations can be made about the crystal structure. Electron micrograph studies show that talc has a layered type crystal structure<sup>[40]</sup>.

Talc is a silicate mineral of the formula  $\text{Mg}_3\text{Si}_4\text{O}_{10}(\text{OH})_2$ . In its powdered form (referred to as talcum powder) it is a loose white particulate with many applications, such as cosmetics and lubricants. For the purpose of this research talcum powder provides a useful matrix for dispersion of luminescent lanthanide complexes, which can then be applied to latent prints and screened for effectiveness. Talcum powder is cheap, with a large surface area, and its perfect basal cleavage<sup>[40]</sup> makes it a smooth flowing powder that is easy to manipulate. Furthermore, talc is considered a non toxic substance and is commercially available to the public. There has been research claiming a relationship between talc inhalation and certain types of cancer<sup>[41]</sup>, however no solid link has yet been proven<sup>[42]</sup>.

Through processing of talcum powder, the particle size and morphology can be altered. Traditional methods utilising a ball mill show an increase

in specific surface area and decrease in particle size of the talcum powder<sup>[43]</sup>. More recent studies have shown that through sonication of talc particles over set lengths of time, the particle size can be reduced to submicron levels<sup>[8]</sup>. Sonication in an acid medium has also proved useful in processing talc into a nano-scale substance<sup>[44]</sup>. In the case of a fingerprinting powder, theoretically the smaller the particle size the better, as smaller particles will give greater resolution of a latent print.

### **3.1.2 Physical makeup of fingerprinting powders**

There is a great variety of print exposing powders available for crime scene investigators. To accommodate the unpredictability of a crime scene, powders with different characteristics are developed to suit different situations. Coloured powders such as white, black and aluminium powders give colour contrast in general dusting situations. Magnetic powders consist of a large portion (typically around 95%) of iron powder, with the remainder made up using a dyed polymer<sup>[7]</sup>. The powders are applied to a print, with excess powder removed using a magnet. This leaves a well resolved print with little excess print powder. Fluorescent printing powders are made up of mostly of an extender (80%) with a fluorescent polymer (20%)<sup>[7]</sup>. The benefits of fluorescent powders are that when exposed to UV excitation, they greatly increase in visibility, and can give high visibility on coloured backgrounds.

### **3.1.3 Use of laser diffraction and SEM for analysis of particle size and morphology**

Common instruments for determining particle size of a substance (such as the Malvern Mastersizer) utilise laser diffraction as a method for analysis. Laser diffraction works by using the theory that the angle at which the particles diffract the laser correlates to the particle size. The common laser

diffraction instrument utilises a set wavelength laser, and a detector that can measure the angles and intensities of the diffracted light pattern. Instruments can use both Mie solution and the Fraunhofer approximation as models on which to calculate the particle size distribution from the light scattering pattern<sup>[45]</sup>.

Laser diffraction techniques have proven to be useful due to their ability to give a quick and straightforward particle size distribution of a sample<sup>[46]</sup>. They can also determine other useful data from samples, such as specific surface area. Due to their efficiency they have become useful for determining the particle size of soil samples, with several literature publications on the subject<sup>[46-47]</sup>. Laser diffraction has proven to have a wide variety of applications, including particle size analysis of pigments in inks<sup>[48]</sup> and lactose powders<sup>[49]</sup>. It has also been used for determining median particle size and size distribution of fingerprinting powders<sup>[50]</sup>.

Scanning Electron Microscopy (SEM) is a highly useful technique for analysing the morphology of particles. This information is derived from the signals produced by interactions of an electron beam with the atoms in the sample. Electron beams are typically produced by a tungsten or LaB<sub>6</sub> filament. On interaction of the electron beam with the atoms in the sample, secondary electrons and back scattered electrons are produced<sup>[51]</sup>. These are recorded by a detector, which converts the information into a monochrome image of the sample.

Use of SEM for analysis of surface and particle morphology is abundant in the literature. The high quality images provide excellent information about both size and morphology of different materials. SEM has been used for various areas of research. Examples of these are size and morphology investigation into particles released from power plants<sup>[52]</sup>, volcanic ash surface area measurements<sup>[53]</sup>, and morphology and size investigations of



Eu<sup>3+</sup> phosphor coatings. SEM has also shown use analysing fingerprinting powders, with one paper detailing the use of SEM to visualise the adhesion of different powders to a latent print<sup>[50]</sup>. Several publications utilise SEM for the analysis of particle size and morphology of latent fingerprint visualising powders <sup>[54]</sup>.

Used together, laser diffraction and SEM are complimentary tools for investigation of particle character. Laser diffraction provides quick and accurate information regarding particle size distribution and surface area. However due to the theoretical nature of its mode of operation, data can be misinterpreted with particularly difficult samples. SEM can corroborate data obtained through laser diffraction, by giving a definitive image of a particle and its morphology. Through using both instruments, detailed and accurate information about particles can be obtained.

Through analysis of the particle size and morphology of talcum powder and existing commercial fingerprinting powders, the particle characteristics that are conducive for exposure of latent fingerprints were studied.

## **3.2 Methods**

### **3.2.1 Materials and instrumentation**

Luminescent fingerprinting powders were made through doping a luminescent metal complex onto talcum powder. The talcum powder used was BDH talcum powder, which had been acid purified by the manufacturer. The metal complexes were synthesised in the laboratory as specified in chapter 2 of this thesis. Table 3.1 gives the compounds used for the powders in this chapter.

<u>Compound</u>	<u>Abbreviation</u>
Eu(acac) <sub>3</sub> (phen)	EU1
Eu(acac) <sub>3</sub> (bipy)	EU2
Eu(tta) <sub>3</sub> (phen)	EU3
Eu(tta) <sub>3</sub> (bipy)	EU4
Tb(acac) <sub>3</sub> (phen)	TB1
Tb(acac) <sub>3</sub> (bipy)	TB2
Tb(tta) <sub>3</sub> (phen)	TB3
Tb(tta) <sub>3</sub> (bipy)	TB4

*Table 3.1: Compounds doped in to talcum powder for particle character analysis.*

The commercial samples used for comparison were Greenwop and Redwop, fluorescent green and red powders respectively. These powders were sourced from Aorangi Forensic Supplies Limited. Particle size and morphological analysis of the processed and unprocessed powders were done using a Hitachi S-4700 Scanning Electron Microscope (SEM) and a Malvern Mastersizer.

### **3.2.2 Manufacture of powders**

For doping of the powders, 0.01 mol of the metal complex was added to a suspension of 2 g of talcum powder in 20 mL of dichloromethane. The mixture was then rotary evaporated on a high speed setting until all solvent was removed. The powder was finally ground in a mortar and pestle to remove clumps.

### 3.2.3 Processing of powders

To investigate the influence of particle size and formation on use as a fingerprinting powder, talcum powder was run through a sonication process to manipulate particle morphology. Samples were selected to be run through a sonication process, after which properties were compared through use of instrumentation detailed earlier. Both standard and doped powders were run through the process, to compare whether processing was more effective before or after addition of luminescent metal complex to the powder.

Sonication operates by the use of ultrasonic waves transferred through solution, which buffer and break down particles over time. For the sonication process, 1 g of powder was added to a conical flask, which was filled with 20 mL of water. These were placed in a sonicating bath for 2 - 8 hours. Upon removal the talcum powder was filtered onto fine mesh filter paper, and dried in the oven for 4 hours at 100 °C. Table 3.2 shows which powders were sonicated for the specified times.

<u>Talcum powder</u>	<u>Time sonicated</u>	<u>Doped Talcum powder</u>
Standard	2 hours	EU1
Standard	4 hours	EU3
Standard	6 hours	TB1
Standard	8 hours	TB3

*Table 3.2: Powders and time sonicated.*

### **3.2.4 Evaluation of the adhesion of powders to latent prints**

To investigate the usefulness of the sonicated talcum powder as a matrix for the luminescent materials, the powders were dusted onto fingerprints applied to glass slides. The effectiveness of the powders was judged on the clarity of the print from the talcum powder alone, as opposed to imaging through excitation of a doped luminescent material.

Thumb prints were deposited onto glass slides by rubbing the thumb across the forehead, and pressing them onto the slide. A small amount of the powder (~0.02 g) was then applied to the top of the slide. This was brushed across the print with a soft makeup brush, until the print was adequately exposed with the white talcum powder.

This process was completed with the 2 hour, 4 hour, 6 hour, 8 hour and unsonicated talcum powder, as well as the Greenwop and Redwop powders. The prints were evaluated by viewing the slide against a dark background, with a good light source. Prints were analysed for detail and clarity given by the powder, and whether print detail was obscured.

## **3.3 Results**

### **3.3.1 Mastersizer analysis**

Particle size distributions of talcum powders were measured using a Mastersizer. Samples were added to a stirred water bath until a suitable obscuration of light scattering was reached, at which point readings were taken. Samples were run of talcum powder and talcum powder that had been doped with metal complexes, to investigate any effect the doping process had on particle size. Figure 3.1 shows the particle size distribution of talcum powder.

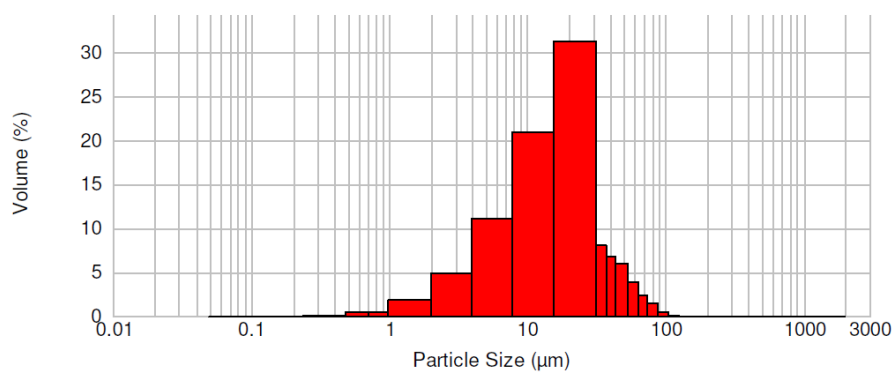


Figure 3.1: Particle size distribution of talcum powder.

Table 3.3 displays the 10<sup>th</sup> percentile, 50<sup>th</sup> percentile and 90<sup>th</sup> percentile particle size in the analysed talcum powders.

<b><u>Sample</u></b>	<b><u>d(0.1) μm</u></b>	<b><u>d(0.5) μm</u></b>	<b><u>d(0.9) μm</u></b>
Talcum powder	4.719	19.842	49.758
EU1	3.743	15.558	44.208
EU2	4.103	17.135	46.633
EU3	3.805	15.470	43.968
EU4	3.725	15.459	43.756
TB1	3.887	15.146	43.391
TB2	3.583	14.348	41.924
TB3	4.997	21.195	51.772
TB4	4.043	16.570	46.159

Table 3.3: Particle sizes of talcum powders.

Analysis of the sonicated samples were also run, with the values shown in Table 3.4.

<u>Sample, time</u> <u>sonicated</u>	<u>d(0.1) <math>\mu\text{m}</math></u>	<u>d(0.5) <math>\mu\text{m}</math></u>	<u>d(0.9) <math>\mu\text{m}</math></u>
Talc powder, 2hr	4.275	16.007	41.549
Talc powder, 4hr	4.225	16.529	42.587
Talc powder, 6hr	4.177	16.271	42.606
Talc powder, 8hr	4.094	15.123	39.479
EU1, 2hr	3.743	13.420	39.762
EU3, 4hr	3.114	11.881	36.110
TB1, 6hr	3.087	11.146	32.391
TB3, 8hr	3.035	10.516	30.522

Table 3.4: Particle sizes of sonicated talcum powders.

From these results, sonication was observed to have a definite reduction on particle size. The size reduction was even greater in the doped powders, possibly due to having been ground in a mortar and pestle following the doping process. Figure 3.2 shows a comparison of standard talcum powder with talcum powder that has been sonicated for 8 hours.

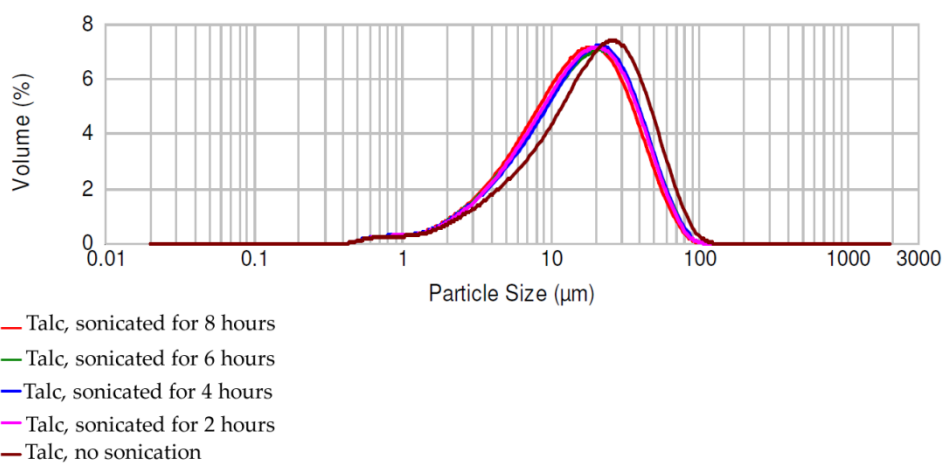


Figure 3.2: Particle size comparison of talcum powder to sonicated talcum powders.

The particle size distribution curve shifts significantly to a smaller distribution of particles. Furthermore, the specific surface area of the unprocessed talcum powder shifted from  $0.609 \text{ m}^2/\text{g}$  to  $0.968 \text{ m}^2/\text{g}$  with 8 hours of sonication. Figures 3.3 and 3.4 show particle size comparisons of the sonicated and non-sonicated EU3 and TB3 talcum powders.

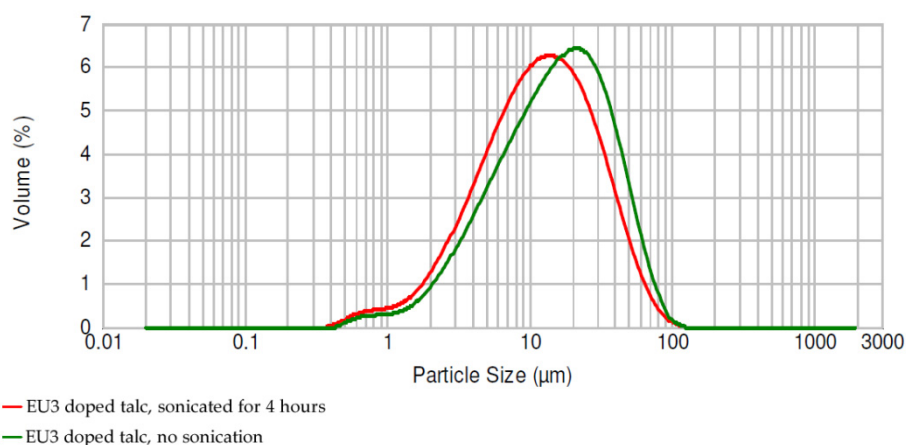


Figure 3.3: Particle size comparison of EU3 talcum powder and 4 hour sonicated EU3 talcum powder.

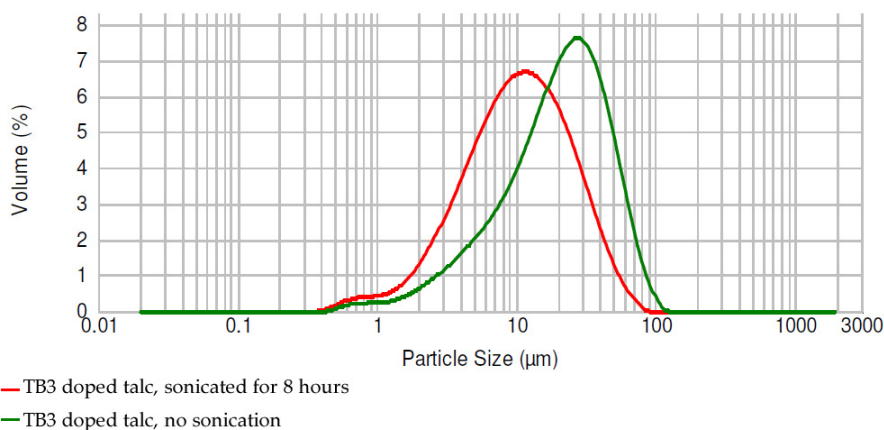
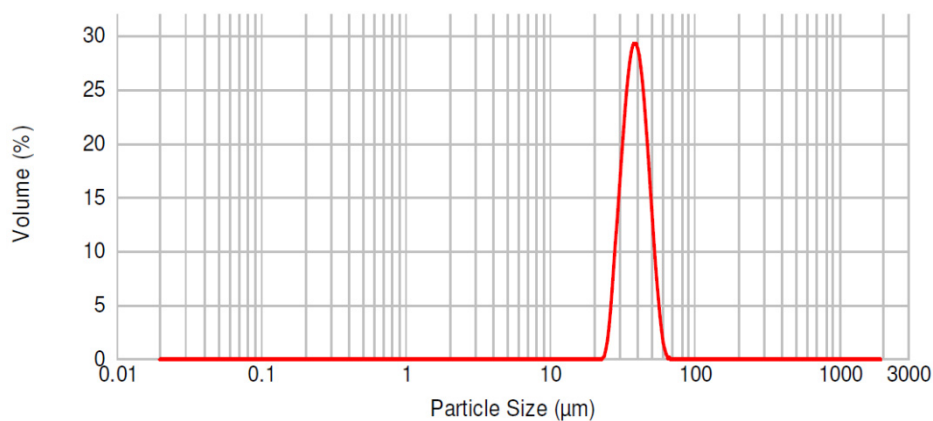


Figure 3.4: Particle size comparison of TB3 talcum powder and 8 hour sonicated TB3 talcum powder.

Both particle distribution curves show distinct shifts to a higher percentage of smaller particle sizes. The change is more noticeable with the TB3 talcum powder, however it should be noted that analysis of this powder pre-sonication gave anomalously larger particle sizes than other

doped talcum powders. Specific surface area also increased, with a shift from  $0.735 \text{ m}^2/\text{g}$  to  $0.917 \text{ m}^2/\text{g}$  in EU3 and  $0.579 \text{ m}^2/\text{g}$  to  $0.968 \text{ m}^2/\text{g}$  in TB3. Figure 3.5 shows the particle size distribution curve of the commercial Greenwop powder.



*Figure 3.5: Particle size distribution of Greenwop powder.*

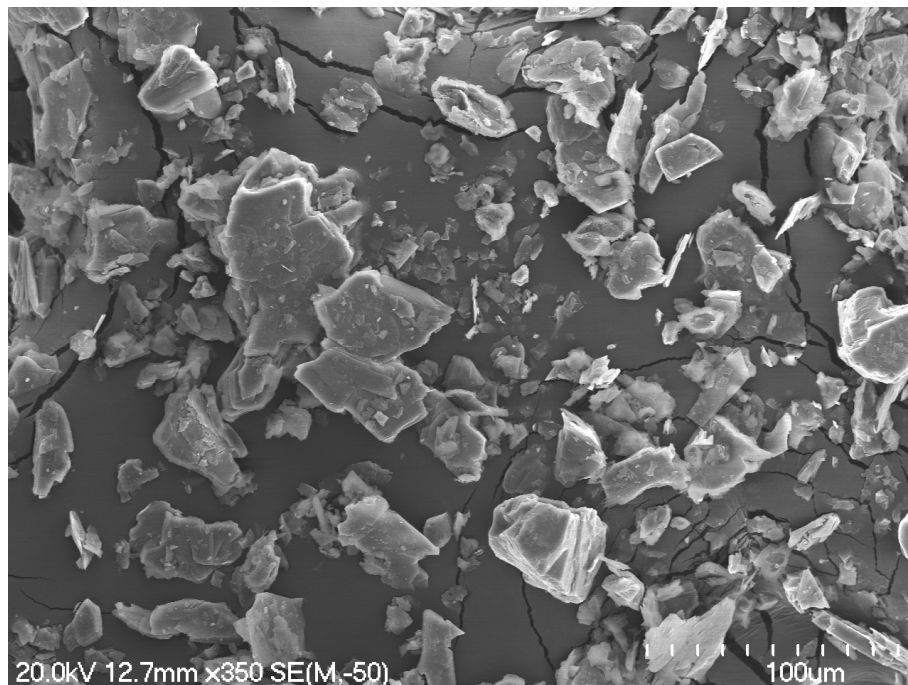
Greenwop was found to have a particle size median of  $38.356 \mu\text{m}$ , which was significantly larger than that of the talcum powders. Also, specific surface area was measured at  $0.159 \text{ m}^2/\text{g}$ , notably smaller in comparison to talcum powder. The distribution curve was a much sharper peak in comparison to the talcum powders, implying a much more homogenous particle size. Analysis of Redwop through use of the Mastersizer proved unsuccessful. Upon reaching an optimum obscuration measurement for analysis, the obscuration increased rapidly giving varying and unreliable data.

### 3.3.2 SEM analysis

To prepare samples for SEM analysis, the powders were applied to an adhesive carbon tape on the sample holder. The samples were then sputtered with platinum, giving an extremely thin coating over the surface of the sample. This is necessary to give electrical conductivity to the compound being analysed, which is necessary for SEM analysis.



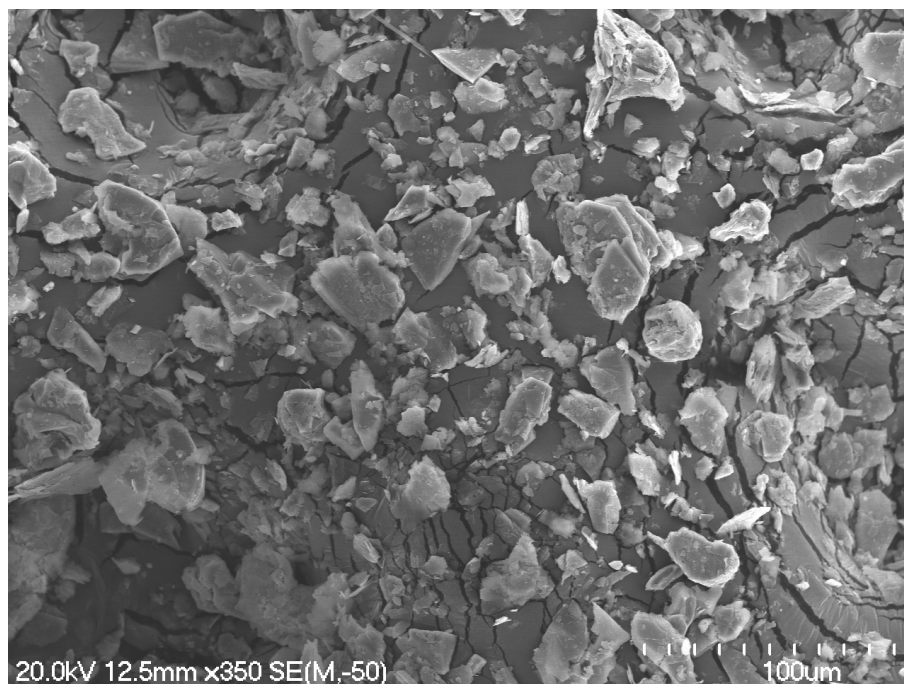
Through SEM analysis, particle size and shape can be analyzed. Selections of samples were used to check agreement with the Mastersizer results. Figure 3.6 shows a SEM image of talcum powder.



*Figure 3.6: SEM image of talcum powder.*

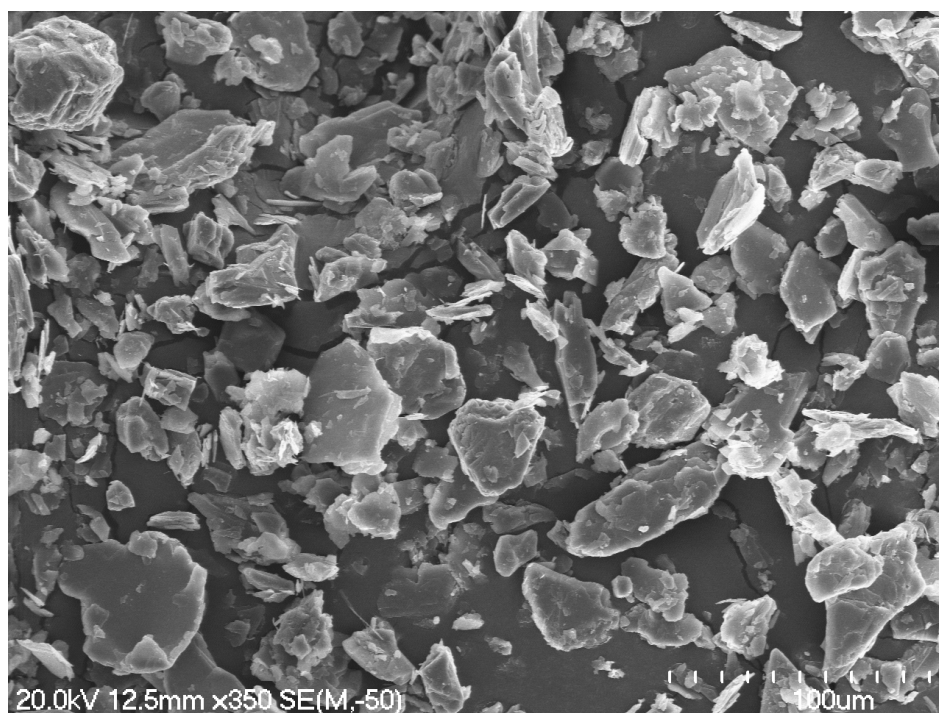
Using the grading on the image, particles of various sizes are observed with many around the 15 - 20  $\mu\text{m}$  size. The characteristic flaky, layered morphology of the talc particles is also present.

Images of the doped talcum powders were also taken using SEM. As suggested by the Mastersizer data, there is no significant difference in particle size observed after the doping procedure has taken place. The image also shows that the morphology remains unchanged. Figure 3.7 shows a SEM micrograph of talcum powder doped with EU3.

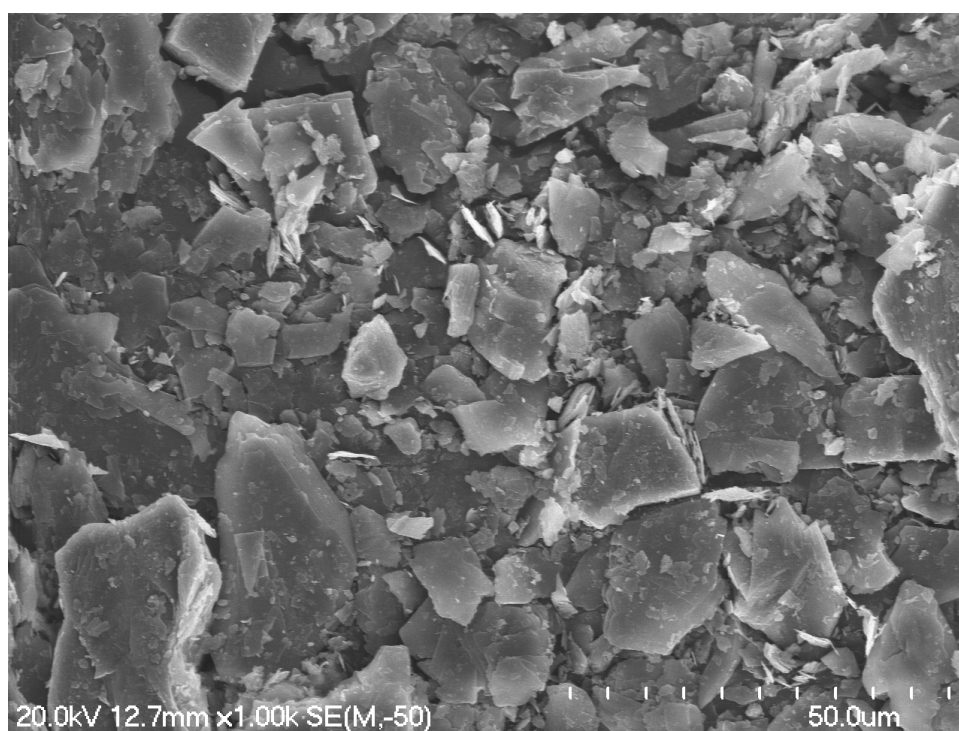


*Figure 3.7: SEM image of talcum powder doped with  $\text{Eu}(\text{tta})_3(\text{phen})$ .*

Sonicated talcum powders were also analysed using SEM. The micrographs reinforced the data taken from the Mastersizer readings, and also displayed that there was no notable effect on particle morphology. Figures 3.8 and 3.9 show SEM images of talcum powder that had been sonicated for 8 hours, and talcum powder doped with  $\text{Eu}(\text{tta})_3(\text{phen})$  that had been sonicated for 4 hours.



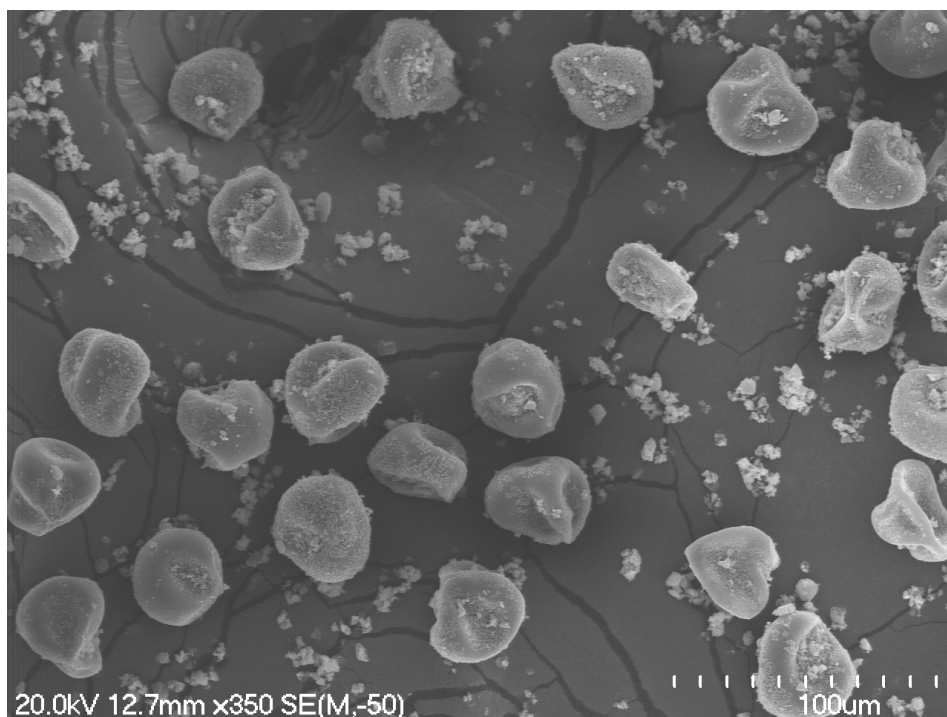
*Figure 3.8: SEM image of talcum powder sonicated for 8 hours.*



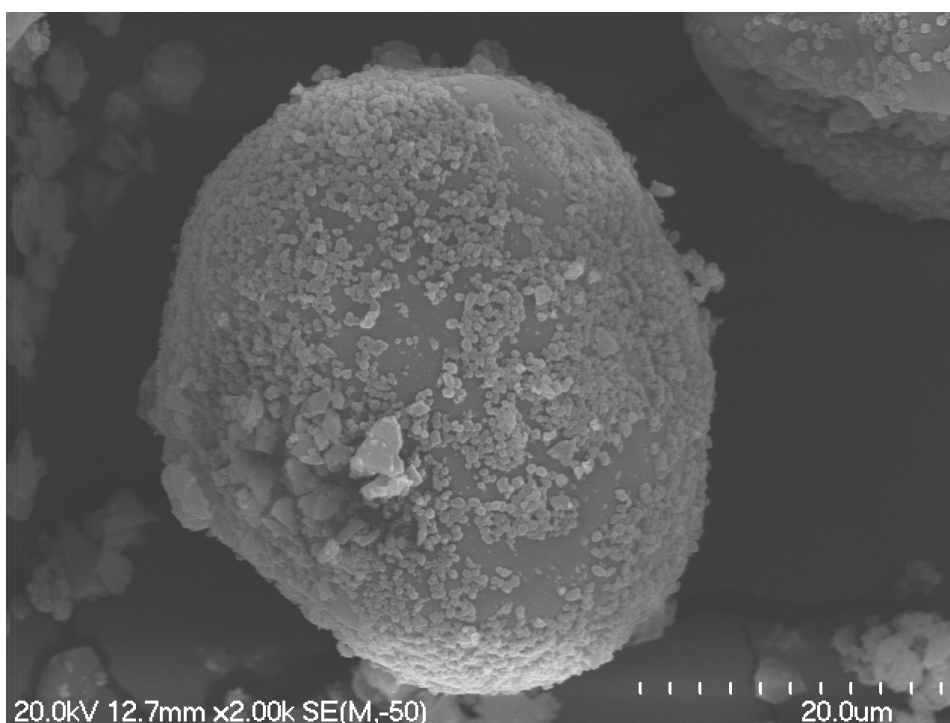
*Figure 3.9: SEM image of talcum powder doped with  $\text{Eu}(\text{tta})_3(\text{phen})$ , sonicated for 4 hours.*

SEM images were taken of the commercial Greenwop and Redwop powders to investigate their particle size and morphology. Figure 3.10

shows a SEM image of Greenwop at 350x zoom, and Figure 3.11 shows a Greenwop particle at 2000x zoom.

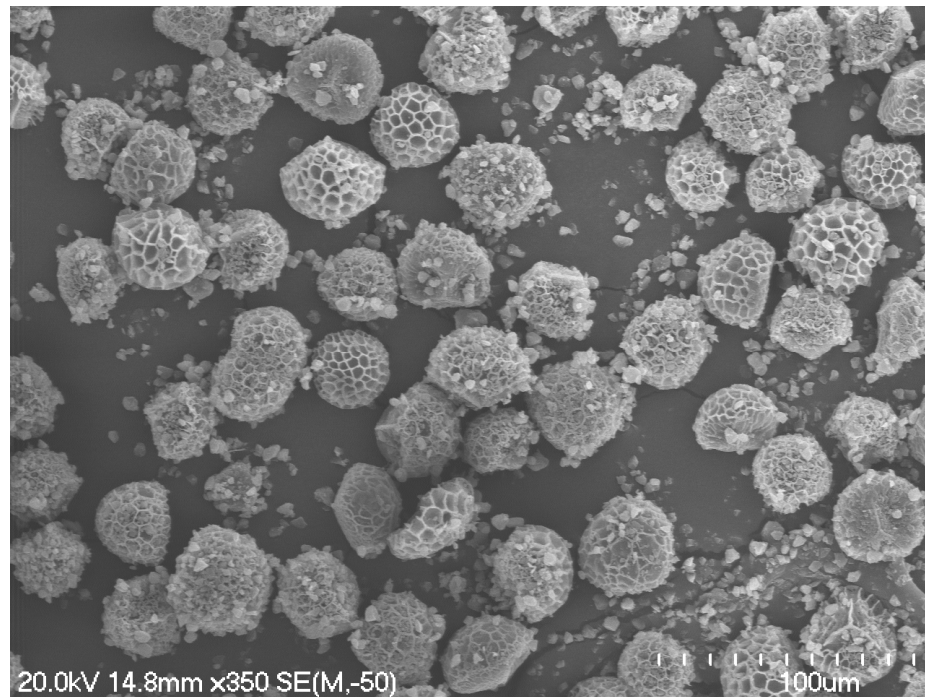


*Figure 3.10: SEM image of Greenwop at 350x magnification.*

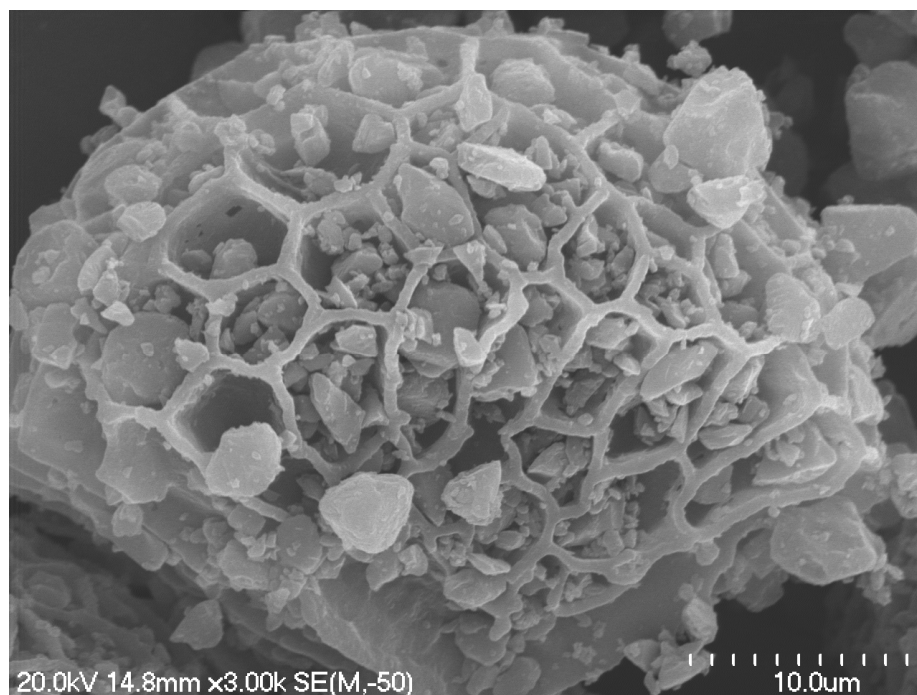


*Figure 3.11: SEM image of a Greenwop particle at 2000x magnification.*

From these images, it was observed that Greenwop consists of particles ~40 microns in size, which are host to a material of much smaller size (1 - 10 microns). Figures 3.12 and 3.13 show SEM images of Redwop at 350x magnification, and 3000x magnification.



*Figure 3.12: SEM image of Redwop at 350x magnification.*



*Figure 3.13: SEM image of Redwop at 3000x magnification.*



These images displayed particles  $\sim 30\ \mu\text{m}$  in size of a honeycomb like structure. Similar to Greenwop, these particles are host to a substance of much smaller size, again of around  $1 - 10\ \mu\text{m}$ .

### 3.3.3 Powder adhesion analysis

All talcum powders when applied to the slide gave clear exposure of the print, with a faint white colour. The Greenwop and Redwop gave clear exposure with strong green and red colours, respectively. Figure 3.14 shows the prints exposed on glass slides by the respective powders.

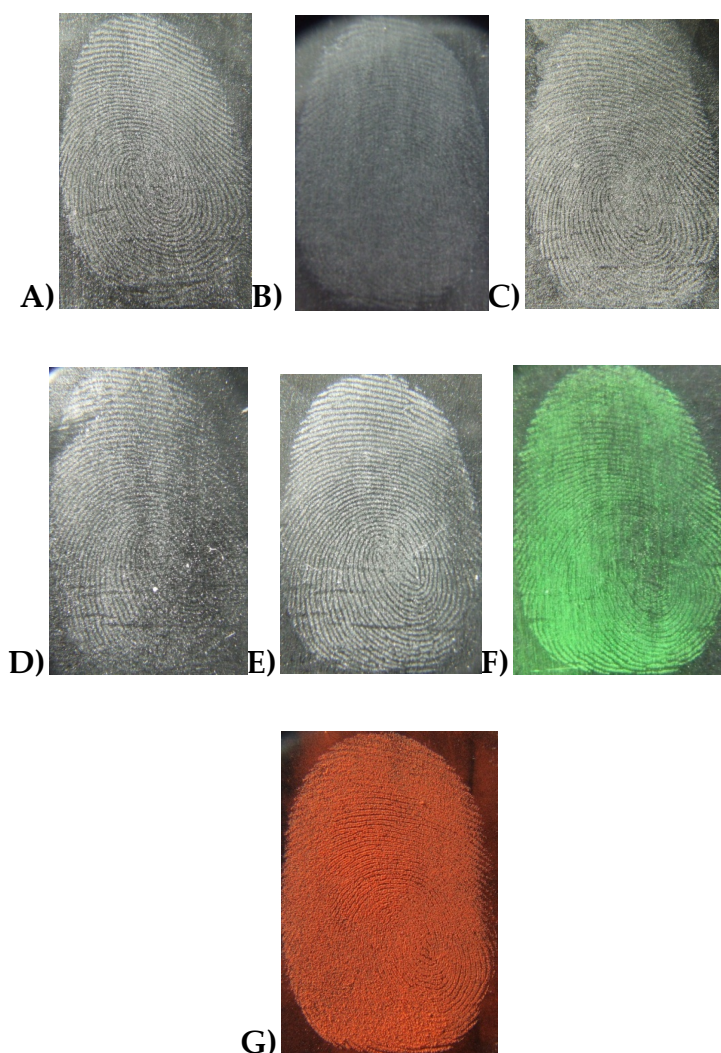


Figure 3.14: Fingerprints exposed by talcum and “wop” powders. From left to right, top to bottom: A) unmodified talcum powder B) 2 hour sonicated, C) 4 hour sonicated D) 6 hour sonicated E) 8 hour sonicated F) Greenwop G) Redwop.

Because there is no way to definitively quantify the quality of a print, the adhesiveness of the powders was evaluated through a subjective analysis by observation. This is discussed further in chapter 5. It was considered that some bias may be introduced when observing the quality of the prints. This bias is introduced through an expectation of the performance of the powders, based on the hypothesis of the effects of manipulating the powders. To overcome this, decisions on print quality were discussed with a PhD student in the laboratory, who was uninformed on the conditions on which the prints were taken. Furthermore, replicate prints were not made, as this experiment was just a trial to investigate observable benefits of the sonication procedure.

It was concluded that the clarity of the prints was not notably influenced by length of time they had been sonicated. The powders behaved similarly when being brushed, and investigation of fine detail in the print did not appear to be noticeably superior when using sonicated powders.

## **3.4 Discussion**

### **3.4.1 Particle size and morphology of talcum powder and doped talcum powders**

Initial Mastersizer experiments indicated that basic talcum powder had a median particle size of  $\sim 19\text{ }\mu\text{m}$ , with a notable distribution. In comparison, the doped talcum powders had particle sizes of  $\sim 15\text{ }\mu\text{m}$ . This was most likely due to the doping process itself, which involved grinding of the powder in a mortar and pestle after removal of the solvent. This likely gave a mechanical breakdown of talc particles. SEM imaging backed up this data, as a range of agreeable particle sizes were observed in the

images. Furthermore the typical talc particle morphology was observed to be unaffected by addition of the metal complex.

Sonicated powders also showed a notable reduction in particle size. Size reduction was more notable in doped talcum powders; again this could be attributed to the mechanical grinding following the doping procedure. Comparison of sonicated talcum powders to standard talcum powders showed a distinct reduction of around 3 microns in the median particle size. Specific surface area also showed an increase after sonication of the talcum powders. Similar to the doping procedure, SEM imaging reinforced the particle size data, while displaying no distinct change in morphology after sonication.

#### **3.4.2 Particle size and morphology of commercial fingerprinting powders**

Initial analysis of the commercial Greenwop powder suggested a much larger median particle size than the talcum powder, but with much more homogeneous size dispersion. Specific surface area was also measured to be significantly smaller than that of talcum powder. However analysis of the particles by SEM indicated these results were unreliable. While the Greenwop powder does consist of homogeneously dispersed particles of around 40  $\mu\text{m}$  in size, these particles are host to a substance of much smaller particle size ( $\sim 1 - 2 \mu\text{m}$ ). It was hypothesised that the larger particles act as a vessel for the smaller, and disperse them as they are brushed across a latent fingerprint. As the smaller particles adhere to the print, the larger particles are removed by the brushing action. This would allow for an even dispersion of the smaller particles without overloading the latent print.



The Redwop powder did not give any reliable results in the Mastersizer, as the obscuration readings fluctuated erratically. SEM analysis showed the powder consisted of honeycomb structured particles around 30  $\mu\text{m}$  in size. These honeycomb structures were packed full of smaller particles, similar to what was observed with Greenwop. A similar mode of action was proposed, with the smaller particles being released upon application to a latent print. SEM images showed both empty and full honeycomb particles. Ideally the smaller particles would be released from the honeycomb structured particle on reaction with the components of a latent fingerprint.

Two online retail sources state that the Greenwop and Redwop powders are made up of a lycopodium base. Plants of the lycopodium genus produce spores<sup>[55]</sup>, which are used to make up lycopodium powder. Lycopodium powder has proven useful as a lubricating dust on latex products<sup>[56]</sup>, a characteristic similar to talcum powder. Literature publications containing SEM images of lycopodium spores back up the information that the Greenwop and Redwop powders are based on these spores<sup>[57]</sup>.

The doping of talcum powder with lanthanide metal complexes was successful in creating a luminescent powder, and subsequent sonication gave a useful method for reduction of median particle size and increase in specific surface area. However in comparison to commercial powders, talcum powder was lacking in certain areas. The commercial powders have been specifically engineered for application to a latent print, using larger particles as a system for applying optimum quantities of smaller particles to the print in question, giving excellent resolution. Furthermore particle size was much more homogenous, meaning the powders give much more reproducible image exposure. Size distribution curves of the

talcum powders show a much wider array of particle sizes, indicating that the powders may not always behave the same (possibly due to an atypically large particle obscuring print detail).

### **3.4.3 Effect of particle size on effectiveness of talcum powder print exposure**

While SEM and Mastersizer analysis determined that sonication did reduce particle size, use and observation of the powders on a glass surface indicated that there was no notable improvement with smaller particle powders. A greater reduction in particle size could perhaps result in a powder with improved print exposure character, however from these trials it was observed that the time required for particle size reduction is inefficient, as the unprocessed powder appears to give equal clarity prints.

## **3.5 Chapter Summary**

Talcum powder was doped with luminescent metal complexes, and was processed using sonication for specified lengths of time. Transmission electron microscopy and laser diffraction analysis were used to determine a reduction in particle size and an increase in specific surface area of the talcum powder, correlating to the length of time that the powders were sonicated. These techniques were also used to compare the talcum powder to commercial print powder. While laser diffraction could not give reliable data on particle size, a much more homogenous distribution of particle size was seen in commercial powders compared to the talcum powders. SEM showed a unique construction of the commercial powders, which differed greatly from the talc particles.

The sonicated talcum powders were evaluated through exposure of a thumb print on a glass slide. Through observation of the prints, it was determined that the smaller particle powders did not have any noticeable

effect on increasing the clarity of the prints. It was concluded that the time required for reducing particle size was undesirable, as the unprocessed powder gave suitable print adhesion and clarity to use as a matrix for the luminescent metal compounds.

## 4 Lanthanide Luminescence

### 4.1 Introduction

The  $[\text{Xe}]4f^n$  electronic configuration of trivalent lanthanide ions gives numerous electronic levels, which provides several spectroscopic properties worthy of investigation. These unique optical properties have resulted in a vast interest in the luminescence that occurs in lanthanide(III) ions, with much research having been undertaken to understand the mechanisms that cause these characteristic energy phenomena.

The IUPAC definition of luminescence is “Spontaneous emission of radiation from an electronically or vibrationally excited species not in thermal equilibrium with its environment”<sup>[58]</sup> This thesis will focus on photoluminescence, specifically the excitation of trivalent lanthanide compounds through the absorption of ultra-violet (UV) light. Through the use of a Jablonski diagram (Figure 4.1), the electronic states of a molecule excited by light absorption can be illustrated.

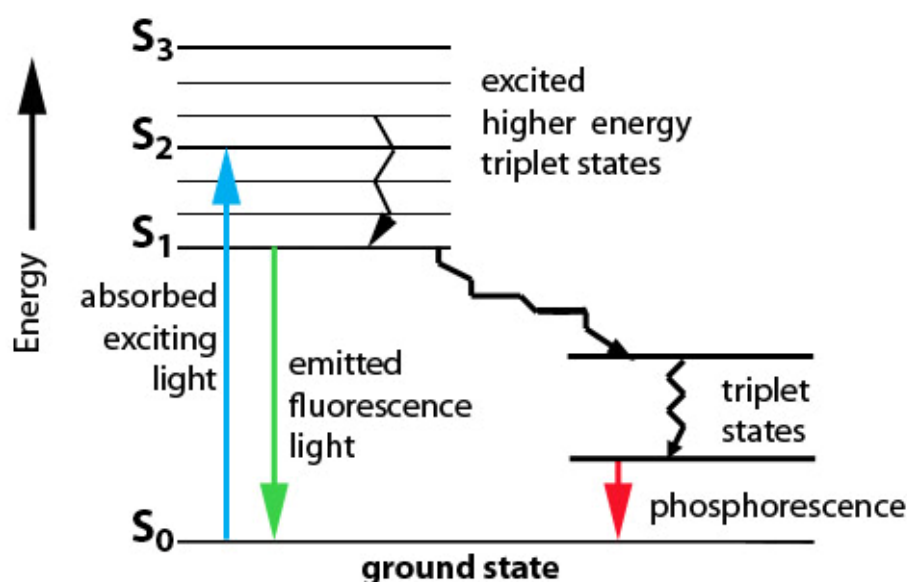


Figure 4.1: Jablonski diagram showing energy transfers and electronic states of a molecule<sup>[59]</sup>.

Through the absorption of light (e.g. UV) the molecule is raised to an excited singlet state from the ground state. Through radiative and non-radiative transitions, the molecule returns to the ground state. The radiative transition is what is observed as fluorescence, while the non-radiative can be various things, such as heat or internal conversion. In the case of the non-radiative process of intersystem crossing, absorbed energy is promoted to a higher triplet state. The triplet state contains “forbidden” energy transitions that are kinetically unfavoured, causing a time delay in the luminescence emission. This process is known as phosphorescence.

#### 4.1.1 Factors influencing luminescent intensity

An important property which determines the emissive strength of a lanthanide(III) ion is the non-radiative deactivation paths. These paths close the energy gap between the emissive state and highest sublevel of the lanthanide(III) ion ground multiplet, as energy is lost through high energy vibrations (such as O-H) in the ligand. As can be observed in the diagram below (Figure 4.2), europium, terbium and gadolinium ions have the largest energy gap making them ideal for use in luminescence applications.

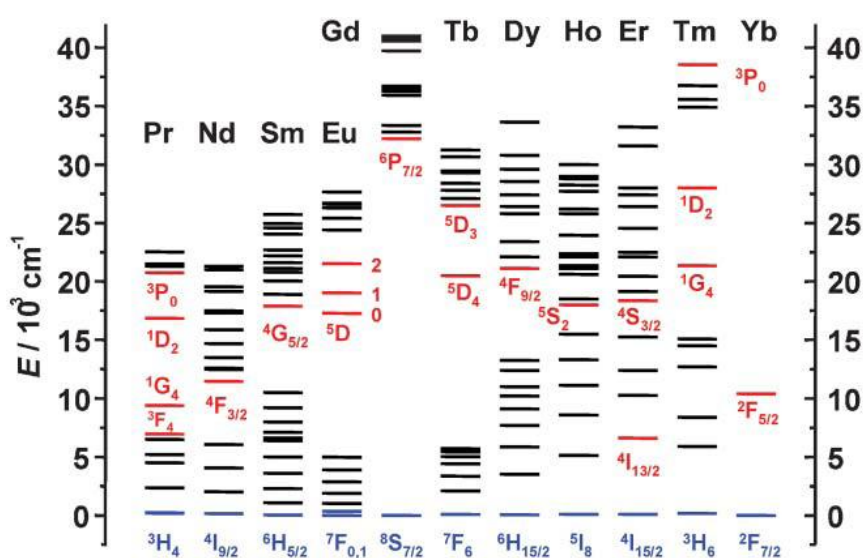


Figure 4.2: Main luminescent levels (red) and fundamental levels of lanthanide(III) ions<sup>[60]</sup>.

Some lanthanide(III) ions, most notably  $\text{Eu}^{3+}$  and  $\text{Tb}^{3+}$  have excited states with lower energy than the triplet states of common ligands. As a result, these ions give strong metal-ion fluorescence, which makes them ideal for luminescence applications. The dominant emissions that give the strong fluorescence are  $^5\text{D}_4 \rightarrow ^7\text{F}_5$  and  $^5\text{D}_0 \rightarrow ^7\text{F}_n$  (where  $n = 0 - 2$ ) for  $\text{Tb}^{3+}$  and  $\text{Eu}^{3+}$  respectively<sup>[15]</sup>.

Laporte selection rules forbid transitions between states of the same  $f^n$  configuration, giving weak absorbance spectra in lanthanide(III) ions. Due to the weak  $f$  orbital-ligand interaction, these transitions have weak intensities. This is in contrast to the strong  $d$  orbital-ligand transitions seen in transition metal compounds, which gives the compounds their characteristic intense colours. While ligand interactions relax this selection rule, oscillator strength and absorbance spectra are still weak for this interaction. This can be resolved through use of an antenna chromophore in the ligand, which absorbs strongly at a specific wavelength and transfers this energy to the metal ion, raising it to a suitable energy for an emission state<sup>[61]</sup>. Ideal compounds for use as these antenna chromophores are  $\beta$ -diketonate ligands. These conjugated compounds can strongly absorb UV light and transfer the energy to the lanthanide ion quickly, due to their direct coordination<sup>[62]</sup>. This phenomenon is known as luminescence sensitisation or the “antenna effect”, which can be explained through a modification of the Jablonski diagram (Figure 4.3).

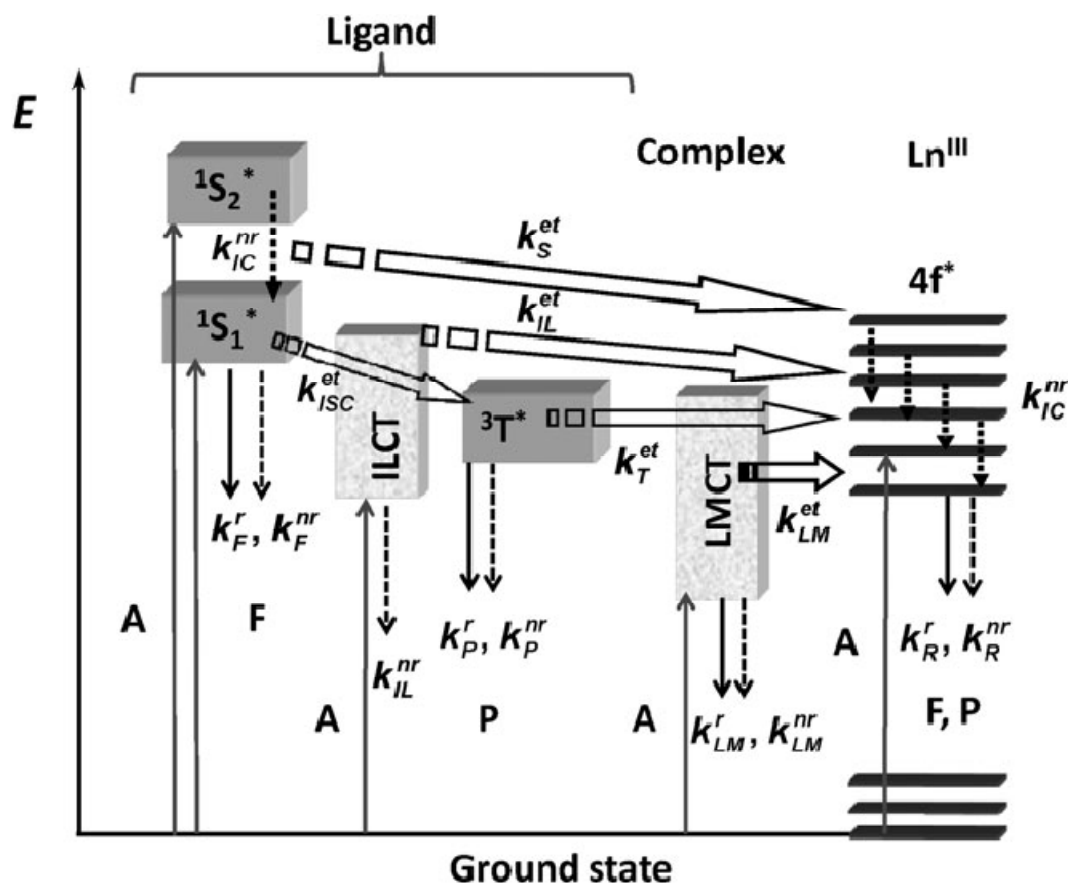


Figure 4.3: Modified Jablonski diagram displaying luminescence sensitisation through ligand interaction<sup>[63]</sup>.  $1S^*$  or  $S$  = singlet state,  $3T^*$  or  $T$  = triplet state,  $A$  = absorption,  $F$  = fluorescence,  $P$  = phosphorescence,  $k$  = rate constant,  $r$  = radiative,  $nr$  = non-radiative,  $IC$  = internal conversion,  $ISC$  = intersystem crossing,  $ILCT$  (indices  $IL$ ) = intraligand charge transfer,  $LMCT$  (indices  $LM$ ) = ligand-to-metal charge transfer.

In Figure 4.3, the solid arrows show absorption, emission and transfer of energy while the dotted arrows represent dissipation of energy in the lanthanide complex. Figure 4.3 shows the absorption of energy and promotion of the molecule to the singlet state as explained previously in the chapter, but with the addition of ligand absorption pathways (observed as intra-ligand charge transfer and ligand-to-metal charge transfer). These additional absorptions and transfers of energy to the lanthanide(III) ion result in greater fluorescent and phosphorescent emissions.

Recent publications have further investigated the design of luminescent lanthanide compounds. Several factors for influencing the luminescent

character were elaborated upon, such as choice of lanthanide cation and choice of antenna ligand. The lanthanide cation can be used to determine colour of luminescence (i.e.  $\text{Tb}^{3+}$  for green,  $\text{Eu}^{3+}$  for red). Antenna ligands can be chosen based on the energy level of their triplet excited state, with a high energy gap between the triplet excited state and the lanthanide cations lowest emitting levels giving more intense luminescence<sup>[64]</sup>. Another study investigated the modification of luminescent character, specifically quantum yield in a  $\text{Eu}^{3+}$  compound by tuning the ligands, thus influencing the environment of the lanthanide ion<sup>[65]</sup>.

#### **4.1.2 Applications of lanthanide luminescence**

The luminescence properties of lanthanide ions are a phenomenon with wide applications detailed throughout the literature. Lanthanide luminescence is a useful tool for bioassays, and is suited to various clinical diagnostic and bio-analytical applications. The long luminescence decay time and large Stokes shift exhibited by luminescent lanthanide ions make them suitable for time-resolved luminescence assays<sup>[66]</sup>. Cathode ray tube televisions have long been the standard for the home entertainment market, and these displays utilise lanthanide phosphors excited by an electron gun as means for a display. With new technologies beginning to dominate the home entertainment market, lanthanide luminescence is still being utilised for potential in OLED (organic light emitting diode) displays. Several papers have been published on the use of lanthanide phosphors in screen displays<sup>[67]</sup>, including one paper which details the manufacture of an OLED by deposition of samarium and europium complexes onto an ITO (indium-tin-oxide) substrate, through spin deposition<sup>[68]</sup>.



The area that this thesis will focus on is the applications of luminescent lanthanide compounds in forensic science, specifically the applications to the exposure of latent fingerprints.

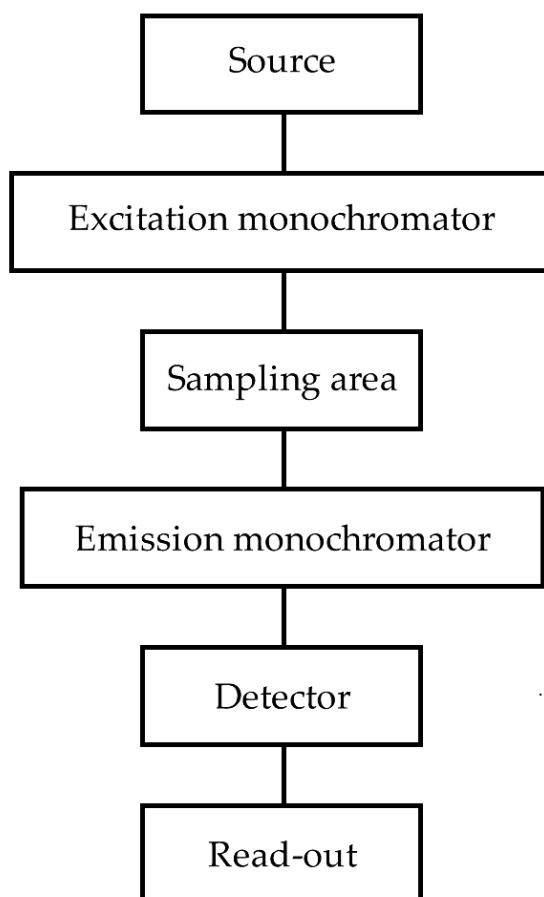
Previous research in this area has investigated the use of lanthanide NMR shift reagents for exposure of latent fingerprints. A paper by Henderson *et al* describes the use of  $\text{Eu}(\text{fod})_3$  for visualising latent prints. The structure of these compounds is similar to that of the  $\text{Ln}(\beta\text{-diketonate})_3$  compounds that are investigated in this thesis. Trials involved dipping of a surface containing a latent print (obtained through running a thumb across forehead to gain an even print) in a solution of  $\text{Eu}(\text{fod})_3$  in petroleum spirits, and illuminating them with a UV light source. The trials were promising, showing well exposed prints on various surfaces. Through ESI-MS studies of  $\text{Eu}(\text{fod})_3$  reacted with various chemical components of latent fingerprints, good evidence was given for the reactivity of  $\text{Eu}(\text{fod})_3$  with lipid and non-lipid components of fingerprints<sup>[26]</sup>.

Other research has investigated doping of ligand sensitised trivalent europium compounds into silicon dioxide based xerogels, which were ground into fine powders. These powders were then brushed onto surfaces of varying porosity on which latent fingerprints had been planted. The study concluded that the xerogel powders were useful fingerprinting agents due to their strong fluorescent emissions and successful exposure on all surfaces<sup>[69]</sup>.

#### **4.1.3 Analysis of luminescent compounds**

The luminescent properties of compounds can be quantified through the use of a fluorescence spectrometer. The general principle for the operation of a fluorescence spectrometer is as follows. UV light from an excitation source (commonly a xenon lamp) is passed through a wavelength selector

(such as a grating monochromator) and interacts with the sample, giving fluorescent emission. These emissions are then passed through another filter to the detector. Figure 4.4 gives a diagram of the operation of a fluorescence spectrometer.



*Figure 4.4: Reproduced diagram of a fluorescence spectrometer.*

Fluorescence spectroscopy has a wide range of applications. It has proven to be useful in medical diagnostics<sup>[70]</sup>, DNA sequencing and bioanalysis<sup>[71]</sup>. Fluorescence spectroscopy has also been used to measure the fluorescence spectra of latent fingerprints through excitation with an Nd-YAG laser<sup>[72]</sup>. Several published methods of latent print exposure using fluorescent techniques acquire fluorescence spectra, as they are useful for determining optimal excitation wavelengths, and alternate emission wavelengths

should the highest intensity emission be interfered with by background fluorescence<sup>[54a, 69, 73]</sup>.

For this thesis a variety of luminescent compounds were synthesised and doped into talcum powder, and the compounds and powders were analysed through the use of a fluorescence spectrometer. A wide range of compounds were used, as to investigate which ligands made the most

<u>Europium compounds</u>	<u>Terbium compounds</u>
Eu(acac) <sub>3</sub> (phen)	Tb(acac) <sub>3</sub> (phen)
Eu(acac) <sub>3</sub> (bipy)	Tb(acac) <sub>3</sub> (bipy)
Eu(tta) <sub>3</sub> (phen)	Tb(tta) <sub>3</sub> (phen)
Eu(tta) <sub>3</sub> (bipy)	Tb(tta) <sub>3</sub> (bipy)
Eu(acac) <sub>3</sub> (phen)	Tb(acac) <sub>3</sub> (phen)
Eu(acac) <sub>3</sub> (bipy)	Tb(acac) <sub>3</sub> (bipy)
Eu(tta) <sub>3</sub> (phen)	Tb(tta) <sub>3</sub> (phen)
Eu(tta) <sub>3</sub> (bipy)	Tb(tta) <sub>3</sub> (bipy)
Eu(acac) <sub>3</sub> (p=O)	Tb(acac) <sub>3</sub> (p=O)
Eu(tta) <sub>3</sub> (p=O)	Tb(tta) <sub>3</sub> (p=O)
[H <sub>2</sub> NMe <sub>2</sub> ] <sub>3</sub> [Eu(2,6-dpa) <sub>3</sub> ].2H <sub>2</sub> O	[H <sub>2</sub> NMe <sub>2</sub> ] <sub>3</sub> [Tb(2,6-dpa) <sub>3</sub> ].2H <sub>2</sub> O

Table 4.1: Compounds that were analysed by fluorescence spectroscopy.

useful compounds. The powders were set in two comparative groups, those with europium (that yielded red luminescence) and terbium

compounds (that yielded green fluorescence). Through comparing spectra of the compounds and their analogous powders, the effect on the luminescence from the doping process could be observed. Table 4.1 shows the compounds that were analysed in this research.

Also analysed were two commercial samples of fingerprinting powders, Redwop and Greenwop. These powders are used for forensic analysis and give red and green luminescence respectively, and were therefore useful as a comparison study for the synthesised compounds.

## 4.2 Methods

### 4.2.1 Chemicals and instrumentation

Lanthanide compounds were all synthesised using  $\text{EuNO}_3 \cdot 5\text{H}_2\text{O}$  or  $\text{TbNO}_3 \cdot 5\text{H}_2\text{O}$  purchased from Sigma Aldrich. Dipicolinic acid and DMF were also purchased from Sigma Aldrich, with drum grade solvents used for synthesis. Fluorescence spectra were recorded using a Perkin-Elmer LS50B fluorescence spectrometer, using FLwinLab software.

### 4.2.2 Synthesis of lanthanide compounds

The  $\text{Ln}(\beta\text{-diketonate})_3(\text{p}=\text{o})$  series of compounds were synthesised by methods detailed in chapter 2, and the  $\text{Ln}(\beta\text{-diketonate})_3(\text{phen/bipy})$  compounds were synthesised by the same method.

The  $[\text{H}_2\text{NMe}_2]_3[\text{Ln}(2,6\text{-dpa})_3] \cdot 2\text{H}_2\text{O}$  compounds were synthesised according to literature methods<sup>[74]</sup>. These were recently published compounds, which were easily synthesised with cheap, available reagents. The structure of the 2,6-dipicolinic acid ligand contained in these compounds is displayed in Figure 4.5. The literature stated that these compounds were stable with high quantum efficiencies, and luminescent

properties. These characteristics made the compounds ideal for investigation into potential application as fingerprinting agents.

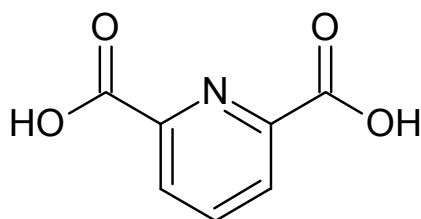


Figure 4.5: Structure of 2,6-dipicolinic acid.

These compounds were then doped into talcum powder using the process detailed in chapter 3.

### 4.2.3 Analysis of luminescent character

#### 4.2.3.1 Fluorescence spectroscopy

The compounds and their powder analogues were analysed using the following procedures. Preliminary tests of appropriate excitation wavelengths were done using a UV lamp, which had two excitation modes (254 nm and 312 nm). Small amounts of sample were placed on a watch glass, and in a darkened room they were exposed to the lamp to visibly gauge luminescent activity. For the spectrometer, a quartz die was used to insert the powder of interest into the spectrometer. The quartz window was covered with the powder (~0.5 g) and placed in the spectrometer. Scans were run with inlet and outlet slit widths of 2.5 nm. Each powder was run twice, scanning for emissions between 250 and 700 nm both times, with the excitations of 254 nm and 312 nm.

#### 4.2.3.2 UV lamp screening

While the fluorescent spectrometer is useful for investigating emission and excitation properties of the powders, the most important property is the direct visualisation of the print. Using the standard experimental set up described in chapter 5, the powders were screened for their luminescent

intensity through observation of the exposed fingerprints. The quality of the prints was not primarily considered in this experiment, but the intensity of luminescence from the powder. The powders were given a rating from 1 to 5 of their intensity. This was an arbitrary score used for comparative purposes. The contrast and brightness of some images were modified to try and better recreate the observed prints.

## 4.3 Results

### 4.3.1 Excitation and emission spectra of $\text{Ln}(\beta\text{-diketonate})_3(\text{phen/bipy})$

#### 4.3.1.1 Emission spectra of $\text{Eu}(\beta\text{-diketonate})_3(\text{phen/bipy})$

All compounds of the  $\text{Eu}(\beta\text{-diketonate})_3(\text{phen/bipy})$  type gave spectra with sharp, well defined peaks. The luminescent intensity was stronger on the compounds using 1,10-phenanthroline as the neutral ligand. The dominant emissions were the same in all complexes (510 nm emission at 254 nm excitation, and 625 nm emission at 312 nm excitation). The europium complexes with tta ligands at 254 nm excitation also exhibited lower intensity emissions around 610 nm. Figure 4.6 shows the emission spectrum of  $\text{Eu}(\text{tta})_3(\text{phen})$  excited at 254 nm.

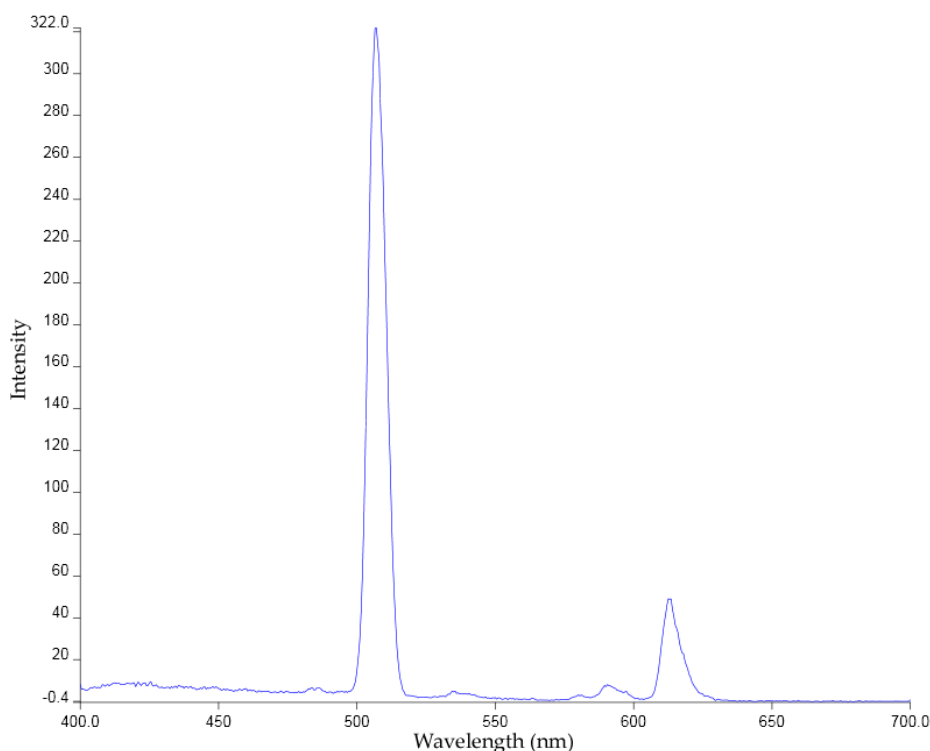


Figure 4.6: Emission spectrum of  $\text{Eu}(\text{tta})_3(\text{phen})$ , excited at 254 nm.

#### 4.3.1.2 Emission spectra of $\text{Tb}(\beta\text{-diketonate})_3(\text{phen/bipy})$

The emission spectra of the  $\text{Tb}(\beta\text{-diketonate})_3(\text{phen/bipy})$  differed to the europium spectra in that the tta complexes exhibited only one dominant emission, while the acac complexes had notably smaller intensity peaks. Also, the dominant emissions in some Tb complexes resulted in flat topped peaks on the spectra, as a result of their high intensity raising them off the scale. Similar to the europium complexes, excitation at 254 nm gave dominant intensity emissions at 510 nm and 312 nm excitation gave dominant emissions at 625 nm. The acac complexes all exhibited smaller intensity peaks at 490 nm and 550 nm under both 312 nm and 254 nm excitation. Figure 4.7 shows the emission spectrum of  $\text{Tb}(\text{acac})_3(\text{phen})$  at 312 nm excitation.

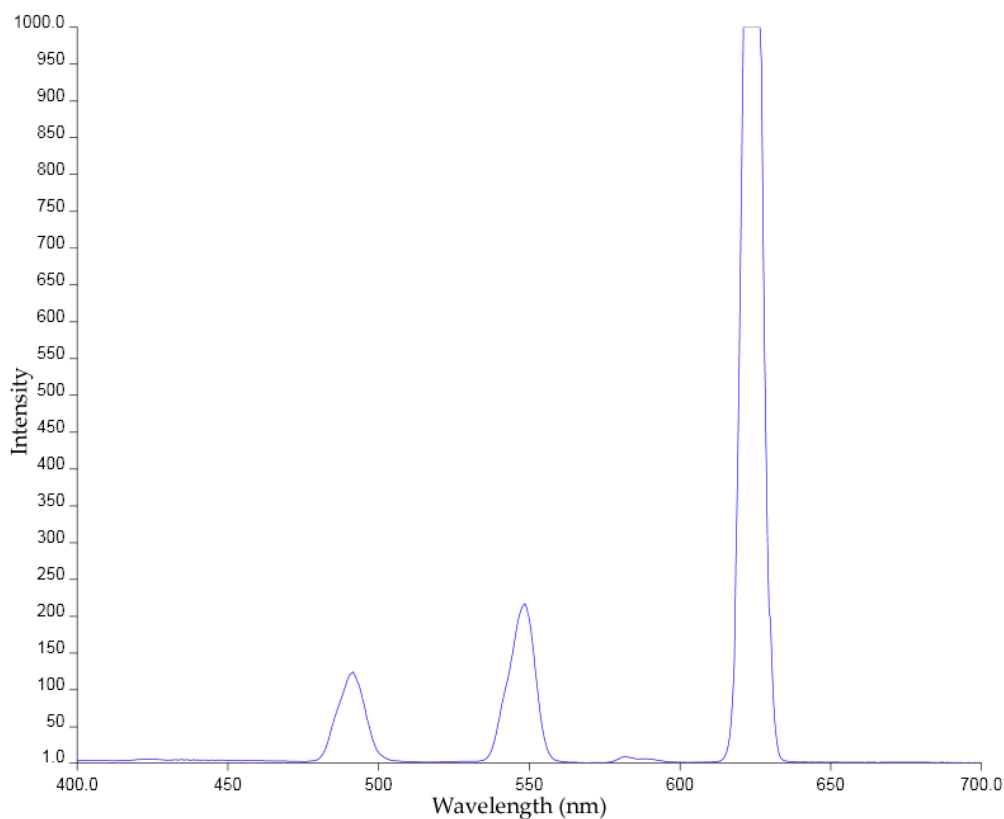


Figure 4.7: Emission spectrum of  $\text{Tb}(\text{acac})_3(\text{phen})$  at 312 nm excitation.

#### 4.3.1.3 Excitation spectra of $\text{Eu}(\beta\text{-diketonate})_3(\text{phen/bipy})$

The spectra for all compounds were very similar, with the only significant differences depending on the set emission wavelength. At 510 nm emission, excitation peaks were observed at 254 nm and 510 nm with higher intensities on the 254 nm peak noted for the acac compounds. At 625 nm emission, excitation peaks were observed at 312 nm and 625 nm, again with greater intensities at the 312 nm peak in acac compounds. Figure 4.8 shows the excitation spectrum for  $\text{Eu}(\text{tta})_3(\text{phen})$  at 625 nm emission.



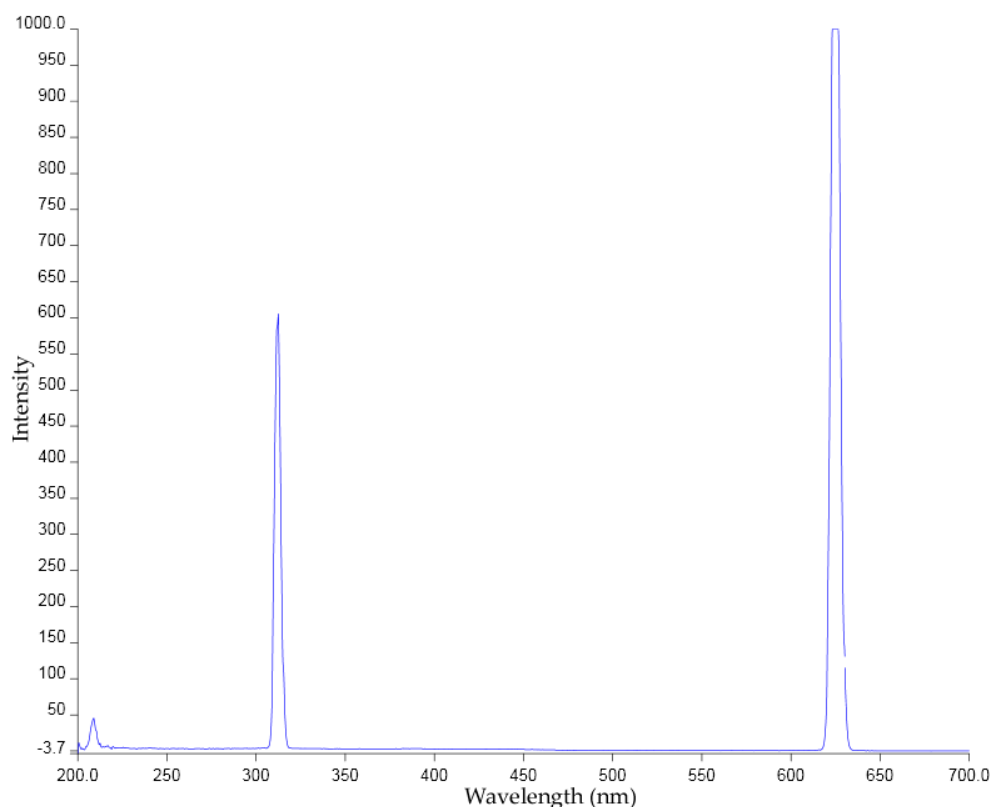


Figure 4.8: Excitation spectrum of  $\text{Eu}(\text{tta})_3(\text{phen})$  at 625 nm emission.

#### 4.3.1.4 Excitation spectra of $\text{Tb}(\beta\text{-diketonate})_3(\text{phen/bipy})$

As with the Eu samples, all compounds show very similar spectra, with the peaks differing between emission wavelengths and intensities varying with different ligands. With the emission fixed at 510 nm, excitation peaks were observed at 254 nm and 510 nm. On all complexes, the dominant peak was at 510 nm, and the intensities gave flat topped peaks on the spectra. The acac complexes had much more intense excitation peaks at 254 nm than the tta complexes. At 625 nm emission, the dominant peaks were at 625 nm with the less intense peaks at 312 nm. Minor peaks were also observed at around 210 nm. Figure 4.9 shows the excitation spectrum of  $\text{Tb}(\text{acac})_3(\text{bipy})$  at 510 nm emission.

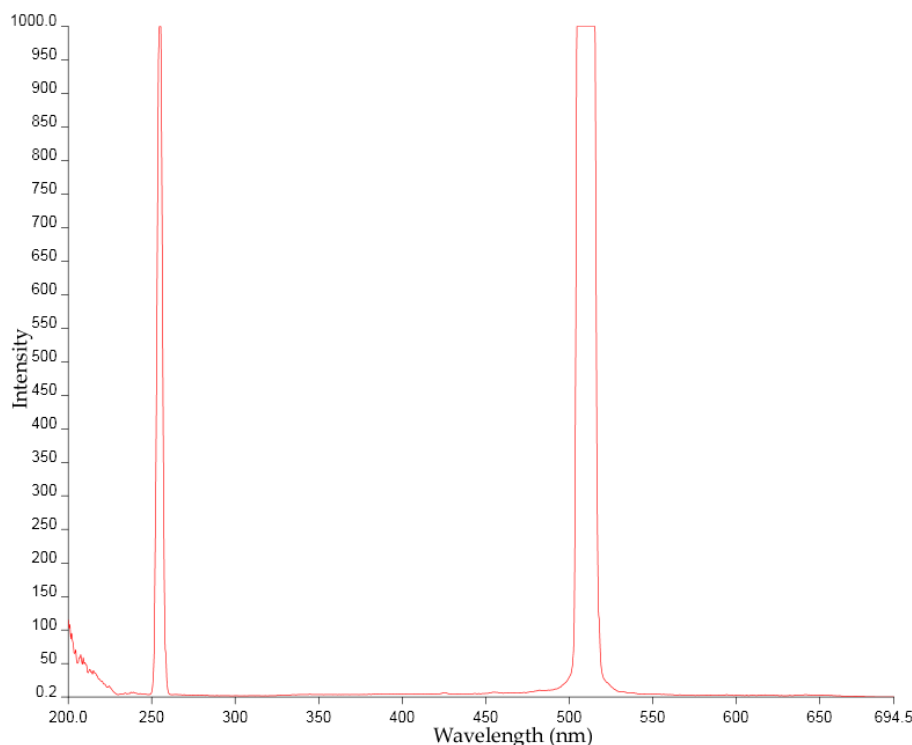


Figure 4.9: Excitation spectra of  $\text{Tb}(\text{acac})_3(\text{bipy})$  at 510 nm emission.

### 4.3.2 Excitation and emission spectra of $\text{Ln}(\beta\text{-diketonate})_3(\text{p}=\text{o})$

#### 4.3.2.1 Excitation and emission spectra of $\text{Eu}(\text{acac}/\text{tta})_3(\text{p}=\text{o})$

At both 254 nm and 312 nm excitation, the dominant peak in the emission spectrum of  $\text{Eu}(\text{acac})_3(\text{p}=\text{o})$  was at 510 nm, with an intensity greater than 1000. At 254 nm excitation, smaller intensity emissions were observed and 490 nm and 550 nm. For  $\text{Eu}(\text{tta})_3(\text{p}=\text{o})$ , excitation at 254 gave a dominant emission at 510 nm with an intensity of 912, with a minor peak at 615 nm. Excitation at 312 nm gave a dominant peak of 545 intensity at 625 nm.

Excitation spectra differed mainly depending on the set emission of 625 nm or 510 nm. At 510 nm emission, excitation peaks were observed at both 254 nm and 510 nm, with more intense peaks observed for the acac ligand. At 625 nm emission, intense excitation peaks were observed at 312 nm and

625 nm, with a minor peak at 210 nm. Figure 4.10 shows the emission spectrum of  $\text{Eu}(\text{tta})_3(\text{p}=\text{o})$  at 254 nm excitation.

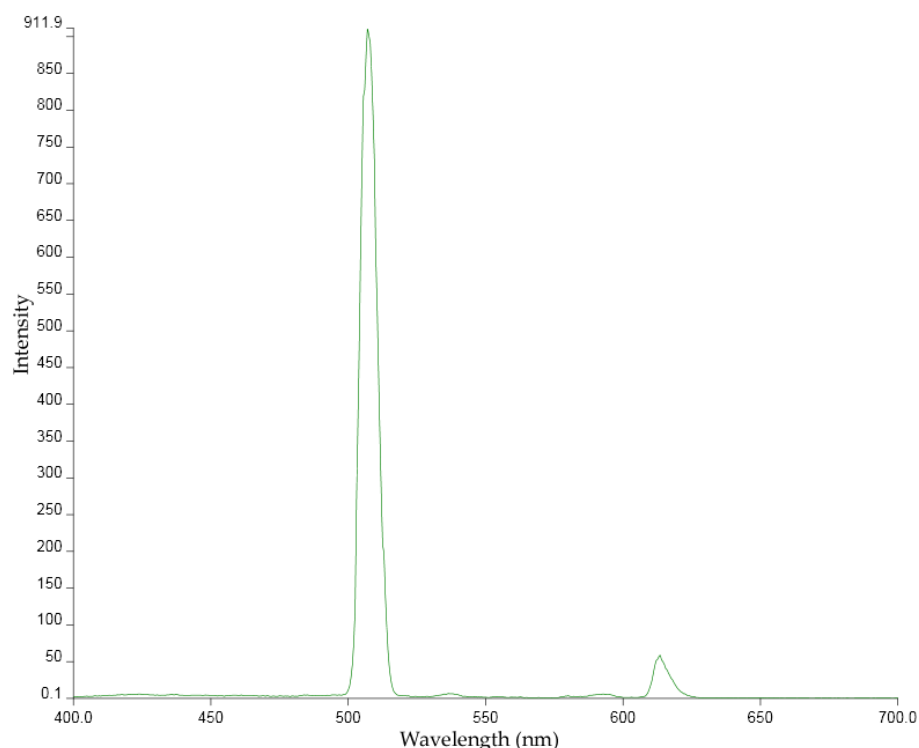


Figure 4.10: Emission spectrum of  $\text{Eu}(\text{tta})_3(\text{p}=\text{o})$  at 254 nm excitation.

#### 4.3.2.2 Excitation and emission spectra of $\text{Tb}(\text{acac}/\text{tta})_3(\text{p}=\text{o})$

The emission spectra for all of the  $\text{Tb}(\text{acac}/\text{tta})_3(\text{p}=\text{o})$  compounds exhibited notable emission peaks at 510 nm and 625 nm, with excitations of 254 nm and 312 nm respectively. The compounds with acac ligands also exhibited minor emission peaks at 490 nm and 550 nm.

The excitation spectra at 510 nm emission displayed excitation peaks at 254 nm and 510 nm, while 625 nm emission showed excitation peaks at 312 nm and 625 nm, with a minor peak at 210 nm. Figure 4.11 shows the excitation spectrum of  $\text{Tb}(\text{tta})_3(\text{p}=\text{o})$  at 625 nm emission.

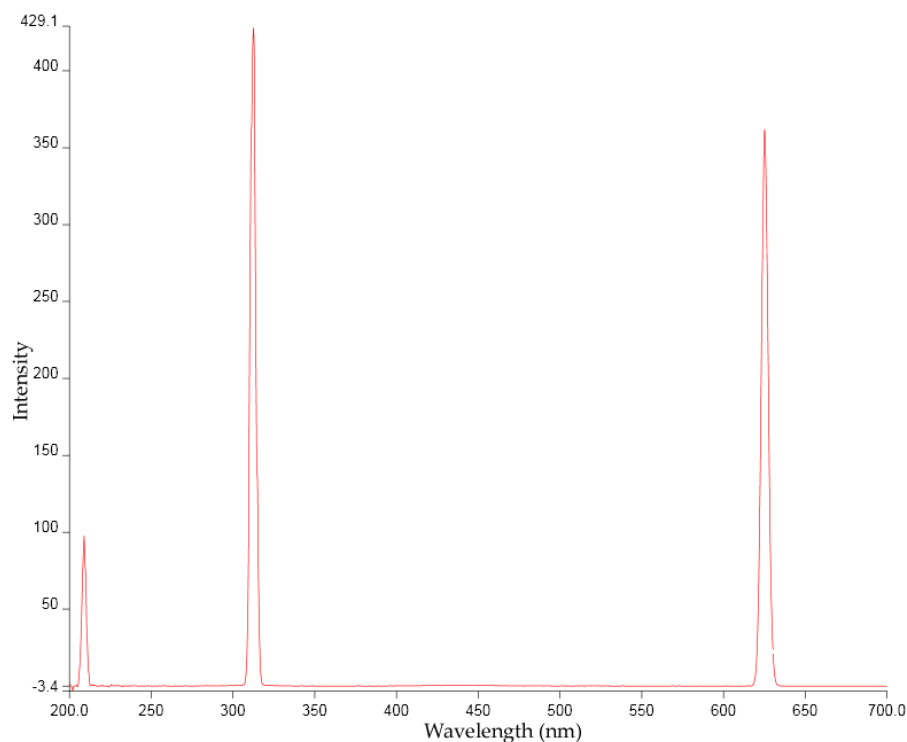


Figure 4.11: Excitation spectrum of  $\text{Tb}(\text{tta})_3(p=0)$  at 625 nm emission.

### 4.3.3 Excitation and emission spectra of Greenwop and Redwop

Similar to the europium and terbium compounds, excitation at 254 nm and 312 nm gave emission at 510 nm and 625 nm respectively. The greenwop had additional broad emission peaks compared to the redwop. Redwop excitation peaks were also similar to the lanthanide compound, with narrow excitations at 254 nm and 510 nm corresponding to 510 nm emission settings, and 210 nm, 312 nm and 625 nm excitation peaks corresponding to a 625 nm emission setting. Greenwop excitation spectra were similar for 625 nm emission, however for 510 nm emission the spectra consisted of broad excitation peaks from 200 nm – 525 nm. While these wavelengths are similar to that of the lanthanide compounds, the MSDS for the “wop” powders indicated the colour is attributable to a dyed polymer.

#### 4.3.4 Excitation and emission spectra of $[\text{H}_2\text{NMe}_2]_3[\text{Eu}(\text{2,6-dpa})_3] \cdot 2\text{H}_2\text{O}$ and $[\text{H}_2\text{NMe}_2]_3[\text{Tb}(\text{2,6-dpa})_3] \cdot 2\text{H}_2\text{O}$

Both europium and terbium compounds show dominant emissions at 510 nm at 254 nm excitation, and at 625 nm emission with 312 nm excitation. Excitation spectra at 510 emission had intense peaks at 254 nm and 510 nm excitation. At 625 nm emission, peaks were most intense at 312 nm and 625 nm, with very minor peaks at 210 nm. Figure 4.12 shows the emission spectrum of  $[\text{H}_2\text{NMe}_2]_3[\text{Eu}(\text{2,6-dpa})_3] \cdot 2\text{H}_2\text{O}$  at 254 nm excitation.

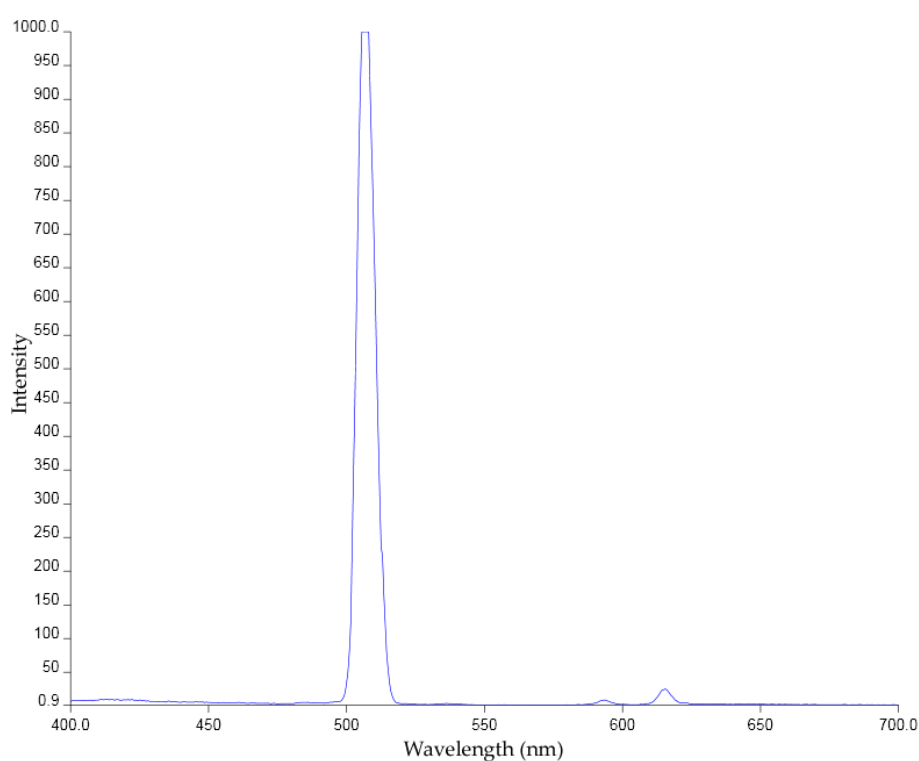


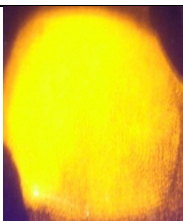
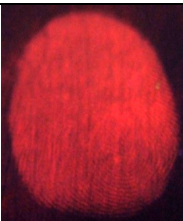
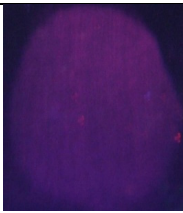
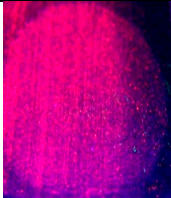
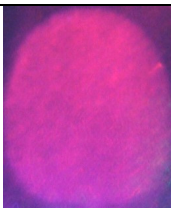
Figure 4.12: Emission spectrum of  $[\text{H}_2\text{NMe}_2]_3[\text{Eu}(\text{2,6-dpa})_3] \cdot 2\text{H}_2\text{O}$  at 254 nm excitation.

#### 4.3.5 Observed luminescent intensity of fingerprint powders

##### 4.3.5.1 Red luminescent fingerprint powders

Table 4.2 displays images of prints exposed with powders that exhibited red luminescence, matched with their designated intensity rating. The talcum powders that directly showed the best red luminescent intensities were those doped with  $\text{Eu}(\text{acac})_3(\text{phen})$ ,  $\text{Eu}(\text{tta})_3(\text{phen})$  and

[H<sub>2</sub>NMe<sub>2</sub>]<sub>3</sub>[Eu(2,6-dpa)<sub>3</sub>].2H<sub>2</sub>O. The score was rated in comparison to the intensity of luminescence from Redwop, which is given a rating of 5. It should be noted that the difficult conditions under which the photos were taken negatively affected the quality of the images.

<u>Compound</u>	<u>Excitation</u>	<u>Image</u>	<u>Rating</u>
Redwop	254 nm		5
Eu(acac) <sub>3</sub> (phen)	254 nm		4
Eu(acac) <sub>3</sub> (bipy)	312 nm		1
Eu(tta) <sub>3</sub> (phen)	312 nm		3
Eu(tta) <sub>3</sub> (bipy)	312 nm		2


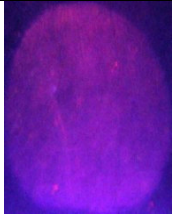
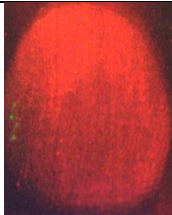
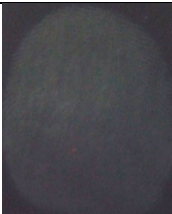

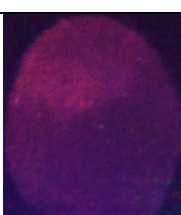
$\text{Tb}(\text{tta})_3(\text{phen})$	312 nm		1
$\text{Tb}(\text{tta})_3(\text{bipy})$	312 nm		1
$[\text{H}_2\text{NMe}_2]_3[\text{Eu}(\text{2,6-dpa})_3] \cdot 2\text{H}_2\text{O}$	254 nm		4
$\text{Eu}(\text{acac})_3(\text{p}=\text{o})$	312 nm		1
$\text{Eu}(\text{tta})_3(\text{p}=\text{o})$	254 nm		4
$\text{Tb}(\text{tta})_3(\text{p}=\text{o})$	312 nm		2

Table 4.2: Summary of powders exhibiting red luminescence.

#### 4.3.5.2 Green luminescent fingerprint powders

Table 4.3 displays images of prints exposed with powders that exhibited green luminescence, matched with their designated intensity rating. For the talcum powders exhibiting green luminescence, the most intense

samples were the talcum powders doped with  $\text{Tb}(\text{acac})_3(\text{phen})$  and  $[\text{H}_2\text{NMe}_2]_3[\text{Tb}(\text{2,6-dpa})_3] \cdot 2\text{H}_2\text{O}$ . The powders were compared to the Greenwop sample, which was given a reference score of 5.

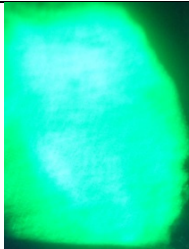
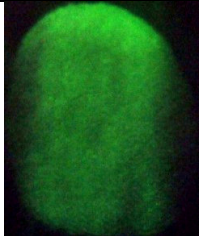
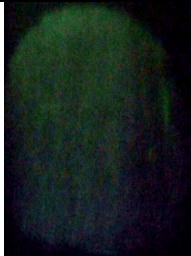
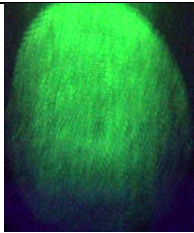
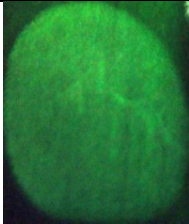
<u>Compound</u>	<u>Excitation</u>	<u>Image</u>	<u>Rating</u>
Greenwop	312 nm		5
$\text{Tb}(\text{acac})_3(\text{phen})$	254 nm		3
$\text{Tb}(\text{acac})_3(\text{bipy})$	254 nm		1
$[\text{H}_2\text{NMe}_2]_3[\text{Tb}(\text{2,6-dpa})_3] \cdot 2\text{H}_2\text{O}$	254 nm		4
$\text{Tb}(\text{acac})_3(\text{p=O})$	312 nm		4

Table 4.3: Summary of powders exhibiting green luminescence.



## 4.4 Discussion

### 4.4.1 Analysis of excitation and emission spectra of lanthanide complexes

Several common results were found through analysis of the fluorescence spectra. The most notable were the occurrence of a dominant emission peak at 510 nm when excited at 254 nm, and a dominant emission peak 625 nm peak when excited at 312 nm. Excitation spectra of 510 nm and 625 nm showed expected peaks at 254 nm and 312 nm respectively, and commonly a minor excitation peak at 625 nm emission. It was worth noting the compounds that exhibited additional excitation and emission peaks, as they can provide an alternate wavelength for excitation when the most intense wavelength is interfered with. Table 4.4 displays the compounds with their alternate emission wavelengths.

<u>Compound</u>	<u>Excitation</u>	<u>Alternate emission</u>
Eu(tta) <sub>3</sub> (bipy)	254 nm	615 nm
Eu(acac) <sub>3</sub> (p=O)	254 nm	550 nm
Tb(acac) <sub>3</sub> (bipy)	254 nm	550 nm
Tb(acac) <sub>3</sub> (bipy)	312 nm	550 nm
Tb(acac) <sub>3</sub> (phen)	254 nm	550 nm
Tb(acac) <sub>3</sub> (phen)	312 nm	550 nm

Table 4.4: Alternate emission wavelengths for lanthanide compounds.

The intensity of the emissions measured by fluorescence spectroscopy is an arbitrary value, and cannot be reliably applied when evaluating the observed visibility of the excited fingerprinting powders. Furthermore, due to interference from the talcum powder, reliable fluorescence spectra of the doped talcum powder could not be obtained. When running fluorescence spectra of the talcum powders, broad peaks were present in the area of the expected peaks from the doped compound.

To determine which powders would be most suitable for trial as fingerprinting powders, the main factor considered was the observed luminescent character of the doped powders.

#### **4.4.2 Analysis of doped talcum powders under UV excitation**

Observation of the powders under UV excitation showed that while measured luminescent intensities could prove useful in indentifying the powders with the most intense luminescence, it was not always accurate. The spectra for the compounds containing a phen ligand generally showed much greater intensities than the compounds with bipy ligands, and this was a trend that was also observed in the activity of the doped powders. However some compounds had luminescent activity that did not reflect that of the recorded spectra. While  $\text{Eu}(\text{tta})_3(\text{phen})$  showed a similar intensity peak to  $\text{Tb}(\text{tta})_3(\text{phen})$ , the observed luminescent intensity of the powder was much less than that of the  $\text{Eu}(\text{tta})_3(\text{phen})$  powder. This was also observed in  $\text{Eu}(\text{acac})_3(\text{p}=\text{o})$  and  $\text{Tb}(\text{acac})_3(\text{p}=\text{o})$ , which had similar intensity peaks on the luminescent spectra, however the Eu compound visibly exhibited much less intense luminescence than the corresponding Tb compound. This was also apparent in the green luminescent compounds. Excluding  $[\text{H}_2\text{NMe}_2]_3[\text{Tb}(\text{2,6-dpa})_3] \cdot 2\text{H}_2\text{O}$ , the luminescent intensities were all measured to be greater than 1000, however in application there was significant difference between them.

One result of note was the observed weak red luminescent emissions from the  $\text{Tb}(\text{tta})_3(\text{phen/bipy/p=o})$  compounds. This was initially thought to be an experimental error, so the compounds were synthesised again but yielded the same result. A search of literature gave no information on red luminescence from terbium compounds.

#### **4.4.3 Effectiveness of the $(\text{Me})_3\text{CN}(\text{CH}_2\text{P}(\text{O})\text{Ph}_2)_2$ ligand compared to 1,10-phenanthroline and 2,2-bipyridine**

The novel  $(\text{Me})_3\text{CN}(\text{CH}_2\text{P}(\text{O})\text{Ph}_2)_2$  ligand was compared to the phen and bipy ligands to measure its effectiveness as a neutral ligand for increasing luminescent activity of the compound. Fluorescence spectroscopy for the  $\text{Ln}(\beta\text{-diketonate})_3(\text{p=o})$  compounds showed sharp, high intensity peaks at the trialled excitation wavelengths of 254 nm and 312 nm. The spectra obtained showed similar characteristics to the established luminescent  $\text{Ln}(\beta\text{-diketonate})_3(\text{phen/bipy})$  compounds.

The observed luminescence from excitation with UV light showed some promising results. The compounds  $\text{Eu}(\text{tta})_3(\text{p=o})$  and  $\text{Tb}(\text{acac})_3(\text{p=o})$  displayed well defined intense luminescence at the specified wavelengths, comparable to the most intense of the traditional  $\text{Ln}(\beta\text{-diketonate})_3(\text{phen/bipy})$  compounds. The  $\text{Eu}(\text{acac})_3(\text{p=o})$  and  $\text{Tb}(\text{tta})_3(\text{p=o})$  samples however did not give intense emissions at either 254 nm or 312 nm. It was concluded that the novel  $(\text{Me})_3\text{CN}(\text{CH}_2\text{P}(\text{O})\text{Ph}_2)_2$  ligand appeared to have useful properties as a neutral ligand to promote luminescence in a compound.

### **4.5 Chapter Summary**

Lanthanide compounds were analysed by fluorescence spectroscopy to investigate their luminescent activity, and talcum powders doped with lanthanide compounds were screened by UV for their observed intensities.

Fluorescence spectroscopy showed that the dominant emissions at 254 nm and 312 nm excitation were 510 nm and 625 nm respectively, with the most intense of these emissions ideally used for exposing the powder when applied to latent fingerprints.

Comparison of the observed luminescent intensities through excitation with UV and the intensity measured by fluorescence spectroscopy showed little correlation. Some compounds with intensity peaks greater than 1000 gave poor observed intensity. This suggested that these peaks may have arisen due to interference from inorganic impurities in the sample.

Through comparison of the novel  $\text{Ln}(\beta\text{-diketonate})_3(\text{p}=\text{o})$  compounds to traditional  $\text{Ln}(\beta\text{-diketonate})_3(\text{phen/bipy})$  luminescent compounds, it was concluded that the novel  $(\text{Me})_3\text{CN}(\text{CH}_2\text{P}(\text{O})\text{Ph}_2)_2$  ligand could be successfully used as a neutral ligand for enhancing luminescence in lanthanide compounds.

From these results, four compounds were chosen to be investigated further for their performance in exposing latent fingerprints. Two compounds were chosen which exhibit red luminescence, and two that exhibit green luminescence. These compounds were as follows.

Red luminescence:

- $[\text{H}_2\text{NMe}_2]_3[\text{Eu}(2,6\text{-dpa})_3] \cdot 2\text{H}_2\text{O}$
- $\text{Eu}(\text{tta})_3(\text{p}=\text{o})$

Green luminescence:

- $[\text{H}_2\text{NMe}_2]_3[\text{Tb}(2,6\text{-dpa})_3] \cdot 2\text{H}_2\text{O}$
- $\text{Tb}(\text{acac})_3(\text{p}=\text{o})$

## **5 Evaluation of doped talcum powders for detection of latent fingerprints**

### **5.1 Introduction**

#### **5.1.1 Methods for print comparison**

With ongoing research into the field of forensic criminology, new methods for exposing latent fingerprints are constantly being developed. A key part of developing new methods is the evaluation of the quality of the prints. Investigation of the literature suggested that there is no standardised method under which a method of latent print exposure can be evaluated for its quality. Due to a lack of a standardised method, the quality of a print exposure method is often down to the subjective perspective of the researcher.

The general aim of research of this nature is to implement more effective and efficient methods of detecting latent fingerprints. To obtain an understanding of the usefulness of a new method, a common technique is to compare the method being trialed against an established method that it could potentially supersede. For example, when trialing a method across a range of surfaces (i.e. smooth and porous) the comparison trials would implement the conventional methods for exposing latent prints on that surface<sup>[75]</sup>.

A common method for investigating the effect of certain environmental conditions involves the deposition of a print on a surface and bisecting the print. One half is then exposed to the conditions, and both halves are developed, giving a direct comparison<sup>[26, 76]</sup>. Because there is no standardised method for quantifying the quality of a print, some studies consider a high quality print as one where all ridge details can be clearly

seen<sup>[77]</sup>. This is important as exposure of the minutiae is vital in successful comparison to a fingerprint database.

Fingerprints taken from criminals make a useful database that can be indexed for future reference. Fingerprints taken from a crime scene are run through an algorithm that attempts to find a match in the database. However for these algorithms to be effective, quality prints must be taken and submitted<sup>[78]</sup>.

### **5.1.2 Powder methods for exposing latent fingerprints**

The general method for exposing prints with powders involves first selecting a powder with a contrasting colour to that of the surface. A gentle brushing technique is used to apply the powder, with excess removed by tapping of the surface. The print can be stored by lifting, which involves the application of adhesive tape to a powder exposed print<sup>[7]</sup>.

The three most common types of fingerprinting powders are regular, magnetic and luminescent. Regular powders work through direct exposure of a latent print on a surface. Magnetic powders can be produced through processing of metals to fine flakes, which adhere to prints. The magnetic flakes can be held at the end of a wand, which brushes across a print, controlling the deposition of the flakes to the print<sup>[79]</sup>. Luminescent powders are the main focus of this thesis. Luminescent powders are applied in the same fashion as regular powders, but strong contrast can be obtained through excitation by a specified light wavelength. Luminescent organic dyes and lanthanide compounds are common techniques for giving a powder luminescent character. One publication details the addition of a lanthanide complex to dendrimers, which can be used to adhere to the residues of a latent fingerprint<sup>[80]</sup>.

One notable drawback of powder methods is the potential health hazards. Several studies were run to test the effect of powders on the level of lead police fingerprint workers were exposed to<sup>[81]</sup>. Use of lead and mercury based powders has been eliminated due to the health risks exposed to users of these powders, although some powders have levels of lead in them. The powders used in this research were talcum powder doped with lanthanide complexes. As detailed in chapter 3, no solid links have been made suggesting health hazards associated with talc. Lanthanides have been suspected to have similar health effects as heavy metals, with some *in vitro* tests indicating function as a  $\text{Ca}^{2+}$  antagonist, similar to  $\text{Cd}^{2+}$ . Studies suggest that lanthanides are not highly toxic, though health effects are highly dependent on the compounds in which the lanthanides are maintained<sup>[82]</sup>.

### 5.1.3 Applications for this research

The research in this thesis is focused on developing a method for latent print exposure based on powder methods. A basic talcum powder doped with a luminescent lanthanide complex will ideally provide an easy and quick dusting method, which can be enhanced by illumination with UV light. To evaluate the effectiveness of this method, it is suitable to compare with other luminescent powders on the market.

As investigated in chapters 3 and 4, Greenwop and Redwop have been used as comparisons for particle structure and luminescent character. As they are dusting powders with green and red luminescent characteristics respectively, they are the product with the most direct comparisons to the powders made for this research.

## 5.2 Methods

### 5.2.1 Materials and instrumentation

Several luminescent powders were investigated for their observed luminescent intensity and fluorescence spectra, and the best were chosen for evaluation of their latent print exposure properties. The powders chosen for trials were:

- $[\text{H}_2\text{NMe}_2]_3[\text{Eu}(2,6\text{-dpa})_3] \cdot 2\text{H}_2\text{O}$
- $\text{Eu}(\text{tta})_3(\text{p}=\text{o})$
- $[\text{H}_2\text{NMe}_2]_3[\text{Tb}(2,6\text{-dpa})_3] \cdot 2\text{H}_2\text{O}$
- $\text{Tb}(\text{acac})_3(\text{p}=\text{o})$

Commercial Greenwop and Redwop powders were used as comparative studies for the various trials, with Greenwop used to contrast powders that exhibited green fluorescence and Redwop for those that exhibited red fluorescence.

A Uvitec If-204.ls 8 watt UV lamp was used to illuminate the powders for visualisation. It had wavelength settings of 254 and 312 nm. Glass microscope slides were used as the glass surface in the standard experimental set up. The powders were applied by the use of a soft badger hair brush, purchased from The Warehouse. A feather brush donated from the Hamilton Police fingerprinting department was also used. In between different powders the brush was rinsed with water, and dried with a paper towel.

### 5.2.2 Fingerprint trials

The standard experimental set up consisted of a glass slide with a latent thumb print, applied by rubbing the thumb across the forehead and pressing on the glass. A spatula tip of powder (~0.01 g) was then



immediately applied to the glass slide, and brushed gently over the print using a badger hair brush. In the case of the Redwop and Greenwop powders, a feather brush was used. Once visible, the print was enhanced using the UV lamp, using the wavelength that gave the best luminescence for the particular powder.

This basic procedure was modified to investigate the effect of a range of different variables on the print powders. The procedure remained constant, except for the variables that are described below.

#### 5.2.2.1 Surface variables

Powders were tested on a range of surfaces to evaluate the effectiveness of the powders in different situations. The surfaces considered were those that might be expected to be found in a crime scene (for example glass representing a window, which may be contacted upon forcing entry). The surfaces tested are detailed in Table 5.1, divided by the surface and the specific item used to represent that surface.

<u>Surface</u>	<u>Item</u>
Glass	Glass microscope slide
Metal	Aluminium Coca-Cola can
Plastic	\$5 New Zealand banknote
Wood	Wooden block

*Table 5.1: Surface trials for fingerprint powders.*

#### 5.2.2.2 Powder quantities

To determine the optimum amount of powder needed to get maximum exposure of a print, varied amounts were applied to prints on a glass slide. The quantities trialled were 0.005 g and 0.02 g.

### **5.2.2.3 Effect of print age**

Trials were conducted to determine the effect of fingerprint age on the influence of development with the powders. Fingerprints were deposited on glass slides, and left for the following periods of time: 6 hours, 24 hours, and 72 hours. The prints were then exposed with powders and compared with the standard prints.

### **5.2.2.4 Effect of temperature variation on print exposure**

Prints left on glass slides were exposed to varied temperatures prior to application of powders to investigate any effect this may have on print quality. Prints were applied to glass slides, and exposed to either 2 minutes in a 100 °C oven, or 2 hours in a fridge. The prints were then exposed with powders and compared with the standard prints.

### **5.2.2.5 Effect of brush on print exposure**

Prints that were deposited on glass slides were dusted with print powders using a feather brush, and the exposed prints then compared to the standard prints that had been exposed with a badger hair brush. Between each powder, the feather brush was rinsed with acetone and water, then lightly blow-dried.

## **5.2.3 Imaging of exposed fingerprints**

To display data for comparative purposes, images of the exposed latent prints under different conditions were taken where possible. Picture quality was at times compromised due to the difficult conditions of photographing under UV light, due to the need for a dark room to visualise the luminescence, but inability to use a flash. Images were taken on a Fujifilm FinePix S-5600 digital camera, stabilised on a tripod. The contrast and brightness of some images were modified to try and better recreate the observed prints.

### 5.2.4 Police fingerprinting laboratory

The doped talcum powder samples were taken to the Hamilton City Police department, for analysis using their fingerprinting laboratory. The powders were trialled by a member of the fingerprinting unit, on a range of surfaces. A Polylight was used to illuminate the powders, however due to the specific wavelengths the doped talcum powders responded to, only the  $\text{Eu}(\text{tta})_3(\text{p}=\text{o})$  powder could be viewed in these conditions. Other powders were trialled solely for their performance in non-UV conditions. The surfaces that were investigated were aluminium, plastic, smooth wood, porous plastic and Formica™ bench top. Prints were placed on the surfaces through random placing of the hand on specific objects. To dust the prints, the powders were loaded onto fibreglass brushes, and gradually adhered to the latent prints.

## 5.3 Results

In each trial, the powders were trialled to observe their ability to visualise a print with and without UV light. The images displayed below are a representation of the prints obtained from each method, however due to the difficult photography conditions mentioned previously not all images gave a fair representation of print quality.

### 5.3.1 Surface trials

#### 5.3.1.1 Glass surface

Table 5.2 displays the exposure of latent prints on glass with powders exhibiting red luminescence. Redwop was used as the standard of comparison.

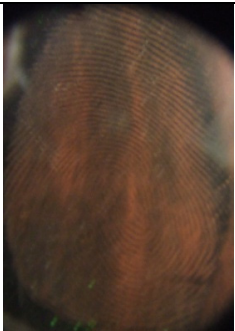
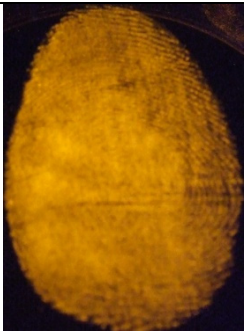

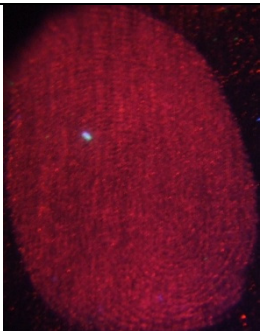

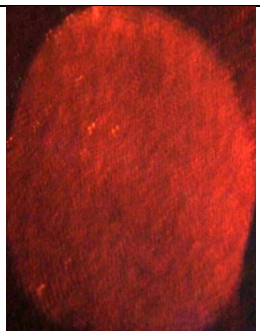
<u>Compound</u>	<u>No UV</u>	<u>UV</u>
Redwop		
Eu(tta) <sub>3</sub> (p=O)		
[H <sub>2</sub> NMe <sub>2</sub> ] <sub>3</sub> [Eu(2,6-dpa) <sub>3</sub> ].2H <sub>2</sub> O		

Table 5.2: Red luminescent powders on glass, displayed with and without UV excitation.

Table 5.3 displays the exposure of latent prints with powders exhibiting green luminescence. Greenwop was used as the standard of comparison.

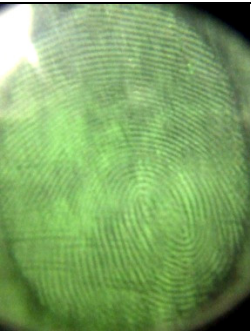
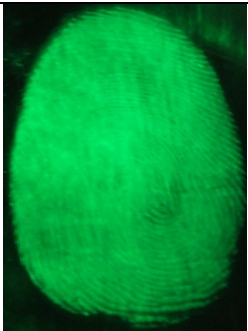

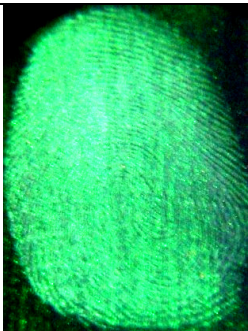

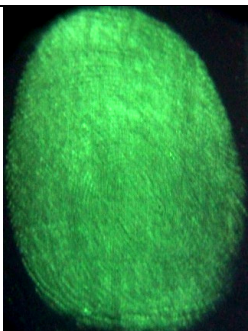
<u>Compound</u>	<u>No UV</u>	<u>UV</u>
Greenwop		
Tb(acac) <sub>3</sub> (p=O)		
[H <sub>2</sub> NMe <sub>2</sub> ] <sub>3</sub> [Tb(2,6-dpa) <sub>3</sub> ].2H <sub>2</sub> O		

Table 5.3: Green luminescent powders on glass, displayed with and without UV excitation.

All powders gave clear, visible prints on the clean glass surface. With no UV illumination, the talcum powders gave much more effective visualisation of the prints as compared to the wop powders. To best visualise without UV the glass had to be placed on a dark surface with a good light source on it. With UV excitation, the wop powders gave more intense exposure of the latent prints. The talcum powders gave notable exposure under UV conditions, with Eu(tta)<sub>3</sub>(p=O) the most intense of the talc powders. However the talcum powders seemed to have a grainy

appearance under UV conditions, where as the “wop” powders gave more significant definition between ridge spaces.

### 5.3.1.2 Aluminium surface

Table 5.4 displays the exposure of latent prints on aluminium with powders exhibiting red luminescence. Redwop was used as the standard of comparison.

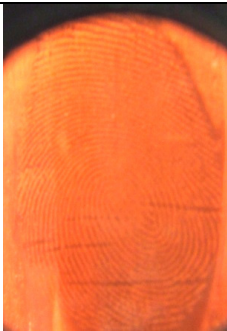

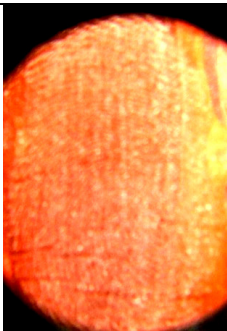
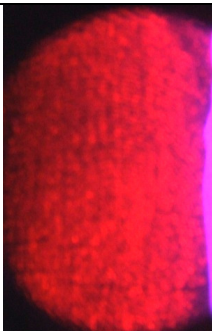

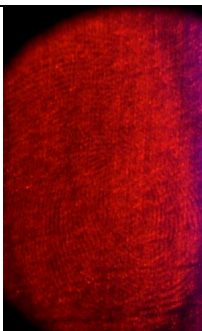
<u>Compound</u>	<u>No UV</u>	<u>UV</u>
Redwop		
Eu(tta) <sub>3</sub> (p=O)		
[H <sub>2</sub> NMe <sub>2</sub> ] <sub>3</sub> [Eu(2,6-dpa) <sub>3</sub> ].2H <sub>2</sub> O		

Table 5.4: Red luminescent powders on aluminium, displayed with and without UV excitation.

Table 5.5 displays the exposure of latent prints on aluminium with powders exhibiting green luminescence. Greenwop was used as the standard of comparison.


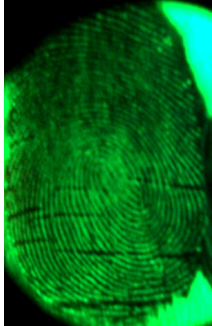

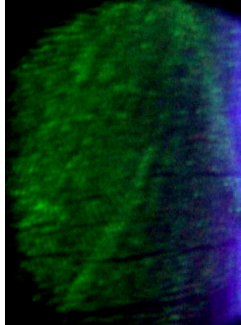
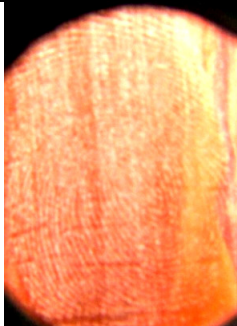
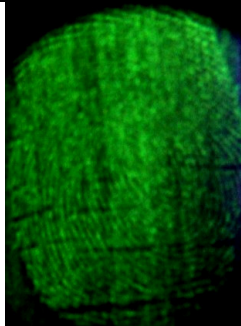
<u>Compound</u>	<u>No UV</u>	<u>UV</u>
Greenwop		
Tb(acac) <sub>3</sub> (p=O)		
[H <sub>2</sub> NMe <sub>2</sub> ] <sub>3</sub> [Tb(2,6-dpa) <sub>3</sub> ].2H <sub>2</sub> O		

Table 5.5: Green luminescent powders on aluminium, displayed with and without UV excitation.

All talcum powders gave observable non-UV print exposure, however the “wop” powders both gave better ridge definition. Under UV excitation, both “wop” powders gave superior definition of the print structure. Of the doped talcum powders, the [H<sub>2</sub>NMe<sub>2</sub>]<sub>3</sub>[Tb(2,6-dpa)<sub>3</sub>].2H<sub>2</sub>O and [H<sub>2</sub>NMe<sub>2</sub>]<sub>3</sub>[Eu(2,6-dpa)<sub>3</sub>].2H<sub>2</sub>O powders gave the best definition under UV and non UV conditions.



### 5.3.1.3 Plastic surface

Table 5.6 displays the exposure of latent prints on a plastic bank note with powders exhibiting red luminescence. Redwop was used as the standard of comparison. No images were taken under a non UV setting for this surface, as no visible print was obtainable for any powder.

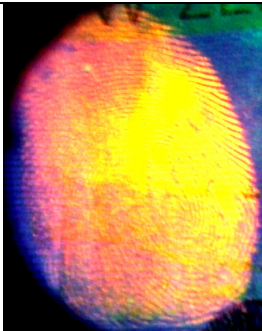
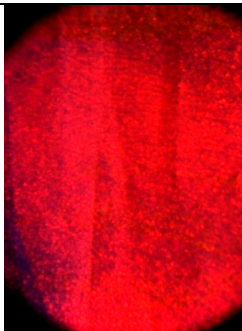
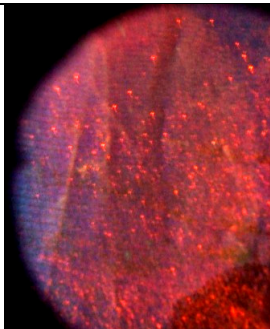
<u>Compound</u>	<u>UV</u>
Redwop	
Eu(tta) <sub>3</sub> (p=O)	
[H <sub>2</sub> NMe <sub>2</sub> ] <sub>3</sub> [Eu(2,6-dpa) <sub>3</sub> ].2H <sub>2</sub> O	

Table 5.6: Red luminescent powders on a plastic bank note, displayed with UV excitation.



Table 5.7 displays the exposure of latent prints on a plastic bank note with powders exhibiting green luminescence. Greenwop was used as the standard of comparison. As above, no images were taken under a non UV setting for this surface, as no visible print was obtainable for any powder. Furthermore, no print was exposed under UV or non UV for the  $\text{Tb}(\text{acac})_3(\text{p}=\text{o})$  powder, so no image was displayed.

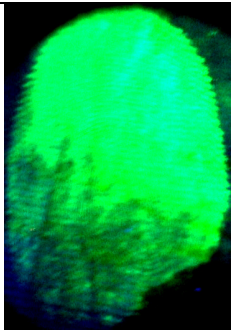
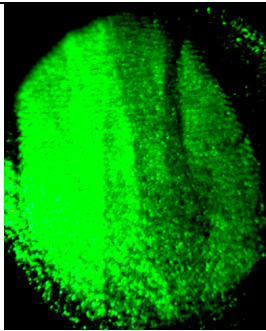
<u>Compound</u>	<u>UV</u>
Greenwop	
$\text{Tb}(\text{acac})_3(\text{p}=\text{o})$	N/A
$[\text{H}_2\text{NMe}_2]_3[\text{Tb}(\text{2,6-dpa})_3] \cdot 2\text{H}_2\text{O}$	

Table 5.7: Green luminescent powders on a plastic bank note, displayed with UV excitation.

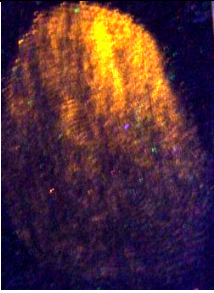
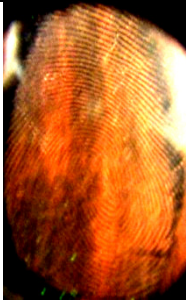


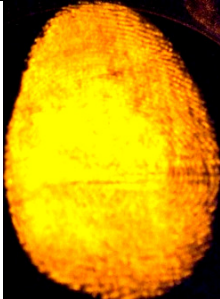
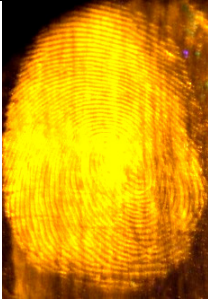



No powders in this trial gave good quality prints. The talcum powder doped with  $\text{Tb}(\text{acac})_3(\text{p}=\text{o})$  resulted in no print under UV or non UV conditions. The “wop” powders displayed greater selectivity in exposing the print without contaminating the background, but ridge detail was still minimal. The most successful talcum powder was from  $[\text{H}_2\text{NMe}_2]_3[\text{Tb}(\text{2,6-dpa})_3] \cdot 2\text{H}_2\text{O}$ , which gave a defined, observable print under UV exposure.

### 5.3.1.4 Wooden surface

No prints of any discernable quality were obtained from the wooden surface. It was the most porous of the surfaces, and the powders exhibited poor adhesion. No quality images were obtained.

### 5.3.2 Powder quantity trials

A comparison of all the powder quantities used that exhibited red luminescence is detailed in Table 5.8. The 0.01 g prints are those from the original glass trial. Redwop is used as the standard of comparison.

		<u>0.005 g</u>	<u>0.01 g</u>	<u>0.02g</u>
Redwop	No UV			
	UV			
Eu(tta) <sub>3</sub> (p=O)	No UV			

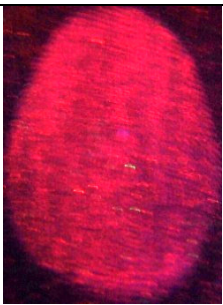
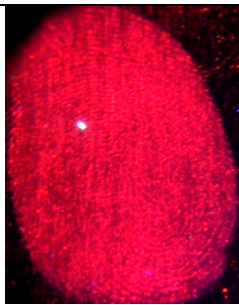
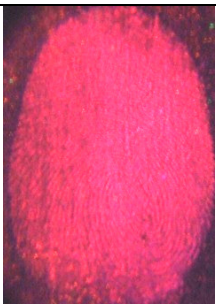



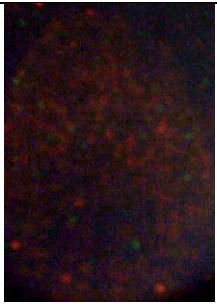
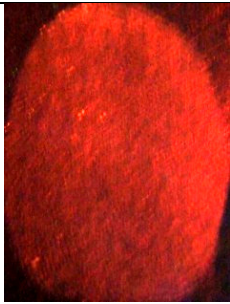
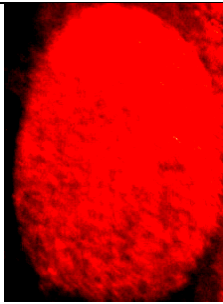
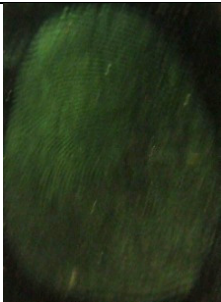

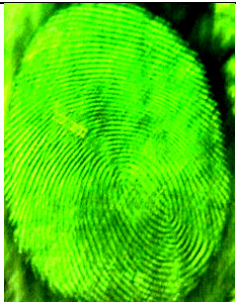
	UV			
[H <sub>2</sub> NMe <sub>2</sub> ] [Eu(2,6-dpa) <sub>3</sub> ].2H <sub>2</sub> O	No UV			
	UV			

Table 5.8: A comparison of red luminescent powders, applied in quantities of 0.005 g, 0.01 g and 0.02 g.

A comparison of all the powder quantities used that exhibited green luminescence is detailed in Table 5.9. The 0.01 g prints are those from the original glass trial. Greenwop is used as the standard of comparison.

		<u>0.005 g</u>	<u>0.01 g</u>	<u>0.02g</u>
Greenwop	No UV			



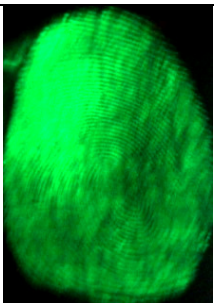
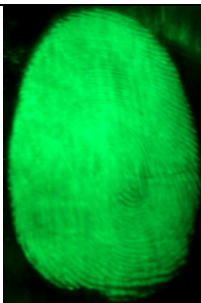
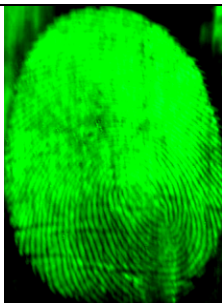

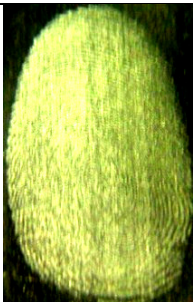

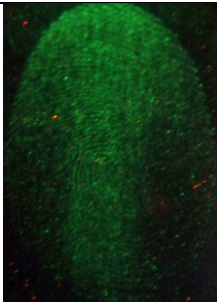
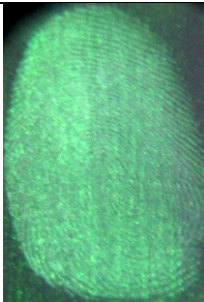
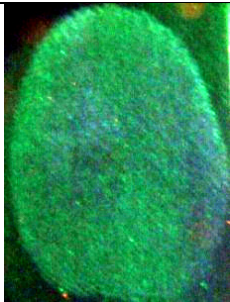



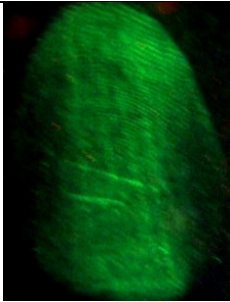
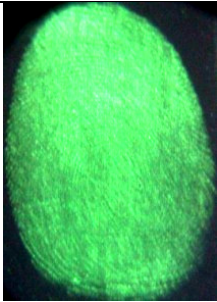
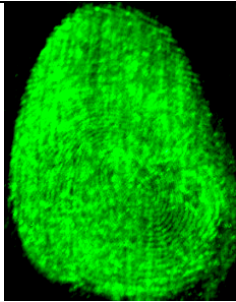
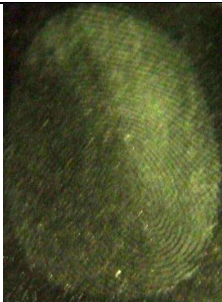

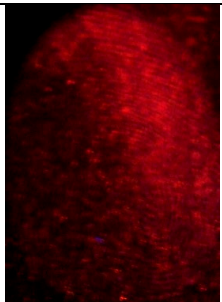
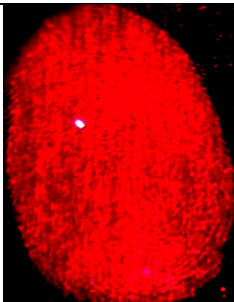
	UV			
Tb(acac) <sub>3</sub> (p=O)	No UV			
	UV			
[H <sub>2</sub> NMe <sub>2</sub> ] <sub>3</sub> [Tb(2,6-dpa) <sub>3</sub> ].2H <sub>2</sub> O	No UV			
	UV			



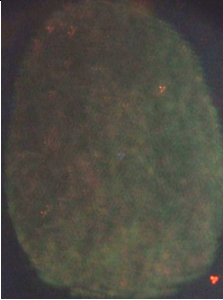
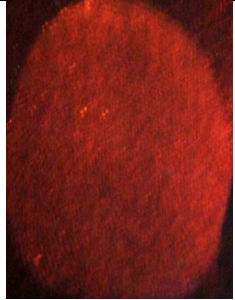


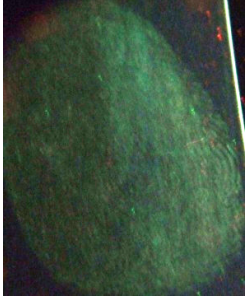
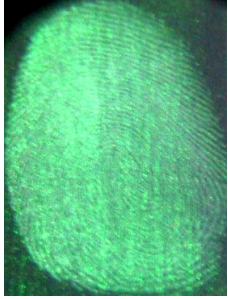


Table 5.9: A comparison of green luminescent powders, applied in quantities of 0.005 g, 0.01 g and 0.02 g.

This prints obtained from this trial indicated that 0.01 g of powder is suitable for giving reproducible imaging of a thumb print. Overall, the 0.02 g prints appeared to have the best detail definition, especially for the “wop” powders. For the talcum powders, it appeared that a limited amount of powder could give good resolution under non UV conditions, however when UV was applied the intensities were weaker than would be ideal.

### 5.3.3 Feather brush trials

Table 5.10 below displays all prints exposed with a feather brush, with images of those prints exposed with a badger hair brush for comparison. No “wop” comparisons were used in this trial as all “wop” powders were applied with the use of a feather brush.

		<u>Feather brush</u>	<u>Badger brush</u>
Eu(tta) <sub>3</sub> (p=0)	No UV		
	UV		

$[\text{H}_2\text{NMe}_2]_3[\text{Eu}(2,6\text{-dpa})_3] \cdot 2\text{H}_2\text{O}$	No UV		
	UV		
$\text{Tb}(\text{acac})_3(\text{p}=\text{o})$	No UV		
	UV		
$[\text{H}_2\text{NMe}_2]_3[\text{Tb}(2,6\text{-dpa})_3] \cdot 2\text{H}_2\text{O}$	No UV		



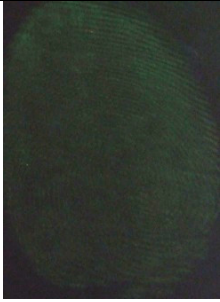
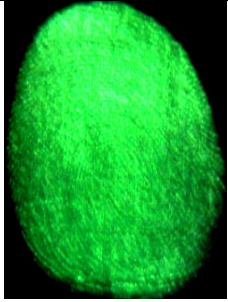
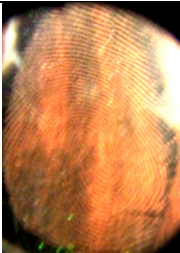

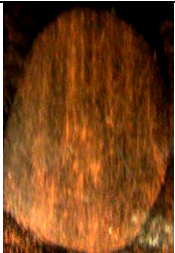

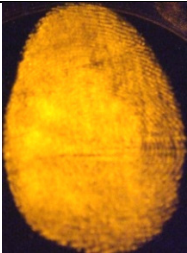
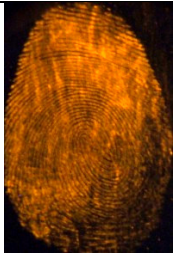
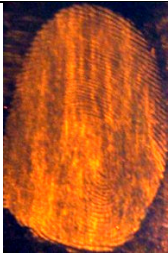
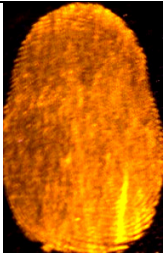
	UV		
--	----	--	---

Table 5.10: Comparison of doped talcum powders when applied with a feather or badger hair brush.

While the feather brush gave notably less overloading of the print with powder, the load was not sufficient to get a good contrasting print. Some good results were obtained with a feather brush under non-UV conditions, however not enough powder was loaded to give any useful intensity when viewed under UV light.

### 5.3.4 Print age trials

Table 5.11 displays a comparison of all powders that exhibited red luminescence across latent prints that had been left for differing time intervals. Redwop was used as a standard for comparing quality of the powders.

		<u>Instant</u>	<u>6 hours</u>	<u>24 hours</u>	<u>72 hours</u>
Redwop	No UV				
	UV				


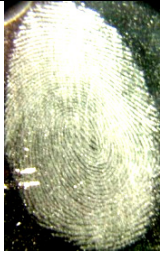
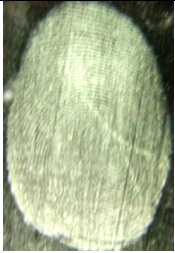

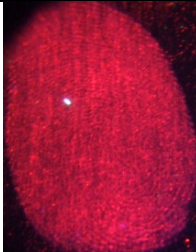
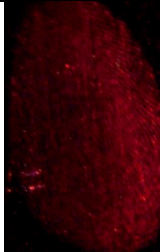
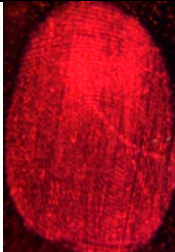
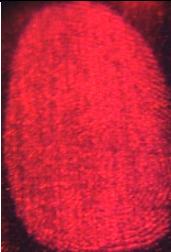



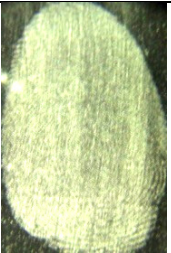
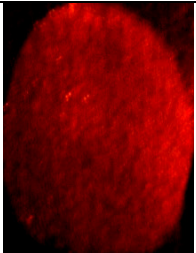
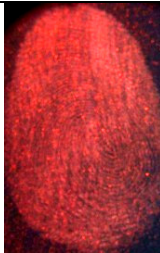
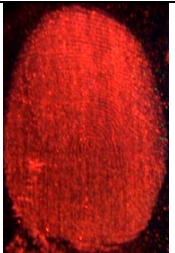
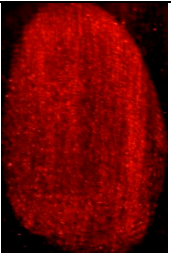

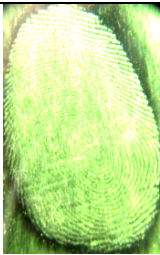
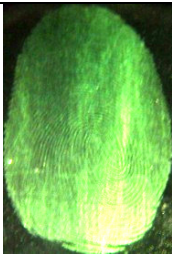
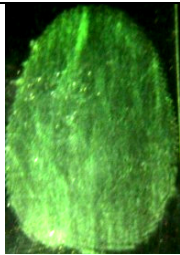
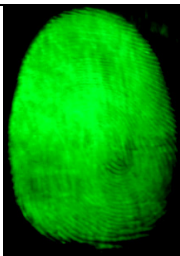
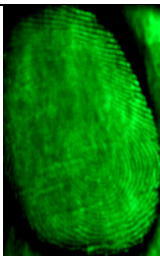
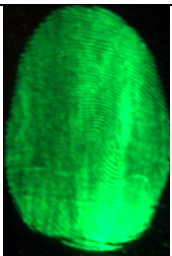
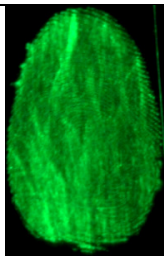



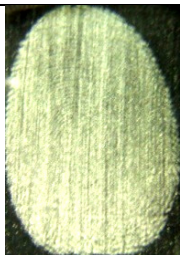
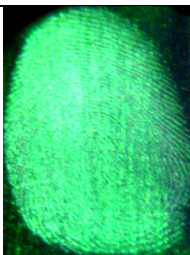
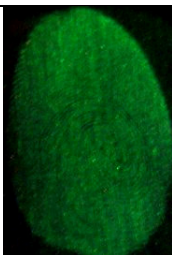
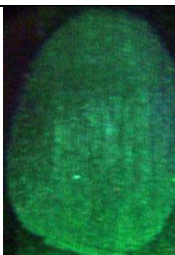
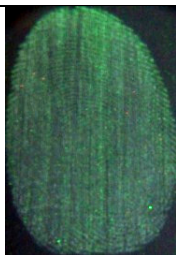
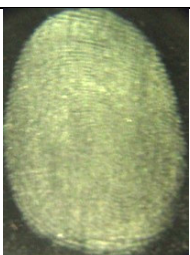


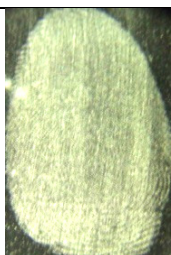
Eu(tta) <sub>3</sub> (p =o)	No UV				
	UV				
[H <sub>2</sub> NMe <sub>2</sub> ] [Eu(2,6- dpa) <sub>3</sub> ].2H <sub>2</sub> O	No UV				
	UV				

Table 5.11: A comparison of red luminescent powders, applied to prints immediately, after 6 hours, after 24 hours and after 72 hours.

Table 5.12 displays a comparison of all powders that exhibited green luminescence across latent prints that had been left for differing time intervals. Greenwop was used as a standard for comparing quality of the powders.



		<u>Instant</u>	<u>6 hours</u>	<u>24 hours</u>	<u>72 hours</u>
Greenwop	No UV				
	UV				
Tb(acac) <sub>3</sub> (p=0)	No UV				
	UV				
[H <sub>2</sub> NMe <sub>2</sub> ] <sub>3</sub> [Tb(2,6-dpa) <sub>3</sub> ].2H <sub>2</sub> O	No UV				

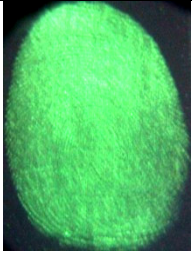
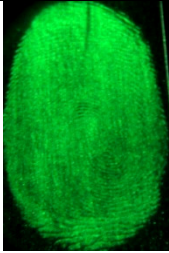
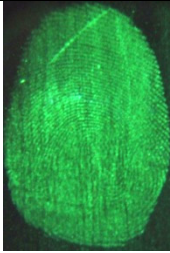
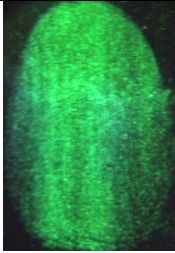
	UV				
--	----	---	---	---	---

Table 5.12: A comparison of green luminescent powders, applied to prints immediately, after 6 hours, after 24 hours and after 72 hours.

The effects of delayed exposure of the prints appeared to have no notable effect on the quality of the prints. Definition of ridges could be obtained on prints of all time intervals, and there appeared to be no effect on the adhesion of the powders to the latent prints.

5.3.5 Temperature trials

The exposure of the prints on glass to heat appeared to have no effect on the quality of exposure, and the prints obtained were vastly similar to those from the glass surface trial. The prints on the glass surfaces that were exposed to frigid conditions became damp, and the moisture interfered with the powder exposure method. The powders could not selectively adhere to the print constituents, and background interference obscured any print definition. The only exception was the  $Tb(acac)_3(p=0)$  print, which managed some print resolution under these conditions. Figure 5.1 shows the print exposed with  $Tb(acac)_3(p=0)$ .

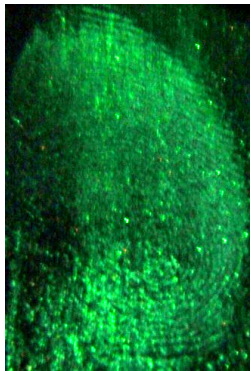


Figure 5.1: Latent print exposed with  $Tb(acac)_3(p=0)$  print under frigid conditions.

### 5.3.6 Police laboratory results

#### 5.3.6.1 Preliminary trials

All four powders were initially trialled on glass under non-UV conditions to investigate their potential. Highly magnified monochrome images of the prints were then taken to get a clear view of the quality of exposure. Figure 5.2 shows the images taken of the prints under non-UV conditions on glass.

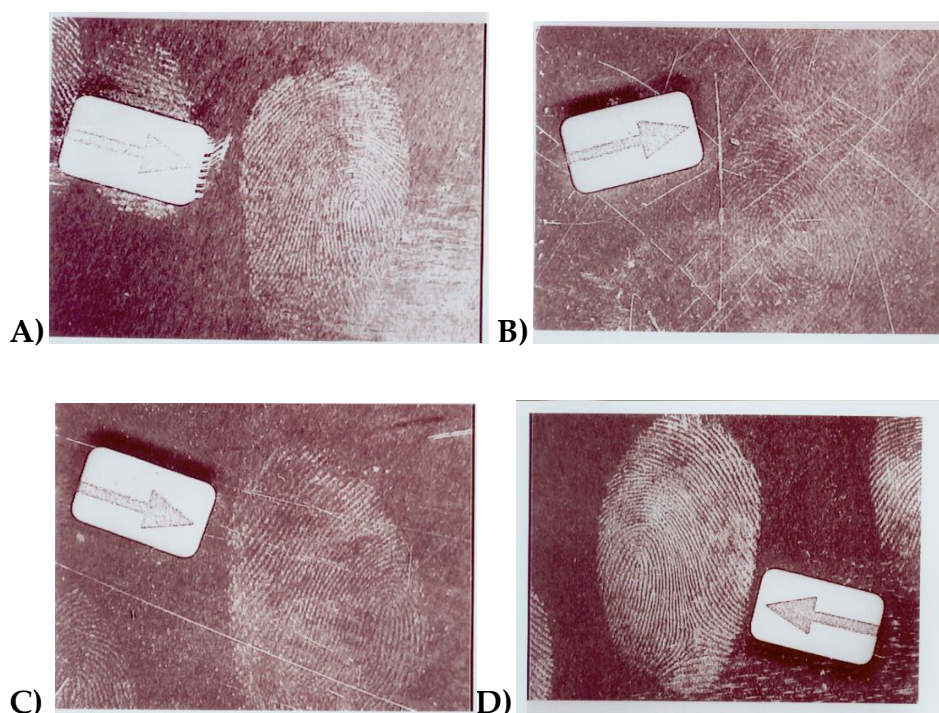


Figure 5.2: Images of talcum powder exposed prints on glass with no UV. A)  $\text{Eu}(\text{tta})_3(p=0)$  B)  $[\text{H}_2\text{NMe}_2]_3[\text{Eu}(2,6\text{-dpa})_3] \cdot 2\text{H}_2\text{O}$  C)  $\text{Tb}(\text{acac})_3(p=0)$  D)  $[\text{H}_2\text{NMe}_2]_3[\text{Tb}(2,6\text{-dpa})_3] \cdot 2\text{H}_2\text{O}$ .

All powders gave some exposure of the latent prints, however the best quality prints were obtained with the  $[\text{H}_2\text{NMe}_2]_3[\text{Tb}(2,6\text{-dpa})_3] \cdot 2\text{H}_2\text{O}$  powder. From the observations of the officer assisting with the trials, this powder gave excellent print definition while not distributing powder to the background. Lifts were also done using adhesive tape to preserve the prints, and worked effectively. An image was also taken of the  $\text{Eu}(\text{tta})_3(p=0)$  powder, illuminated by a UV light source at 350 nm. Figure



5.3 displays this image, compared with the image of the  $\text{Eu}(\text{tta})_3(\text{p}=\text{o})$  powder under non-UV conditions.

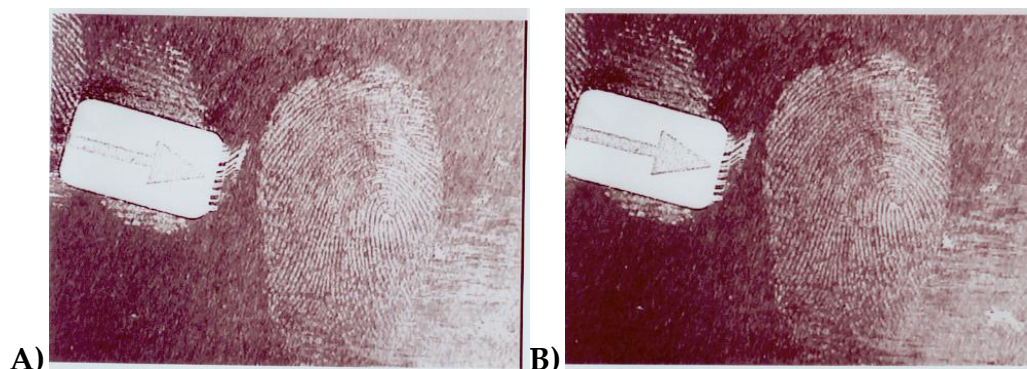


Figure 5.3: Images of prints exposed with  $\text{Eu}(\text{tta})_3(\text{p}=\text{o})$  powder. A) no UV B) 350 nm excitation.

Under the photography conditions, the powder was effective both with and without UV excitation.

#### 5.3.6.2 Surface trials and luminescent imaging

Due to the superior non-UV performance of the  $[\text{H}_2\text{NMe}_2]_3[\text{Tb}(\text{2,6-dpa})_3] \cdot 2\text{H}_2\text{O}$  powder and the fact that luminescent activity could only be obtained from the  $\text{Eu}(\text{tta})_3(\text{p}=\text{o})$  powder with the police Polylight, only these two powders were used for subsequent trials.

Initial trials on surfaces were undertaken with no UV illumination. On the aluminium surface, both powders gave some exposure of latent prints, but background interference was noticeable. Both powders performed better on smooth plastic, with print details easily observable. The wood surface gave faint prints for both powders, with some ridge detail observable. The porous plastic surface gave no prints for either powder. Under non-UV conditions, the Formica™ bench top gave no well observable prints.

Luminescent imaging was undertaken of the  $\text{Eu}(\text{tta})_3(\text{p}=\text{o})$  powder. Figures 5.4 through 5.6 show high quality images of the prints taken on the glass, smooth plastic and aluminium. The yellow tint observed in these images is a result of the lens filter that was used.

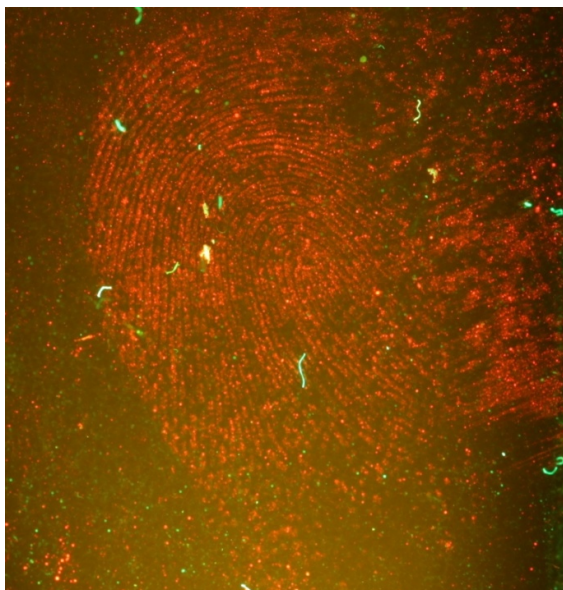


Figure 5.4: Fingerprint on glass exposed with  $\text{Eu}(\text{tta})_3(\text{p=O})$  powder, exposed with 350 nm light.

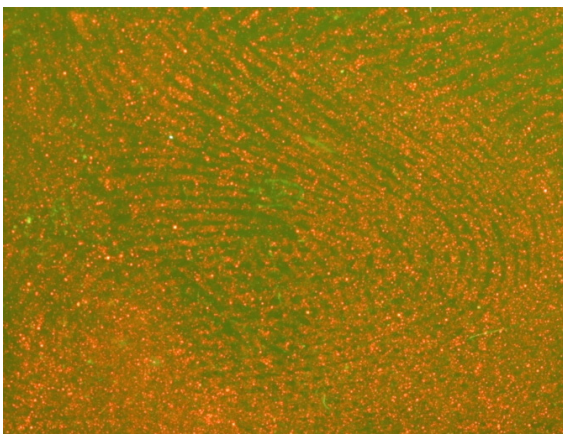


Figure 5.5: Fingerprint on plastic exposed with  $\text{Eu}(\text{tta})_3(\text{p=O})$  powder, exposed with 350 nm light.

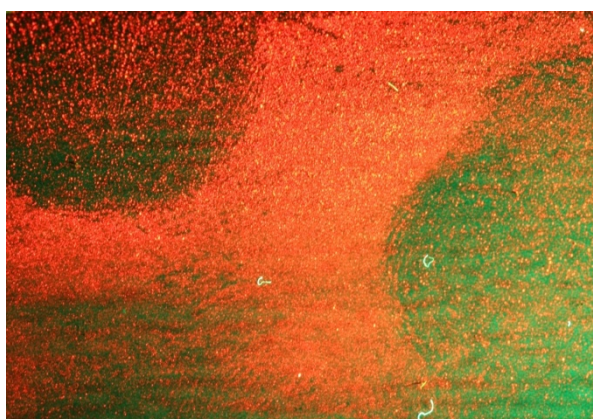


Figure 5.6: Fingerprints on aluminium exposed with  $\text{Eu}(\text{tta})_3(\text{p=O})$  powder, exposed with 350 nm light.

The best contrast is observed on the glass print. Across all prints, a noticeable speckling effect can be observed, which compromised the quality of the prints. Severe adhesion of the powder to the background of the aluminium can be observed, however it was suggested this was as a result of the specific item used, not from the aluminium itself.

## **5.4 Discussion**

### **5.4.1 Quality of doped talcum powders compared to commercial Greenwop/Redwop samples**

When trialled on a glass surface, the most obvious difference between the “wop” and talcum powders was the specificity of which the powders adhered to the latent fingerprint. The “wop” powders gave much more definitive ridges and troughs contrasting to the glass surface, where as the talcum powders seemed to overload these troughs, obscuring detail. This difference was notable across all surface trials, and when viewed under UV conditions this overloading gave a “grainy” effect which compromised clarity.

One possible benefit the talcum powders have against the “wop” powders is their dual appearances under non-UV and UV conditions. The talcum powders give the options for white prints which can further be enhanced by illumination with UV light. The “wop” powders exhibit fluorescence in the same colour as their powder, which means any strong background colour interference could compromise clarity under non-UV and UV conditions.

Overall, the clarity and definition of the “wop” powders was superior to that of the talcum powders in these trials. Regardless, the talcum powders still gave promising results under many conditions.

#### **5.4.2 Factors influencing best use of the doped talcum powders for latent print exposure**

The talcum powders showed the ability to expose prints with reasonable definition on a range of surfaces. The glass and aluminium surfaces gave the best results, while the plastic application showed some print exposure. It is important to note that the nature of the surfaces could have a large influence on the quality of the print that is obtained. While the Banknote gave relatively poor prints compared to the glass and aluminium, a smoother plastic surface with less background colour interference would likely give much clearer prints. This is backed up by results from the police station fingerprinting trials, where a clear plastic surface gave clear, defined prints when exposed with a doped talcum powder.

From testing the appropriate quantities, it appeared that prints could be overloaded with the talcum powders. Using a scarce amount of powder gave better resolution and contrast of ridges in the print under non-UV conditions; however by loading the print with too little powder luminescent intensity was compromised. From this, the best approach may be a gradual application of the powder, first exposing it in non-UV conditions, the subsequently loading the print with more powder to increase UV intensity. The use of a feather brush helped avoid overloading the print, however again luminescent intensity was weak from the feather brush application. This could also be overcome by repeated applications of the powder until desired intensities were achieved.

The delay in exposure of the prints appeared to have no effect on the quality that was achieved. All time delays gave the same relative quality of print with each powder. It is worth considering that these time delays occurred in a lab setting, where interference from outside sources is

minimal. This meant that the glass on which the prints were placed was not exposed to any conditions which could have a dramatic effect on the exposure quality.

### **5.4.3 Assessment of powders by police fingerprinting officers**

Through discussion with members of the Hamilton City police fingerprinting unit, conclusions were reached on the performance of the powder. As discussed earlier in this chapter, because there is no way to empirically quantify the quality of a print exposed by a specific powder, it is often a case of personal preference for individual officers as to what powders are used in practice.

One distinct benefit agreed upon by the officers was the dual ability of the powders to expose under non-UV and UV conditions. Because of this property, the talcum powders could be used as a broad powder for detecting prints on a surface, and then used to further expose good quality individual prints which could then be viewed under UV conditions. One main drawback which was noticed in the use of the  $\text{Eu}(\text{tta})_3(\text{p=O})$  powder under UV conditions was the speckling effect that occurred. This could be attributed to particles of the  $\text{Eu}(\text{tta})_3(\text{p=O})$  compound that were not equally distributed through the talcum powder. This could be remedied through a milling procedure that gives a more homogeneous powder.

The general consensus was that the talcum powders have promise in their use as latent fingerprinting agents. The biggest upside to these powders was seen as their ability to act as a basic white dusting powder, and then provide alternate means of imaging through UV excitation. Improvements could be made through reduction of the speckling effect seen when exposed by UV light and less attachment of the powders to the background of the item being dusted.



It is important to note the differences between the police laboratory trials and the trials undertaken in the research lab. The trials in the police laboratory were designed to replicate more likely scenarios whereas a strictly scientific approach was taken in the research laboratory. One example of this was deposition of fingerprints on the trialled surfaces. Uniformed, reproducible prints were specifically placed on surfaces for the research trials, as opposed to more random prints that were placed from handling the surfaces for the police trials. Furthermore, the brushes used in the police trials were fibreglass brushes, which gave a much better delivery of the powder to the print surface, as opposed to the badger hair brush used in research trials, which at times had a destructive effect on the prints.

## **5.5 Chapter summary**

Talcum powder doped with four promising luminescent lanthanide compounds were trialled for their ability to expose latent fingerprints. The powders were trialled across several different variables including surface, powder quantity, age of latent print, temperature, and the brush used. The powders were compared to commercial powder samples Greenwop and Redwop to gain insight into how they compared against established luminescent powders. While the commercial “wop” powders proved to give superior print definition than the doped talcum powders, the talcum powders successfully gave exposure of latent prints under a range of conditions, with and without UV illumination.

Trials undertaken at a police fingerprinting lab were used to obtain a professional opinion on the quality and usefulness of the powders. Members of the police fingerprinting unit concluded the doped talcum powders made for good printing powders, with their ability to visualise

prints under non UV and UV conditions especially useful. Recommendations were also made for possible improvements, specifically removing the effect of speckling under UV excitation, and improving selectivity of the powder to the print and not the background.

It was concluded that these lanthanide doped talcum powders expose latent prints best on smooth surfaces, specifically glass. A gradual application of the powder is useful for exposing a print under non UV conditions, without overloading and spoiling clarity and definition. To enhance intensity under UV conditions, more powder can be loaded on with subsequent brushing.

## 6 Conclusions and recommendations

### 6.1 Conclusions

#### 6.1.1 Synthesis of $(\text{Me})_3\text{CN}(\text{CH}_2\text{P}(\text{O})\text{Ph}_2)_2$ ligand and $\text{Ln}(\beta\text{-diketonate})_3(\text{p}=\text{o})$ compounds

Through a slightly modified literature procedure, the  $(\text{Me})_3\text{CN}(\text{CH}_2\text{P}(\text{O})\text{Ph}_2)_2$  ligand was synthesised. A range of characterisation techniques were used to confirm successful synthesis of this ligand. When sufficient evidence was obtained, the  $\text{Ln}(\beta\text{-diketonate})_3(\text{p}=\text{o})$  compounds were synthesised and characterised by the same methods. Characterisation data suggested that these compounds were also successfully synthesised. Further analysis of luminescent character through fluorescence spectroscopy and direct visualisation with a UV light source indicated intense luminescent emissions could be obtained from the  $\text{Ln}(\beta\text{-diketonate})_3(\text{p}=\text{o})$  compounds. This suggested the initial hypothesis that the  $(\text{Me})_3\text{CN}(\text{CH}_2\text{P}(\text{O})\text{Ph}_2)_2$  ligand would work as an effective neutral ligand for blocking inner coordination sites in the lanthanide complex in place of traditional ligands such as 1,10-phenanthroline, were correct.

#### 6.1.2 Analysis of particle character of doped talcum powders

Talcum powder was doped with a series of  $\text{Ln}(\beta\text{-diketonate})_3(\text{phen/bipy})$  compounds, and the particle character was analysed by Scanning Electron Microscopy (SEM) and laser diffraction methods. Commercial Greenwop and Redwop fingerprinting powder samples were also analysed by these methods to compare particle structure. Experiments to determine the effects of particle modification by sonication of the powders were also undertaken.

Doping of the compounds into the powder yielded a decrease in size of the talc particles of  $\sim 4\ \mu\text{m}$ . This was attributed to part of the doping process where the powders are ground with a pestle and mortar to ensure homogeneity. Sonication appeared to yield a decrease in particle size and an increase in specific surface area, two characteristics which were hypothesised to improve performance in exposing latent fingerprints. However any improvements were not sufficient enough to justify including powder sonication as an efficient step in the manufacture of doped talcum powders.

The “wop” samples showed they consisted of lycopodium spores roughly  $30\ \mu\text{m}$  in size, packed with smaller particles of  $\sim 10\ \mu\text{m}$  size. The smaller particles appeared to have a similar flaky morphology as the talcum powder. It is postulated that the spores in the “wop” powders act as vessels for distributing the smaller particles to the residues of latent prints, following which the spores are brushed away.

### **6.1.3 Analysis of luminescent character of lanthanide complexes**

A range of lanthanide compounds were analysed for their luminescent character,  $\text{Eu/Tb}(\beta\text{-diketonate})_3(\text{phen/bipy})$ ,  $\text{Eu/Tb}(\beta\text{-diketonate})_3(\text{p=O})$  and  $[\text{H}_2\text{NMe}_2]_3[\text{Eu/Tb}(2,6\text{-dpa})_3]\cdot 2\text{H}_2\text{O}$ . Fluorescence spectroscopy and direct visualisation with a UV lamp with excitation wavelengths of 254 nm and 312 nm were used to determine the compounds of strongest luminescent intensity.

The dominant emission wavelengths were determined to be at 510 nm for 254 nm excitation, and 625 nm for 312 nm excitation. While fluorescence spectroscopy was often a good indicator of exhibited luminescent intensity, some compounds which exhibited peaks of over 1000 intensity did not

produce strong intensities when excited by a UV wavelength. These exceptions could be attributable to inorganic impurities in the sample.

#### **6.1.4 Evaluation of doped talcum powders for their performance in exposing latent fingerprints**

Four powders were selected and trialled for their use in exposing latent fingerprints. Several variables were tested including surface, powder quantity, age of latent print, temperature, and the brush used. Further tests were also done with the assistance of the Hamilton City police fingerprinting department. Commercial Greenwop and Redwop samples were used as comparisons for powder performance, as they were established powders that perform a very similar role.

In direct comparison with the Wop samples the doped talcum powders were inferior, in terms of clarity of print exposure. Definition of ridge patterns was much clearer with the “wop” powders, especially under UV conditions.

Despite this the powders still had some promising applications. They worked best on smooth surfaces, especially glass. One noted advantage is the ability of the doped talcum powders to expose prints with the white colour of basic talcum powder, and then provide alternate means of exposure through UV excitation. As they stand as luminescent fingerprinting powders they are not as effective as the industrially established “wop” powders, however improvements could make them viable alternatives.

## **6.2 Future recommendations**

While sufficient characterisation evidence was collected to assume the successful synthesis of the  $(\text{Me})_3\text{CN}(\text{CH}_2\text{P}(\text{O})\text{Ph}_2)_2$  ligand and the  $\text{Ln}(\beta-$

diketonate)<sub>3</sub>(p=O) ligands, X-ray diffraction studies would provide useful information and further certainty about the compounds. Further research could also be done to modify the phosphine oxide ligand. Aminomethylphosphine oxides are versatile ligands, and the *tert*-butyl group could be substituted to change the properties of the lanthanide compounds.

Additional research into the processing of the doped talcum powder could greatly enhance the powders ability to expose latent fingerprints. Longer sonication times on a large scale, or perhaps processing of talcum powders in a colloid mill could yield smaller particle size powders. However it seems that with smaller particle size, an affinity for the print residue is equally important, otherwise background interference of the print becomes a problem.

There are many possible routes that can be explored when further researching methods for improving latent print exposure. Several factors could improve the powders, such as increasing luminescent intensity by increasing concentration that is doped into the powder, improving homogeneity of the powders to reduce the speckling effect, use of a brush that best suits the powder and a greater affinity for the latent print residue. However for future research, a survey of police fingerprinting officers may yield useful advice. Through communicating with members of a fingerprinting unit, it seemed personal preference was often a large factor in why a powder was used. To create a powder that could break into the market, a valuable avenue of inquiry could be a list of preferences of those who will be using the product the most.

## 7 References

- [1] N. Grew, *Philosophical Transactions of the Royal Society of London* **1684**, 14, 566.
- [2] F. Galton, *Finger Prints*, Macmillan and Co., London, **1892**.
- [3] F. E. Inbau, *Journal of Criminal Law and Criminology (1931-1951)* **1934**, 25, 500.
- [4] C. Weyermann, C. Roux, C. Champod, *Journal of Forensic Sciences* **2011**, 56, 102.
- [5] D. E. Newton, *Forensic Chemistry*, Facts on File Inc., New York, **2007**.
- [6] J. B. Cheng, D. W. Russell, *The Journal of Biological Chemistry* **2004**, 239.
- [7] G. S. Sodhi, J. Kaur, *Forensic Science International* **2000**, 120, 172.
- [8] L. A. Pérez-Maqueda, A. Duran, J. L. Pérez-Rodríguez, *Applied Clay Science* **2005**, 28, 245.
- [9] P. Czekanski, M. Fasola, J. Allison, *Journal of Forensic Sciences* **2006**, 51, 1323.
- [10] S. Morimoto, A. Kaminogo, T. Hirano, *Forensic Science International* **1998**, 97, 101.
- [11] C. Pounds, R. Grigg, T. Mongkolaussavaratana, *Journal of Forensic Sciences* **1990**, 35, 169.
- [12] I. M. Alaoui, E. R. Menzel, *Forensic Science International* **1996**, 77, 3.
- [13] N. Benedict, *Arizona Law Review* **2004**, 46, 519.
- [14] J.-C. G. Bünzli, N. André, M. Elhabiri, G. Muller, C. Piguet, *Journal of Alloys and Compounds* **2000**, 303-304, 66.
- [15] S. Cotton, *Lanthanide and Actinide Chemistry*, John Wiley & Sons Ltd Sussex, **2006**.
- [16] J. W. Mitchel, C. V. Banks, *Talanta* **1972**, 19, 1157.
- [17] Y. Hasegawa, Y. Wada, S. Yanagida, *Journal of Photochemistry and Photobiology* **2004**, 5, 183.
- [18] H. Coates, P. A. Theodore, in *United States Patent Office* (Ed.: A. W. M. Limited), England, **1962**.
- [19] J. Fawcett, P. A. T. Hoye, R. D. W. Kemmitt, D. J. Law, D. R. Russell, *Dalton Transactions* **1993**, 2563.
- [20] C. Sivriev, L. Žabski, *European Polymer Journal* **1994**, 30, 509.
- [21] Jurgen, G. E. Krauter, M. Beller, *Tetrahedron Letters* **2000**, 56, 771.
- [22] M. Keles, O. Altan, O. Serindag, *Heteroatom Chemistry* **2008**, 19, 113.
- [23] M. Keles, Z. Aydin, O. Serindag, *Journal of Organometallic Chemistry* **2007**, 692, 1951.
- [24] C. C. Hinckley, *Journal of the American Chemical Society* **1969**, 5160.
- [25] M. Bednarski, S. Danishefsky, *Journal of the American Chemical Society* **1983**, 105, 3716.
- [26] J. P. Caldwell, W. Henderson, N. D. Kim, *Journal of Forensic Sciences* **2001**, 46, 1332.
- [27] X. Gan, B. M. Rapko, E. N. Duesler, I. Binyamin, R. T. Paine, B. P. Hay, *Polyhedron* **2005**, 24, 469.
- [28] T. H. Siddal, *Journal of Inorganic and Nuclear Chemistry* **1963**, 25, 883.
- [29] H. Eccles, A. Naylor, *Chemistry and Industry* **1987**, 174.
- [30] E. M. Bond, X. Gan, J. R. Fitzpatrick, R. T. Paine, *Journal of Alloys and Compounds* **1998**, 271-273, 172.
- [31] X.-M. Gan, I. Binyamin, B. M. Rapko, J. Fox, E. N. Duesler, R. T. Paine, *Polyhedron* **2006**, 25, 3387.
- [32] A. Kochel, *Inorganica Chimica Acta* **2009**, 362, 1379.
- [33] N. Dodoff, N. Spassovska, S. Varbanov, G. Borisov, *Journal of Inorganic Biochemistry* **1990**, 39, 201.
- [34] H. Xu, K. Yin, L. Wang, W. Huang, *Thin Solid Films* **2008**, 516, 8487.

- [35] L. R. Melby, N. J. Rose, E. Abramson, J. C. Caris, *Journal of the American Chemical Society* **1964**, *86*, 5117.
- [36] H. Bauer, J. Blanc, D. L. Ross, *Journal of the American Chemical Society* **1964**, *86*, 5125.
- [37] S. Priya, M. S. Balakrishna, J. T. Mague, S. M. Mobin, *Inorganic Chemistry* **2003**, 1272.
- [38] R. Frański, B. Gierczyk, *Rapid Communications in Mass Spectrometry* **2005**, *19*, 2979.
- [39] J. Dilag, H. Kobus, A. V. Ellis, *Forensic Science International* **2009**, *187*, 97.
- [40] I. S. Stemple, G. W. Brindley, *Journal of the American Chemical Society* **1960**, *43*, 34.
- [41] R. Baan, *Inhalation Toxicology* **2007**, *19*, 213.
- [42] M. Huncharek, J. F. Geschwind, B. Kupelnick, *Anticancer Research* **2003**, *23*, 1955.
- [43] F. Dellisanti, G. Valdrè, M. Mondonico, *Applied Clay Science* **2009**, *42*, 398.
- [44] N. H. Jamil, S. Palaniandy, *Powder Technology* **2010**, *200*, 87.
- [45] W. Nai-Ning, Z. Hong-Jian, Y. Xian-Huang, *Advanced Powder Technology* **1992**, *3*, 7.
- [46] G. Eshel, G. Levy, U. Minglegrin, M. Singer, *Soil Science Society of America* **2004**, *68*, 736.
- [47] S. Wanogho, G. Gettinby, B. Caddy, *Forensic Science International* **1987**, *33*, 117.
- [48] M. McGarvey, D. McGregor, R. B. McKay, *Progress in Organic Coatings* **1997**, *31*, 223.
- [49] H. Adi, I. Larson, P. Stewart, *Powder Technology* **2007**, *179*, 90.
- [50] B. J. Jones, A. J. Reynolds, M. Richardson, V. G. Sears, *Science & Justice* **2010**, *50*, 150.
- [51] L. Reimer, *Scanning electron microscopy: physics of image formation and microanalysis*, Second ed., Springer, Munster, **1998**.
- [52] F. Goodarzi, *Fuel* **2006**, *85*, 273.
- [53] O. Ersoy, *Journal of Volcanology and Geothermal Research* **2010**, *190*, 290.
- [54] a) M. J. Choi, T. Smoother, A. A. Martin, A. M. McDonagh, P. J. Maynard, C. Lennard, C. Roux, *Forensic Science International* **2007**, *173*, 154; b) L. Wang, M. Yin, C. Guo, W. Zhang, *Journal of Rare Earths* **2010**, *28*, 16.
- [55] J. Dawson, R. Lucas, Random House Auckland, **2004**.
- [56] M. Balick, J. Beitel, *Economic Botany* **1989**, *43*, 373.
- [57] J. H. Wilce, *American Fern Journal* **1972**, *62*, 65.
- [58] A. D. McNaught, A. Wilkinson, (Ed.: IUPAC), Blackwell Scientific Publications, Oxford, **2006**.
- [59] in <http://web.uvic.ca/ail/techniques/epi-fluorescence.html>, Victoria University, **2005**.
- [60] J.-C. G. Bünzli, C. Piguet, *Chemical Society Reviews* **2005**, *34*, 1048.
- [61] D. Parker, J. A. G. Williams, *Dalton Transactions* **1996**, 3616.
- [62] N. M. Shavaleev, G. Accorsi, D. Virgili, Z. R. Bell, T. Lazarides, G. Calogero, N. Armaroli, M. D. Ward, *Inorganic Chemistry* **2005**, 61.
- [63] S. V. Eliseeva, J.-C. G. Bünzli, *Chemical Society Reviews* **2010**, 187.
- [64] L. Armelao, S. Quici, F. Barigelli, G. Accorsi, G. Bottaro, M. Cavazzini, E. Tondello, *Coordination Chemistry Reviews* **2010**, *254*, 487.
- [65] C. Freund, W. Porzio, U. Giovanella, F. Vignali, M. Pasini, S. Destri, A. Mech, S. Di Pietro, L. Di Bari, P. Mineo, *Inorganic Chemistry* **2011**, *50*, 5417.
- [66] J. Yuan, G. Wang, *TrAC Trends in Analytical Chemistry* **2006**, *25*, 490.
- [67] a) C.-H. Kim, I.-E. Kwon, C.-H. Park, Y.-J. Hwang, H.-S. Bae, B.-Y. Yu, C.-H. Pyun, G.-Y. Hong, *Journal of Alloys and Compounds* **2000**, *311*, 33; b) R. P. Rao, D. J. Devine, *Journal of Luminescence* **2000**, *87-89*, 1260.



- [68] N. K. Za'aba, W. H. A. Majid, E. Kusriani, M. I. Saleh, *AIP Conference Proceedings* **2009**, *1150*, 291.
- [69] L. Liu, S. K. Gill, Y. Gao, L. J. Hope-Weeks, K. H. Cheng, *Forensic Science International* **2007**, *176*, 163.
- [70] A. Shahzad, M. Edetsberger, G. Koehler, *Applied Spectroscopy Reviews* **2010**, *45*, 1.
- [71] F. V. Bright, *Analytical Chemistry* **1988**, *60*, 1031A.
- [72] N. Akiba, N. Saitoh, K. Kuroki, *Journal of Forensic Sciences* **2007**, *52*, 1103.
- [73] L. K. Seah, U. S. Dinis, W. F. Phang, Z. X. Chao, V. M. Murukeshan, *Forensic Science International* **2005**, *152*, 249.
- [74] T. J. Mooibroek, P. Gamez, A. Peveč, M. Kasuni, B. Kozlevčar, W.-T. Fu, J. Reedijk, *Dalton Transactions* **2010**, *39*, 6483.
- [75] G. Payne, B. Reedy, C. Lennard, B. Comber, D. Exline, C. Roux, *Forensic Science International* **2005**, *150*, 33.
- [76] I. H. Yu, S. Jou, C.-M. Chen, K.-C. Wang, L.-J. Pang, J. S. Liao, *Forensic Science International* **2011**, *207*, 14.
- [77] O. P. Jasuja, G. D. Singh, G. S. Sodhi, *Forensic Science International* **2006**, *156*, 237.
- [78] M. Liu, *Pattern Recognition* **2010**, *43*, 1062.
- [79] J. D. James, C. A. Pounds, B. Wilshire, *Powder Metallurgy* **1991**, *34*, 39.
- [80] E. R. Menzel, *Vol. US 6306662 (B1)* Texas Tech University, United States, **2001**.
- [81] a)L. Rabjerg, P. Jennum, M. Hl., *Scandinavian journal of work, environment & health* **1983**, *9*, 511; b)F. C. G. Souter, C. Van Netter, R. Brands, *International Journal of Environmental Health Research* **1992**, *2*, 114.
- [82] S. Hirano, K. T. Suzuki, *Environmental Health Perspectives* **1996**, *104*, 85.